DISS. ETH NO. 26024

Experimental and Modeling Framework for the Production of Cell and Protein-Based Biopharmaceutical Products

A thesis submitted to attain the degree of
Doctor of Sciences of ETH Zurich
(Dr. sc. ETH Zurich)

presented by

Ernesto Scibona

M.Sc. in Biomedical Engineering, Politecnico di Milano
born on 14.09.1990
citizen of Italy

accepted on the recommendation of
Prof. Dr. Massimo Morbidelli (ETH Zurich), examiner
Prof. Dr. Markus Aebi (ETH Zurich), co-examiner

2019

Abstract

The advent of biological drugs has revolutionized the pharmaceutical industry by bringing to the market therapeutic agents capable of combining high potency with extremely high selectivity. Despite the financial success, this sector is constantly evolving to keep pace with the approval of an increasingly sophisticated catalogue of biotherapeutics.
The present work aims at developing novel experimental and modeling strategies to optimize the production of cell and protein based biotherapeutics with tailored quality attributes. The first part of this thesis reports the development of two expansion processes to scale-up the cultivation of human pluripotent stem cells and T cells. Pluripotent stem cells can be expanded as floating aggregates in low-footprint suspension-based systems, but all currently reported processes rely on serial dissociation and reaggregation procedures to control the aggregate diameter below a critical size to maintain acceptable levels of pluripotency and cell viability. These procedures require the interruption of the culture and are usually associated with a reduced yield due to cell loss. This issue was solved through the development of a scalable bioreactor-based platform capable of maintaining a steady-state size distribution of stem cell aggregates through pulses of hydrodynamic shear stress, allowing the prolonged expansion of viable and phenotypically undifferentiated stem cells at high density. In the case of T cells, several studies have linked the clinical success rate of cell-based immunotherapies to the number of infused cells and to T cell-related attributes such as longevity, proliferative potential and metabolism. At the same time, most of the methods for T cell expansion in clinical trials are based on small-scale system in combination with medium formulations that aim at maximizing the growth rate of T cells at the expense of extensive differentiation in short-

lived effector cells. To provide a better alternative to conventional processes, an initial screening process was performed to optimize the medium formulation for providing the best trade-off between the inhibition of effector cell differentiation and the promotion of proliferation. After determining the optimal conditions for T cell expansion using small-scale system, the expansion step was translated to stirred tank bioreactors, resulting in the scalable generation of large numbers of T cells with an early memory phenotype.
The second part of this thesis aims at providing mathematical modeling tools for the mechanistic understanding of the N-linked glycosylation pathway. This post-translational modification is crucial for the thermodynamic stability of proteins and is regarded to as one of the most important quality attributes for therapeutic recombinant proteins such as monoclonal antibodies. First, a flux analysis methodology was applied to study the glycosylation heterogeneity of a model protein bearing multiple oligosaccharides. This methodology correctly described site-specific processing and was successfully applied in the determination of enzymatic bottlenecks for sugar maturation after alterations in the primary structure of the protein. Secondly, a mathematical model was developed to study the maturation and secretion of monoclonal antibodies by providing a kinetic description of intracellular N-glycan processing. Taken together, these two approaches provide a platform to quantify possible alteration in the N-Glycosylation machinery to produce proteins with tailored oligosaccharides.

Sommario

L'avvento dei farmaci biologici ha rivoluzionato l'industria farmaceutica introducendo sul mercato agenti terapeutici in grado di combinare un'elevata potenza con una estrema selettività verso i propri target. Nonostante il successo finanziario, questo settore è in continua evoluzione per stare al passo con l'approvazione di un catalogo sempre più sofisticato di prodotti bioterapeutici.

Il presente lavoro di tesi mira a sviluppare nuove strategie sperimentali e di modellazione per ottimizzare la produzione di agenti terapeutici basati su cellule e proteine. La prima parte di questa tesi riporta lo sviluppo di due processi di espansione per migliorare la coltivazione di cellule staminali pluripotenti umane e cellule T. Le cellule staminali pluripotenti possono essere coltivate come aggregati in sistemi in sospensione, ma tutti i processi attualmente pubblicati per la loro espansione si basano su procedure di dissociazione seriali al fine di controllare il diametro degli aggregati al di sotto di una dimensione critica per mantenere livelli accettabili di pluripotenza e viabilità. Queste procedure richiedono l'interruzione della coltura e sono solitamente associate a una resa ridotta a causa della inevitabile perdita di cellule. Questo problema è stato risolto attraverso lo sviluppo di una piattaforma scalabile basata su bioreattori agitati, in grado di mantenere una distribuzione di dimensione degli aggregati stazionaria attraverso impulsi di stress di taglio idrodinamico, consentendo l'espansione prolungata di cellule staminali vitali e fenotipicamente indifferenziate ad alta densità. Nel caso delle cellule T, diversi studi hanno collegato il tasso di successo clinico delle immunoterapie basate su cellule al numero di cellule infuse e agli attributi correlati alle cellule T quali longevità, potenziale proliferativo e metabolismo. Allo stesso tempo, la maggior parte dei metodi

per l'espansione delle cellule T utilizzati in studi clinici si basa su un sistemi di piccola scala in combinazione con formulazioni di medium che mirano a massimizzare il tasso di crescita delle cellule T a scapito di una significative differenziazione in cellule effettrici, caratterizzate da una bassa persistenza *in vivo*. Per fornire un'alternativa migliore ai processi convenzionali, è stato eseguito un processo di screening iniziale per ottimizzare la formulazione di medium al fine di fornire il miglior trade-off tra l'inibizione della differenziazione e la promozione della proliferazione delle cellule T. Dopo aver determinato le condizioni ottimali per l'espansione delle cellule T utilizzando un sistema in piccola scala, lo step di espansione è stato traslato in bioreattori agitati, portando alla generazione di un elevati numeri di cellule T con un fenotipo indifferenziato.

La seconda parte di questa tesi punta a fornire strumenti di modellizzazione matematica per la comprensione del progesso di N-glicosilazione. Questa modifica posttraduzionale è cruciale per la stabilità termodinamica delle proteine ed è considerata uno degli attributi di qualità più importanti per le proteine ricombinanti terapeutiche come gli anticorpi monoclonali. Il primo lavoro presentato si basa sull'analis dei flussi per studiare l'eterogeneità della N-glicosilazione di una proteina modello che presenta più strutture oligosaccaridiche sulla superficie. Questa metodologia descrive correttamente il processamento sito-specifico ed è stata applicata con successo nella determinazione delle limitazioni enzimatiche per la maturazione dello zucchero a seguito di alterazioni nella struttura primaria della proteina. In secondo luogo, un modello matematico è stato sviluppato per studiare la maturazione e la secrezione di anticorpi monoclonali fornendo una descrizione cinetica del processamento intracellulare degli zuccheri. Questi due approcci forniscono una piattaforma per quantificare possibili alterazioni nel sistema intracellulare di N-glicosilazione per produrre proteine con profili di oligosaccaridi desiderati.

Acknowledgments

The development of this work (...and of myself) would have not been possible without the invaluable contribution of the people who accompanied me over the last years.

First of all, my gratitude goes to Professor Massimo Morbidelli for i) answering positively to the email I sent him on the 15^{th} October 2012, where I asked him if it was a good idea to follow the course of applied physical chemistry in Milan, ii) taking me under his wing, iii) giving me all the scientific freedom and support, iv) his confidence in me.

Thanks to no lesser extent to Professor Markus Aebi for bringing up a wonderful collaboration, his support and appreciation in my work, the interesting discussions and for accepting to be my co-examiner.

Thanks to Thomas Villiger, Daniel Karst and Sandro Hutter for the priceless support during my master's and PhD thesis and for being an inspiration outside of work. Thanks to Professor Miroslav Soos for his (not only) scientific inputs and for always being there where I needed feedback and consultations. Thanks to Ilaria and Marie-Estelle for the successful collaborations and for the nice time spent together. Thanks to Daniel Baur for the great help in coding and computations. Thanks to my students Filippo, Luis and Maddalena, without your outstanding contribution this work wouldn't have been possible.

Thanks to Alberto for countless reasons. Thanks to my office mates Ruben and Marcel for the nice time spent together. Thanks to all the lab colleagues and collaborators for their support and providing a great working environment. Special mention to my sport buddies Anna, Fabio and Bettina.

Thanks to Professor Moscatelli for the nice collaboration, the interesting discussions and all the support. Thanks to Matteo and Nicolò for the wonderful time spent together in and out of the lab.

Finally, thanks to all the friends and family for their support and the time spent together.

Contents

List of Figures

List of Tables

Chapter 1

Introduction

1.1 Biopharmaceutical Market

The term biopharmaceutical was invented in the 1980s to indicate a class of therapeutic entities produced "*through biotechnological techniques*" [1]. This description was referred only to proteins expressed in biological system and stayed valid until recently, when the advent of novel therapeutic modalities based on nucleic acids or entire cells required the inclusion of additional criteria. Nowadays, biopharmaceuticals (or biotherapeutics) are defined as ''*natural or genetically modified products derived from microbial or yeast fermentations, mammalian or insect cell cultures, or from natural sources, or they are exact copies of such molecules made by chemical synthesis*" [2]. For the last 30 years, the biopharmaceutical industry in its entirety has been constantly growing in terms of R&D expenditure, manufacturing capacity and number of marketed products, with a global revenue reaching 275 billion $/year in 2018 and a compound annual growth rate estimated around 12-13% according to the 15^{th} Annual Report and Survey of Biopharmaceutical Manufacturing Capacity and Production. This success can be attributed to several factors. From a financial standpoint, biopharmaceuticals are sold through value-based pricing strategies, resulting in margins higher than 60% for originator drugs [3]. Compared to conventional drugs like small molecules, biopharmaceuticals provide different targets and novel therapeutic mechanisms, paving the way for the treatment of a broader class of diseases [4]. Moreover, biological products bind their targets through antigen-receptor interactions, resulting in a higher specificity and a significant reduction in off-target effects. The improved efficacy and safety profiles largely contributed to an unprecedented success in clinical trials for biopharmaceuticals [5], resulting in twofold regulatory approval rates for biotech products compared to standard drugs [6]. This commercial success was accompanied by a dramatic increase in the volumetric yield of the associated manufacturing processes, allowing a significant decrease in production costs for many biopharmaceuticals.

1.2 Industrial Production of Biopharmaceuticals

The manufacturing of biopharmaceuticals starts with the identification of a suitable expression organism that can efficiently produce clinically efficient and safe active pharmaceutical ingredients (APIs), or, in particular cases (e.g. human plasma, cell therapies), with the definition of the source of the biological material of interest. After the

initial screening process, a small-scale investigation is performed to evaluate the optimal process conditions and medium formulation for the cultivation of the organism of choice and the purification of the API. The results are then transferred to a pilot scale process to produce the initial batches of materials to supply preclinical studies [7]. In case of success, the entire process is scaled up, characterized, transferred to the manufacturing site and validated to match the expected market demand of the drug. The unit operations for the production of biopharmaceuticals follow a common flowsheet, which is usually separated into upstream and downstream processes. The upstream part typically covers cell expansion, production culture and product harvesting. Downstream processing is instead responsible for the isolation, purification and clarification of the product. In contrast to conventional drugs, biopharmaceuticals are large, structurally complex entities that exist as heterogeneous mixtures due to their biological synthesis route. For example, protein-based pharmaceuticals differ in terms of post-translational modifications (PTMs), chemical or enzymatic modifications, conformational diversity and aggregation [8], while cell-based drugs may be characterized by differences in phenotype, differentiation status, metabolism, genome integrity, telomer length and several others. All these characteristics represent critical quality attributes (CQAs) of the final product and often have a profound impact on its efficacy, safety and biodistribution [9, 10]. Although a certain degree of heterogeneity is usually tolerated by regulatory agencies, several strategies have been developed in controlling this heterogeneity of biological drugs, including host cell engineering, clone selection, medium screening and definition of optimal process parameters [11]. Despite the increasing demands, the pharmaceutical industry is facing important operational decisions to position itself in the future market. For established classes of drugs such as monoclonal antibodies (mAbs), the efforts will be focused on controlling their critical quality attributes (CQAs) to face the increasing competition posed by biobetters and biosimilars. At the same time, novel therapeutic modalities like cell and gene therapies will require the development of tailored manufacturing platforms to quickly produce small batches of personalized products within a limited timeframe. These technological improvements in the manufacturing of biopharmaceuticals will only be possible through a deeper understanding of the input-output relationship between culture-related parameters and the intrinsic machinery of the cell itself.

1.3 Scope of the thesis

This thesis aims at tackling the aforementioned challenges in the production of specific biopharmaceutical products and can be conceptually divided in two parts, with the first three chapters centered around cell-based therapies and the last two aiming at developing a mechanistic, model-based understanding of the N-linked glycosylation processing for proteins produced in mammalian hosts.
Chapter two aims at reviewing the main culture systems and expansion processes used for the production of cell therapy products (CTPs), highlighting the need to implement scalable, cost-efficient technologies together with process optimization strategies to bridge the gap between basic scientific research and commercially available therapies. Chapter three is dedicated to the development of a scalable bioreactor-based platform for human expansion of human pluripotent stem cells (PSC), which is capable of maintaining a steady-state size distribution of PSCs aggregates, overcoming one of the main limitations in the manufacturing of PSC-based products and advancing towards automation and continuous processing in the manufacturing of cell-based therapies. Chapter four reports the development of a scalable process to generate large number of T cells with improved antitumor efficacy in serum-free conditions, covering medium development, determination of optimal process conditions, and translation from small-scale static systems to benchtop stirred tank bioreactors.
The second part of the thesis focuses on mathematical modeling of N-glycosylation for proteins produced in mammalian hosts. Besides playing a fundamental role in several intracellular pathways, this post-translational modification is of paramount importance for the therapeutic efficacy of many recombinant proteins and is one of the main criteria for the approval of biologics under the designation of biosimilar. In this respect, Chapter five aims at quantifying the activity and heterogeneity of Golgi-resident enzymes in the processing of a glycoprotein bearing multiple glycosylation sites through a flux-analysis methodology to identify site-specific enzymatic bottlenecks of N-glycan processing, while Chapter six presents a model-based, kinetic description of intracellular N-glycan processing of mAbs along the entire secretory pathway.

Chapter 2

Expansion Processes for Cell-Based Therapies

This chapter is based on the following publication: E. Scibona, M. Morbidelli. *Expansion processes for cell-based therapies*, submitted.

2.1 Introduction

Small molecules and recombinant proteins currently dominate the pharmaceutical market. Despite the development of more advanced biological drugs such as bispecific antibodies, fusion proteins and antibody-drug-conjugates (ADC), there is still no definitive cure for many of the major disease families, including diabetes, myocardial infarction and neurodegenerative disorders, with currently marketed substances only achieving a delay in disease progression or in the occurrence of complications [12]. Cell-based therapies, defined as the administration of living cells as drug product [13], are expected to bring a revolution in the pharmaceutical industry by providing novel therapeutic mechanisms that can address several of the currently unmet clinical needs. Compared to small molecules and biologics, living cells are complex entities, capable of integrating signals from the surrounding environment, executing precise responses according to the inputs received [4]. When used as therapeutic agents, cells are able to exert more advanced modes of action compared to conventional treatments, such as migration and accumulation at specific areas, on-demand production of paracrine or systemic factors, self-regulating dosage in response to the disease burden through proliferation or apoptosis [4] and long-lasting regeneration of entire tissues [14]. Moreover, synthetic biology techniques can be used to design novel biological mechanisms to enhance their safety and efficacy profiles, possibly introducing novel functionalities [15]. The concept of exploiting human cells as therapeutic entities is not new, and dates back to the 1950s with the pioneering work on bone marrow (BM) transplants to treat hematological malignancies and blood transfusions [16]. Despite their great potential, there were no significant breakthroughs in cell-based therapies for over 40 years, with the exception of epidermal cell transplantation for the treatment of large burns [17]. The field has gained worldwide interest in the last two decades due the discovery of new cell types, the development of more reliable cultivation methods and more precise gene editing techniques. Nowadays, the number of clinical trials involving Cell Therapy Products (CTPs) is continuously on the rise [18], and it is characterized by a wide diversity in terms of both the targeted conditions and cell type used for the treatment. To date, 22 CTPs have been granted marketing authorization in the EU and US, and the number is expected to rise significantly over the next decade given the recent successes in cell-based immunotherapies. The list includes nine autologous (patient-to-self) and three allogeneic (donor-to-many) therapies, presented in Table 2.1 and Table 2.2 respectively. The total number of ap-

proved CTPs also includes seven products approved in the US for cord blood storage and three *in vivo* genetic modification of cells using viral vectors, which fall under the same regulation but are beyond the scope of the review and are listed in Tables A.1 and A.2 for the sake of completeness. Although the number of marketed CTPs is very limited compared to conventional drug classes, the ''Report on Biomedicine in Development from the Pharmaceutical Research & Manufacturers of America" [19] shows that 115 biological drugs in human clinical trials or under review by the Food and Drug Administration (FDA) in 2013 contained cells or genes as active pharmaceutical ingredients (API). For comparison, 338 monoclonal antibodies (mAbs), 250 vaccines and 93 other recombinant proteins were at the same stage of development when the report was written, highlighting how the variety of future therapeutics might change significantly in the near future [2].

Table 2.1: Allogeneic cell-based therapies approved in EU and US.

Product	**Cell Type**	**Dosage**	**Indication**	**Manufacturer**
Gintuit	Keratinocytes and fibroblasts	$> 4 \cdot 10^6$ cells	Oral soft tissue regeneration	Organogenesis Incorporated
Zalmoxis	T cells	10^7 cells/kg	Hematological malignancies	MolMed S.p.A
Alofisel	AT-MSC	$1.2 \cdot 10^8$ cells	Chron's disease	TiGenix - Takeda

Within the complex manufacturing scheme of CTPs, almost all therapeutic cells used in a non-minimally-manipulated setting, according to the definition of the Food & Drug Administration [20], require extensive culture *ex vivo* to increase their number before formulation and infusion. The need for implementation of at least one expansion step in CTP manufacturing is manifold. First, the number of cells purified during biopsies is usually not sufficient to display significant therapeutic efficacy. Secondly, in case of allogeneic therapies, the production of large batches of cells drives the economics of the entire process. Finally, the infusion of higher number of cells does often correlate with a positive outcome for many therapies, as it is the case for T lymphocytes [21], mesenchymal stromal cells (MSCs) [22], hematopoietic progenitor cells (HPCs) [23] and several others [24]. Despite numerous advances in the cultivation methods, the production of large numbers of cells with desired safety and potency profiles is one of the main bottlenecks in cell therapy in terms of yield, cost and manufacturing time [25]. The translation to robust, scalable, automated and low-cost industrial processes is a step

Table 2.2: Autologous cell-based therapies approved in EU and US. Therapies withdrawn from the market are indicated with the symbol *.

Product	Cell Type	Dosage	Indication	Manufacturer
Laviv	Fibroblasts	$> 4 \cdot 10^7$ cells	Nasolabial fold wrinkles	Fibrocell Technologies, Inc
MACI*	Chondrocytes	$5 \cdot 10^5$ cells/cm^2	Cartilage regeneration	Vericel Corporation
Kymriah	T cells	10^8 cells	B-cell Leukemia	Novartis
Yescarta	T cells	$2 \cdot 10^8$ cells	Large cell lymphoma and B-cell lymphoma	Kite Pharma-Gilead
ChondroCelect*	Cartilage cells	$0.8 - 1 \cdot 10^6$ cells/cm^2	Knee repair and cartilage diseases	TiGenix N.V.
Holoclar	Corneal epithelial cells and stem cells	$0.8 - 3 \cdot 10^5$ cells/cm^2	Limbal stem-cell deficiency	Holostem Terapie Avanzate
Strimvelis	Transduced CD34+ cells	$2{-}20{\cdot}10^6$ cells/kg	ADA-SCID	GlaxoSmithKline
Spherox	Chondrocytes	n.a.	Cartilage defects	Co.don ag
Provenge*	T cells	$> 50 \cdot 10^6$ cells	Prostate Cancer	Dendreon Corporation

that needs to be addressed in order to exploit the full potential of cell therapies in a commercial setting [26], similarly to what happened for breakthrough biological drugs such as monoclonal antibodies [27]. To put this concept into perspective, the first recombinant protein (human Somatostatin) was produced in the late 1970s at Genentech [28], and the first regulatory approval occurred in 1982 (recombinant Insulin, Genentech). The commercial success of this technology came more than three decades later, since in year 2001 recombinant proteins generated only 7% of the total revenue of the top ten most selling drugs, a value that increased to 71% in 2012 [29]. This success was accompanied by a dramatic increase in the volumetric yield of the manufacturing processes, which led to a significant decrease in production costs [30]. For example, production runs nowadays can easily achieve 10-15 g/L product titers, while the industrial standard in the mid-1980s was around 0.05-0.1 g/L. As noted by Wurm et al. [31], this productivity increase results mostly from process development and optimization, while the contribution of advances in DNA engineering has been very limited. In this respect, the major innovations in recombinant protein manufacturing involved the transition to closed systems, which could be scaled up and monitored, the use of serum-free medium

formulations and the implementation of novel bioreactor operating modes (i.e. fed-batch and perfusion). Until now, most of the developments in cell therapies has been carried primarily in academic and research institutions at lab-scale using standard cultivation techniques, with limited efforts devoted to industrial aspects such as process scalability and optimization. For this reason, CTP manufacturing is still considered as an emerging area in the biopharmaceutical industry.

The aim of this review is to characterize the main types of therapeutic cells used in clinical trials with respect to their expansion processes. We first provide an overview of the common CTP manufacturing processes and review the main systems used for cell expansion in the pharmaceutical industry. We then review and categorize the main cell types used in clinical trials based on the protocols used for their expansion. Finally, we discuss possible future strategies to be implemented, following the established trends registered for biological drugs manufacturing.

2.2 General Concepts for the Manufacturing of Cell-Based Therapies

The complexity of cell therapy poses several challenges for the manufacturing of these products at a commercial-scale level [26]. Nowadays, many of the processes and unit operations in CTP production are similar to what is already implemented in biological drug manufacturing, especially for upstream processing (USP). On the other hand, downstream processing (DSP) is significantly different, since the cells represent the product themselves and need to be maintained vital before formulation, preventing the use of filtration and low pH viral inactivation procedures. Despite the differences in terms of cell type and application, most of the non-minimally manipulated CTPs are manufactured according to the general scheme depicted in Figure 2.1. In the autologous setting, lot production is performed on an individual basis and is initiated from the patient's own biopsies (Figure 2.1 A). The biopsy is processed in specialized centers, where the cell population of interest is isolated and cultured *in vitro*. During this stage, the cells can either be simply expanded to increase their number or manipulated in order to change their phenotype or genotype, so as to provide the cells with the functionalities required to exert their therapeutic mechanism *in vivo*. Possible manipulations include gene editing, genetic reprogramming, differentiation and exposure to antigens

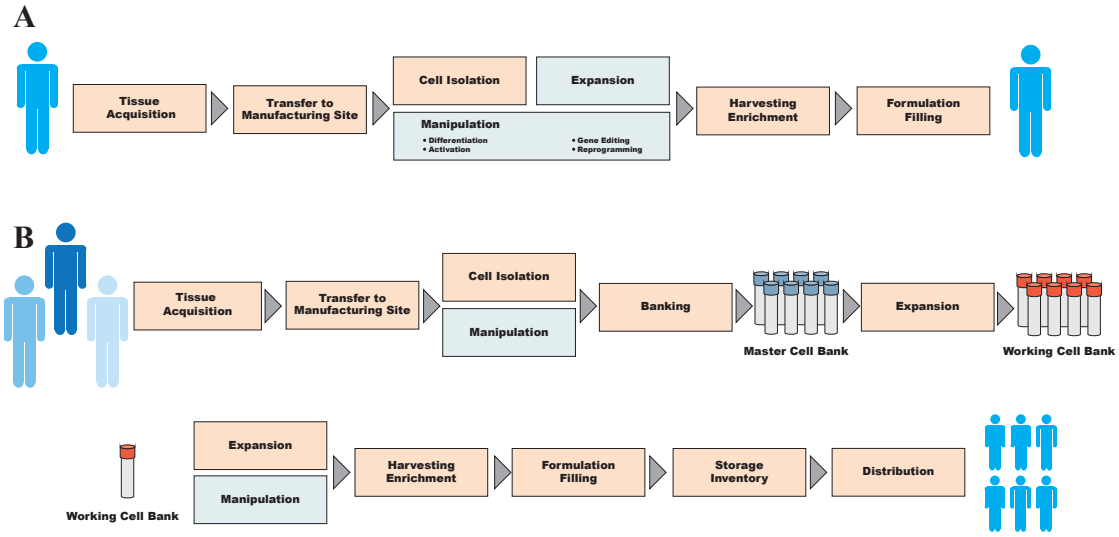

Figure 2.1: General manufacturing flowsheets for autologous (A) and allogeneic cell-based therapies (B). Steps that are not universally implemented are represented in light blue.

or other chemical clues. Upon obtainment of the desired amount of clinically relevant cells, they are subjected to extensive quality control/quality assurance protocols, and then harvested from the culture system. In autologous therapies, harvesting is usually followed by concentration, buffer exchange and possibly cryopreservation before infusion or transplantation. Cells for autologous therapies are usually regarded to as safe in terms of immunologic aspects, but need to be manufactured within a time frame that meets the needs of the patient [32]. For example, the target turnaround time for the manufacturing of KYMRIAH® CAR-T cells has been set to 22 days [33]. Altough not in the focus of this review, it is worth mentioning that the need for delivering a customized product within a limited timeframe will probably impose a paradigm shift in the business strategies and organization for the manufacturing of autologous therapies. One possible solution involves the adoption of a decentralized manufacturing model, which aims at optimizing delivery time and flexibility to local demand fluctuations through the use of satellite facilities and personalized supply chains, as reviewed in [34, 35].

Allogeneic cell therapies (Figure 2.1 B) rely on cells from selected donors that are tolerated by the immune system of many patients. Compared to autologous therapies, the availability of the starting material and the time constraints connected to the manufacturing process are greatly reduced thanks to the generation of master cell banks (MCBs). These master cell banks are generated from biopsies taken from selected

healthy donors, whose cells are expected to be tolerated by the immune system of several recipients. Allogeneic CTP manufacturing follows the same scheme as autologous therapies in terms of unit operations, but each step is usually operated at a larger scale. In case of autologous therapies, the number of cells to be infused corresponds roughly to the size of the production batch, and the production costs for a single dose are therefore those associated to the entire batch. Manufacturing of allogeneic therapies is closer to the mass production paradigm used for biologics, where several doses are produced per single lot, requiring the entire production process to be scaled-up to match commercial-scale needs [36]. It is worth noting that immortalized cell lines are also being tested in the clinics in the context of cell therapies. Examples include the non-Hodgkin's lymphoma derived NK-92 cell line for cancer treatment (clinical trial identifiers NCT03656705 and NCT03383978), human myeloid leukemia derived dendritic cells (DCOne) for cancer vaccines (NCT01373515) and the neural stem cell line CTX for ischemic middle cerebral artery (MCA) stoke (NCT02117635). Compared to cells taken directly from living tissues, these cell lines have unlimited proliferative potential and can be maintained as more homogeneous populations, heavily simplifying their manufacturing procedures. Due to their tumorigenic nature, they need to be irradiated before infusion, thus improving the overall safety profile of the therapy, but drastically reducing the *in vivo* persistence of these cells.

2.3 Technologies for Cell Expansion

Expansion is a critical step in both autologous and allogeneic settings since it determines not only the number, but also the phenotype and therapeutic properties of cells infused. Considering single doses or grafts, the optimal number of cells differs significantly for the main therapies investigated in research and clinical trials (Figure 2.2). Generally speaking, the number of cells is lower for small tissue grafts such as corneal or retinal replacements (10^5 cells) and for cells that are known to expand highly *in vivo* upon transfusions, such as hematopoietic stem cells (HSCs) and chimeric antigen receptor (CAR) T cells. The use of terminally differentiated non-dividing cells such platelets and red blood cells might instead require much higher dosages, estimated to be in the order of 10^{11-12} cells per infusion. Given the different scales needed to produce the required dosages depending on the application, and cell-specific properties such as growth rate, metabolic activity, sensitivity to environmental conditions including anchorage de-

pendence, it is unlikely that a single universal cultivation platform would accommodate every need [37].

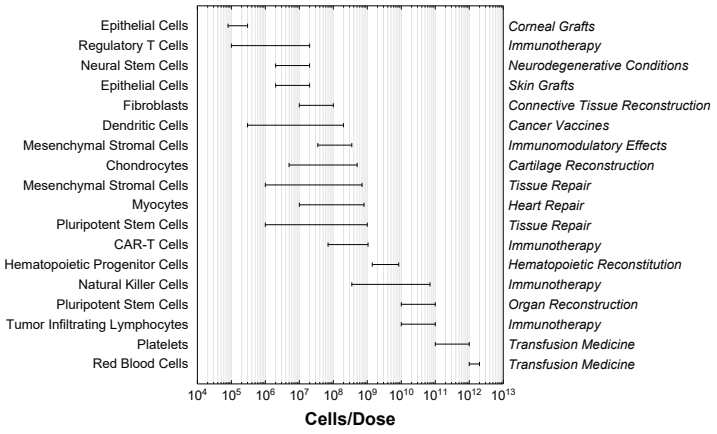

Figure 2.2: Typical dosages for the most common cell therapies. The values are taken from the references provided in SI Table 3 and normalized with respect to i) patients weighting 70 kg, ii) 1 cm^2 for corneal grafts and iii) 20 cm^2 for skin grafts.

Additionally, media formulation, soluble factors and immobilized ligands need to be tailored specifically for the final cell phenotype and quality attributes desired [38]. Despite these differences, all culture systems have to meet the same basic requirements needed to create suitable conditions for cell survival and proliferation. First, environmental variables such as pH, temperature, dissolved oxygen (DO) and CO_2 need to be maintained at their optimal values for the cell population of interest. Secondly, gas and heat exchange within the system must be ensured, together with a mean to sample, while maintaining sterility throughout the entire cultivation. Currently, the vast majority of the systems used for the cultivation of therapeutic cells is not new, and derives directly from the established fermentation platforms developed for the cultivation of bacteria, yeast and animal cell lines.

2.3.1 Static Culture Systems

Static systems are defined by the absence of any mechanical, pneumatic or hydraulic power input [39]. The most common static systems are tissue culture (TC) and multiwell plates. They are simple sterile plastic containers in either polystyrene or polypropylene, do not contain sensors or instrumentation and necessarily rely on external incubators

for controlling temperature, humidity and pH. When seeded, the cells spread across the available surface, which is then covered by a thin layer of medium to allow gas exchange through the headspace. They can also be applied for the cultivation of suspension cells with the same principles, but in this case no adherent layer is formed. Besides simplicity and low cost, the main advantages are the possibility of visual and microscopic inspection of the culture and the ease to accommodate difficult procedures such as transfections, differentiation protocols or co-culture assays. On the other hand, these systems are not scalable except by the addition of more units in parallel, and are usually limited to batch-wise operation mode, with media exchanges performed every 1-4 days depending on the metabolic activity of the cells. The surface area for single units ranges from few cm^2 to 300 cm^2, while culture volume for standard flasks and well plates ranges from few microliters to the hundreds of milliliters.

Multitray Systems

Multitray systems consist of several stacks of culture plates aseptically connected to provide surfaces in the order of 10^{4-5} cm^2. Scaling-up is performed through the serial addition of aseptically connected multiple units, providing a significant increase in surface area compared to TC flasks in a single device. Culture protocols such as seeding, harvesting and media exchanges can be directly translated from culture on TC plates. Due to their static nature, these systems tend to establish gradients in pH and pO_2 levels in the liquid phase, potentially introducing heterogeneities that would decrease the reproducibility of the expansions or reduce the growth rate of the cells. Moreover, the lack of sensors does not allow the maintenance of optimal set points for some physicochemical variables. For example, pH levels may drop during the culture due to lactic acid accumulation, and oxygen levels can decrease if the cell density in the plates becomes too high. These systems have been often used for the production of vaccines [13], and are being tested in research for the cultivation of adherent cells, in particular MSCs [40].

Gas-Permeable Systems

Conventional TC plates do not allow the use of more than 1 mL of medium per cm^2 of culture to prevent limitations in oxygen transfer to the cells lying at the bottom of the plate. In case of high cell densities, this amount of liquid becomes quickly limiting for supplying growing cells with glucose and other metabolites, and cultures require regular

passaging to maintain the cells in an healthy state [41]. Gas-permeable plastic culture ware such as the G-Rex systems (Wilson Wolf, USA) and conventional Teflon bags are designed to provide gas exchange through their surfaces, accommodating more medium per surface area of culture without the need for mixing. They still require to be placed in incubators to maintain optimal temperature and possibly humidity set points. These systems have successfully been applied for the cultivation of T cells and other immune system cells, providing a valuable alternative to conventional methods [41–43] due to their versatility (the working volume ranges from few milliliters up to the liter scale) and simple design.

2.3.2 Dynamic Culture Systems

In dynamic cell culture systems the culture broth is continuously agitated to provide a uniform environment, preventing the formation of physicochemical gradients and improving the mass and heat transfer. Generally speaking, suspension-based systems have the advantage to provide a higher yield (intended as total number of cells) with a lower footprint compared to their planar counterpart. Similar to TC flasks, the simplest small-scale dynamic culture systems (i.e. spin tubes, shake flasks and roller bottles) are sterile plastic tubes, which usually lack instrumentation and control, and require a humidified CO_2 incubator to be operated. Initially developed for the cultivation of various immortalized suspension cell lines, they have been surpassed by more sophisticated systems for the industrial production of recombinant proteins or cell-based products, but still play a significant role for small-scale screening of medium compositions and process conditions [44, 45].

Dynamic well-mixed systems have been initially developed and optimized for the cultivation of suspension cells. Suspension culture is also possible for anchorage-dependent cells, which by definition require the adhesion to a suitable surface in order to survive and proliferate. This transition has been achieved through several strategies. Microcarriers are solid beads with diameters typically ranging from 100 to 300 µm, which are maintained in suspension by the motion of the fluid while providing a support for anchorage-dependent cells. This strategy leads to a uniform culture environment with high surface to volume ratios, increasing significantly the scalability of the system compared to static dishes. Microcarriers have been extensively characterized and optimized in terms of bulk properties, surface charge, porosity, and coating

chemistry (Merten, 2015), as well as in their hydrodynamic behavior in agitated systems [46]. Moreover, surface functionalization with specific ligands allows cultivation of a broad variety of cells and stem cells [47]. In the last years, the cultivation of cells as multicellular aggregates (also called spheroids) has gained a lot of attention for many anchorage-dependent stem cells. The main motivation for growing cells as aggregates is to avoid the use of exogenous supports while exploiting basic principles of normal tissue organization, giving cells the opportunity to arrange in a 3D setting, similar to living tissues [48, 49]. In this configuration, cells self-assemble and interact under natural forces, permitting them to generate their own extracellular matrix (ECM), which serves as support for the cells to survive in suspension and reproduces the cell-to-cell and cell-to-matrix signaling networks present *in vivo* [50, 51]. Furthermore, spheroids are free of exogenous biomaterials, which could cause problematic responses upon cell transplantation [52], and simplifies downstream processing for cell-based products, since fewer purification treatments are needed. Spheroid culture is not applicable to every cell type, since downregulation of proliferation-related genes upon aggregation might occur, as it is the case for MSCs [53]. Moreover, agglomeration of cells into clusters exceeding 200-300 μm tends to induce apoptosis due to nutrient limitations in the core of the aggregates [54]. This strategy provides another level of complexity, since aggregate breakage procedures need to be introduced throughout the process in order to control their size. Microencapsulation has been proposed as a strategy to immobilize cells in order to protect them against the high shear levels present in dynamic systems [55]. This technique does however not solve the problems related to mass transfer limitations and has potential issues concerning scalability and purification procedures to get rid of the exogenous materials used for encapsulation.

Dynamic systems, in particular stirred tank reactors, are the main industrial choice for production of recombinant proteins due to their scalability, flexibility and thorough characterization. Bioreactors are closed systems providing a sustainable environment for biochemical reactions and cell proliferation [39]. They easily scale to match production needs, facilitate mass transport and allow monitoring and feedback control of the culture environment and automation of the feeding strategy or other manufacturing steps. Other advantages include reduced working volumes and easier compliance with GMP regulations due to their closed-system nature [56]. Although several categories of fixed and fluidized bed bioreactors have been developed for microbial and animal cell fermentation for the production of recombinant proteins, cell-based therapies are mostly

employing the stirred tank and rocking bioreactor platforms [57].

Stirred Tank Bioreactors

Stirred tanks represent the main platform used in the biopharma industry for the production of recombinant proteins, with scales ranging from 15 mL to 15000 L. They consist of closed, aerated vessels equipped with a motor-driven impeller to drive the fluid agitation. The main purpose of the impeller is to provide sufficient mixing of the culture broth without harming the cells [58] or, in case of microcarriers or multicellular aggregates, to achieve homogeneous dispersion and sufficient mass transfer at the lowest possible shear [59]. These systems have been widely investigated from the hydrodynamic point of view, and acceptable operating conditions can be obtained using modelling techniques [60], and scale-up principles are very well characterized compared to other reactor types. Compared to static systems and most of the small-scale dynamic systems, stirred systems can accommodate fed-batch feeding strategies and perfusion operations in a manual or automated fashion. For the latter, the reactor needs to be aseptically connected to a cell retention device to allow continuous removal of nutrient-depleted medium. The most common strategy for fluid filtration in industrial processes involves the use of porous hollow fibers or screen filters, operated in cross-flow filtration with tangential flow (TFF) or alternating tangential flow (ATF). For cell therapy, simpler technologies such as glass filter tubes [61], centrifugation, sedimentation and ultrasound-based separation have been employed, although they are more complicated to implement and operate in large scale systems [62].

Stirred tank bioreactors have been widely applied in research for the expansion of mesenchymal stromal cells [63], pluripotent stem cells [64], hematopoietic progenitors [65], T lymphocytes [66] and many others, with scales ranging from 0.1 to 150 L, in both reusable and single-use setups. Despite its flexibility to accommodate different types of cells at several scales, this platform is yet very scarcely employed for the clinical manufacturing of cell therapies.

Rocking Bioreactors

Rocking bioreactors are pre-sterilized disposable plastic bags, which rely on a continuous rocking motion to provide efficient mixing. Oxygen supply is achieved through the headspace gas and, in some instances, it can be increased with the use of gas-permeable

walls. This technique allows a better oxygen supply compared to spinner flasks and reduces the shear acting on the cells with respect to impeller-mixed systems, making the platform more suitable for the expansion of shear-sensitive cells. This system has been applied in the biotech field for the cultivation of several cell lines with performances comparable to standard stirred platforms, and is now being implemented as expansion platform for T cells in clinical trials [67]. Bags are available as single use devices with volumes ranging from 0.5 to 500 L, eliminating the needs for sterilization procedures, reducing the risks of cross-contamination and increasing the ease of implementation in existing facilities. Similar to stirred tanks, these systems can also be operated in fed-batch and perfusion operation modes when combined with ATF or TFF equipment [68]. On the other hand, wave-mixed bag systems are less efficient at maximizing mass transfer [13], posing a possible limitation in case of very high-density cultures.

2.4 Expansion Processes for Therapeutic Cells

Considering the vast majority of non-minimally manipulated cell therapies, the devices and protocols used for *ex vivo* culture expansion must address the need of producing a sufficient number of cells that match the desired targets in terms of product quality attributes. The conjugation of these two aspects often generates a trade-off: when subjected to extensive cultivation, cells are often prone to develop phenotypic changes (e.g., differentiation, senescence or immunogenicity) or genetic changes (e.g., mutations, gene deletions or chromosomal aberrations) that can severely undermine the safety and the efficacy profiles of the drug product. Therefore, higher yield due to prolonged expansion often correlates with the selection of more proliferative cell subpopulations, which can be less efficient *in vivo* for their designed function or even tumorigenic (Merkle et al., 2017). For example, it has been demonstrated that maximizing the growth rate of T lymphocytes, usually achieved by supplementation of high doses of IL-2, results in the differentiation towards short-lived effector cells [69], which are characterized by reduced longevity and proliferative potential *in vivo* with respect to early memory lymphocytes [70]. The expansion process must be designed according to several factors [38]. First, it must comply the regulatory guidelines for clinical approval and market authorization. This aspect includes the implementation of GMP-compatible protocols and consumables, ensure appropriate quality control mechanisms by defining assays to evaluate potency and safety of the product, and perform the appropriate risk

analyses [71]. Optimal operating conditions and critical process parameters must be identified and their impact on product quality must be carefully assessed, as extensively discussed in [10]. Finally, precise cost-reduction strategies must be implemented to ensure long-term sustainability and viability on the market.

Compared to conventional biologics, where a limited number of platforms can be used to manufacture hundreds of different products, the technologies for the cultivation of therapeutic cells need to be tailored to accommodate cell-specific protocols and clinically sufficient dosages (Figure 2.3). Although in principle one could expect the development of cell-specific platforms, most of the technologies used for therapeutic cell expansion result from a direct translation of platforms already implemented in the biotech industry. Additionally, for most of the clinically-investigated cells, only a limited number of the avialable manufacturing platforms has been applied, with the exception of mesenchymal and pluripotent stem cells [72]. To provide an overview of the field, we categorized the main cell types investigated in the clinic upon the underlying technologies used for their expansion.

2.4.1 Expansion Processes for Low-Dosage Therapies based on Adherent Cells

The vast majority of therapies that require the production of up to 10^8 anchorage-dependent cells are based on the use of TC Plates or TC Flasks, where cells are grown until confluency and routinely passaged to increase the final yield. This system is usually most commonly used in the early-phase process development for almost all putative cell therapies due to its simplicity. Despite many therapies require the use of more sophisticated systems to produce sufficient number of cells, planar systems are generally sufficient for the production of several types of therapies based on adherent cells such as fibroblasts, chondrocytes and keratinocytes, as well as other tissue specific cells and stem cells.

Cultured Skin Grafts

Skin is a highly regenerative organ with a turnover rate of approximately 30 days [73]. Regeneration is driven by highly proliferative stem cells, which generate *in vitro* colonies called holoclones *in vitro* [74]. Holoclones can be cultured *in vitro* for long periods and their progeny is capable of forming functional epidermis [75]. Skin grafts

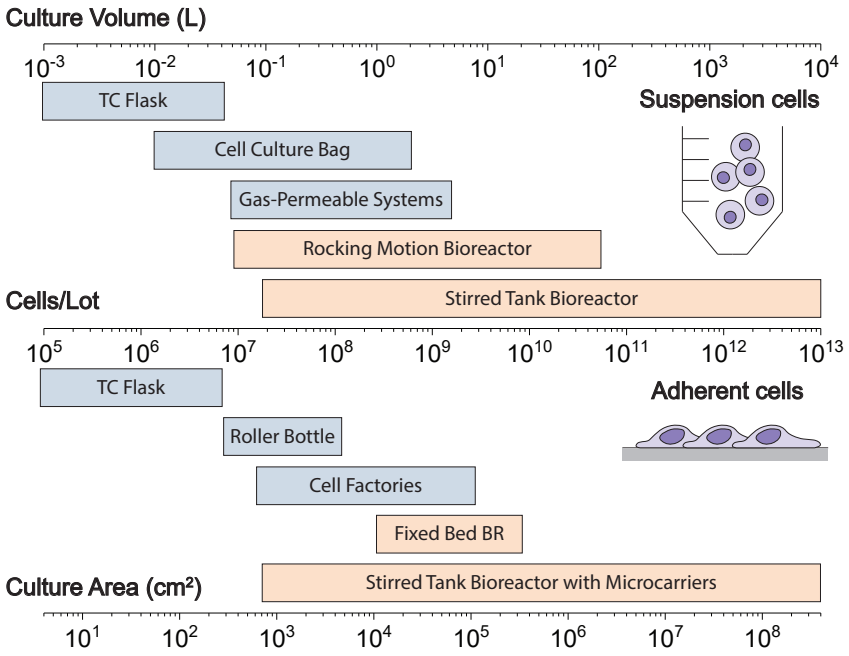

Figure 2.3: Overview of the main technologies used for therapeutic cell expansion. For suspension cells, a viable cell density of 10^6 cells/mL is considered. For adherent cells, the graph assumes a cell concentration of 25000 cells/cm^2 and a surface area of 16000 cm^2/L for microcarrier systems. Orange boxes indicate systems amenable to online instrumentation and process intenfisication strategies.

are mostly applied to treat large burns. The first skin grafts were produced by cultivating autologous holoclone-derived sheets of keratinocytes taken from biopsies of third degree burn patients on 3T3 fibroblast feeders and successfully implanted [76]. Despite the presence of xenogeneic material, the use of lethally irradiated murine fibroblasts as feeder cells is still considered the gold standard for the production of dermal grafts due to their extensive promotion of keratinocyte proliferation. Of note, the FDA-approved product Epicel is manufactured with this protocol, while other marketed products such as Apligraf® and GINTUIT™ are based on static monolayer cultivation of allogenic keratinocytes but do not explicitly disclose the use of feeder cells. The cultivation of epithelial progenitors requires approximately from one to three weeks depending on the quality of the donor material and the extension of the burned area [77]. Cultured skin grafts can also be applied for rare genetic diseases in combination with DNA editing techniques. For example, genetically modified autologous keratinocytes cultured on

feeder layers have been recently used to regenerate a functional epidermis on a single patient with junctional epidermolysis bullosa (JEB) [78].

Corneal Replacements

Epithelial stem cells are also present in the limbus, located at the border between the cornea and the sclera [79]. These stem cells are capable of forming long-term self-renewing holoclone-colonies and are responsible for the continuous regeneration of the transparent and non-vascularized corneal epithelium. Chemical or physical burns can disrupt this process and cause corneal opacity and loss of vision due to the invasion of bulbar conjunctival cells [80]. This condition can be treated by transplanting cultured limbal tissue grafts. Currently, the only approved CTP for corneal replacement is Holoclar®, regulated as Advanced Therapy Medicinal Product (ATMP) in Europe. Similarly to skin grafts, Holoclar® is manufactured staring from autologous limbal stem cells, which are expanded on irradiated mouse 3T3 feeder cells on circular fibrin substrates [81]. Comparable procedures have been followed in several other clinical trials for limbal deficiencies, reviewed extensively by Baylis et al. [82]. Usually, the expansion of limbal stem cells for graft production does not exceed 20 days since the graft dimension is fairly small (maximum 7 cm^2) [82].

2.4.2 Expansion Processes for Hematopoietic Progenitors and Immune System Cells

Hematopoietic and immune system cells are widely used in clinical trials for hematopoietic reconstitution, cancer treatment and cancer vaccine development. These cells are usually capable of survival and proliferation in suspension and are often used in combination with gene editing techniques to provide novel functionalities or restore genetic defects. The dosages vary significantly among the cell type and the disease area targeted. Hematopoietic progenitor cells and CAR-T cells are known to expand highly *in vivo*, and are therefore infused at around 10^6 cells/kg. Tumor infiltrating lymphocytes and natural killer cells must on the other hand be infused at much higher dosages to show clinical efficacy. These cells have been mostly expanded using static systems like Teflon bags, TC flasks and gas-permeable flasks, but are rapidly transitioning towards more scalable, and closely monitored bioreactor systems.

Hematopoietic Progenitor Cells

Long-term repopulating hematopoietic stem cells (HSCs) give rise to all mature blood cell types and are the only cells capable of regenerating a fully functional hematopoietic system for the entire lifespan of an organism. Although the first HSC transplant dates back to the 1940s, its clinical application became widespread only after the discovery of the human leucocyte antigen (HLA) histocompatibility system in the 1970s [16]. Nowadays, HSC transplantation represents the only possible cure for several hematopoietic malignancies, with autologous treatments being slightly more common than the allogeneic counterpart (approximately 58% of the total transplantations done in Europe in 2014) [83]. HLA matching is one of the main limitations for allogeneic BM transplant, with 30% to 40% of patients excluded from therapy due to the lack of donors [84]. HLA matching is less restricted for CB-derived HSCs, thereby extending the availability of HSC transplantation to a higher portion of the population [85]. Several clinical studies have indicated cell dosage as a critical parameter for successful engraftment, recommending a minimum threshold of $2 - 3 \cdot 10^7$ nucleated cells/kg or, alternatively, $3 - 4 \cdot 10^6$ CD34+ cells/kg [86, 87]. Unfortunately, the number of HSCs in CB immediately after harvesting is limited and sufficient only for pediatric patients, and multiple HLA-matches cords are needed to treat adults [14]. To address this challenge, several studies have focused on developing strategies for expanding CB-derived HSCs *ex vivo* [23, 88–91]. The expansion of undifferentiated HSCs has proved to be a difficult task, since the self-renewal capacity of HSCs *in vitro* is severely limited by the secretion of inhibitory feedback signals, leading to the production of differentiated cells with limited regenerative potential *in vivo* [23]. High throughput screenings of chemical compounds have identified several agonists of HSCs self-renewal. Small molecules such as SR-1 and UM171, recently discovered nicotine derivatives, are now being used in clinical trials in addition to more standard cytokines, including SCF, THPO, SF-O3, G-CSF, Flt3L, IL-3,IL-6, reviewed in [92].

The expansion of UCB products used in clinical trials lasts on average 14 to 21 days and has mainly been performed using culture bags [89, 90] and TC Flasks in presence of Notch ligands [93] or MSCs (de Lima et al., 2012). Although most of the published strategies rely on standard passaging procedures with complete medium exchanges every 4-7 days, Csaszar et al. reported the use of an elegant fed-batch strategy, where the dilution caused by media addition is used to decrease the effect of endogenously-

produced factors [23]. Overall, the use of expanded CB-derived cells appears to be safe and accelerates initial hematopoietic engraftment, possibly due to the higher cell dosage used, but larger randomized clinical trials are needed [87]. Although not in the focus of this review due to the lack of expansion steps, it is worth mentioning that HSCs can also be genetically modified to treat congenital defects such as immune deficiencies, anemias and metabolic diseases. The benefits for gene therapies targeting stem cells are long lasting and a single treatment is usually sufficient. Up to now, only one stem cell-based gene therapy has been approved (Strimvelis, GSK) for the treatment of ADA-deficient patients.

2.4.3 T Lymphocytes

T cells are now widely recognized as a new class of therapeutic agents to cure B cell malignancies, with the noteworthy approval of two CD19 CAR-T cell therapies, and hold great promise for the treatment of other advanced therapy-resistant tumors [94]. Three main forms of adoptive cell therapy (ACT) using T lymphocytes are currently being developed and tested in clinical trials. In a first approach, tumor infiltrating lymphocytes (TIL) are surgically extracted from tumor biopsies, expanded *ex vivo* to clinically suitable numbers and re-infused to the patient. While TIL therapy relies on tumor recognition by the purified lymphocytes to be effective, T cell receptor (TCR) engineered T cells and chimeric antigen receptor (CAR) T cells rely on synthetic biology techniques to change their properties and improve their function by targeting novel epitopes present on tumor cells.

Tumor Infiltrating Lymphocytes

TIL therapy is based on the isolation of autologous lymphocytes from dissected mm-sized tumor fragments. These lymphocytes are first selected for high tumor recognition and subsequently expanded to clinically relevant numbers by serial passaging before reinfusion [43]. This strategy has been initially employed with remarkable success for metastatic melanomas, and is now being tested for ovarian, kidney, head and neck cancers together in conjunction with lymphodepletion. In the case of TIL therapy, cell dosage strongly correlates with tumor regression, with infusion of more cells correlating with objective response rate (ORR) in animal models and clinical trials [21]. The optimal dosage of TILs varies upon tumor type and stage but is generally very high

(10^{10-11} cells), leading to long culture times, usually ranging from four to eight weeks. TIL manufacturing is conventionally divided in two parts. The first part involves the isolation and selection of tumor-reactive lymphocytes from tumor fragments. This step is usually achieved by *ex vivo* co-culture of TILs with tumor cells in multiwell plates in presence of high doses of IL-2 (>1000 U/mL) and selection of the most reactive TIL populations [95]. The second part of TIL bioprocessing is usually referred to as Rapid Expansion Protocol (REP) and is used to produce the high number of cells needed for ACT [96]. The vast majority of REPs for TIL relies on the use of irradiated feeder cells in presence of IL-2 and anti-CD3 antibodies to activate the cells in absence of tumor-specific antigens. Irradiated PBMCs have for long been the main choice for TIL expansion [97–99], but are now being replaced by GMP-compliant cell lines such as K562 cells in order to reduce variability in the process [96]. Earlier studies reported the use of TC flasks and static culture bags in the REP combined with repeated passaging [43, 95, 97]. These types of equipment are now less and less used for TIL cultivation due to the numerous containers needed to reach the required cell doses, the lack of automation and the risk of contamination due to the open nature of the system. Alternatively, hollow fiber [100, 101] and more recently WAVE bioreactors [102–104] have been implemented in the REP due to their larger volumes, reduction of cell handling and possibility to automate feeding procedures. The G-REX system also represents a promising system for TIL expansion due to its simplicity and the possibility to easily accommodate the use of feeder cells [42, 105].

Genetically Modified Lymphocytes

Tumor recognition in TIL therapy depends on the endogenous TCR expressed on the infused cells [106]. Gene transfer technologies have gained a lot of interest to develop synthetic receptors to provide lymphocytes novel functionalities and specificities. The two main strategies followed in this respect involve the transfection of synthetic TCRs or chimeric receptors (CARs). Compared to synthetic TCRs, CARs eliminate the need of major histocompatibility complex (MHC) restriction and provide more affinity towards the chosen antigen, although they tend to produce a more severe cytokine release syndrome [107]. Most of engineered T cells manufacturing reported is based on autologous cells and focuses on hematopoietic tumors. Compared to TIL therapy, the reported CAR-T cell dosage is significantly lower, with a median of $1.5 \cdot 10^8$ cells infused for

fixed-dose treatments [108]. This reduction in cell dosage is mainly due to their use for easily accessible liquid tumors and the possibility of CAR T cells to expand *in vivo* more than 1000-fold after infusion [109]. For this reason, the expansion process for CAR-T cells only lasts maximum 14 days and can fit in a 20-25 days manufacturing schedule which also includes apheresis, gene delivery, formulation, cryopreservation and shipping [110]. Prior to expansion, CAR- and TCR-engineered T cells are activated and subjected to gene delivery. Activation methods mostly rely on the use of anti-CD3 antibodies and anti-CD3/CD28 coated beads, with some authors reporting the use of tetramers and artificial antigen presenting cells [111].

Similar to TIL manufacturing, the main expansion systems for CAR-T cells are T flasks, Teflon bags, gas-permeable systems [112, 113] and Rocking Motion bioreactors in continuous perfusion operating mode [114, 115], with the latter representing the current system of choice for clinical expansion [96]. Fully-integrated closed systems are also being developed for CAR-T manufacturing. For example, the CliniMACS Prodigy (Miltenyi Biotec, Germany) system is capable of performing all CAR-T manufacturing steps from fractionation of the starting material to formulation in a single platform in an automated fashion [116].

Regulatory T Cells

Regulatory T cells (T_{reg}) are immunosuppressive lymphocytes, which modulate the effector T cells response through cell-cell interactions and paracrine factors [117]. Clinical studies involving T_{reg} are mostly focused on the treatment of autoimmune diseases such as type-1 diabetes and multiple sclerosis, solid organ transplantation, graft-versus-host disease (GVHD) and Crohn's disease [118]. T_{reg} are present in peripheral and cord blood at very low frequencies (1-5% of circulating CD4+ cells), and an *ex vivo* expansion step is required to achieve sufficient regulatory to effector ratios [119]. Based on mouse models, the effective dose of polyclonal T_{regs} to prevent graft rejections or autoimmunity should be higher than 10^{10} cells [120]. On the other hand, the number of infused cells reported in literature is much lower, typically in the order of 10^5-10^7 cells, and only rarely exceeding 10^9 cells [117], mostly due to insufficient expansion rates *in vitro* of the cells and loss of function upon extended cultivation. The duration of the expansion step for T_{reg}-based trials ranges from one to three weeks. The reference protocol for T_{reg} culture involves the use of CD3/CD28 beads for activation together with

IL-2 and rapamycin for effector T cells depletion [121]. Contrary to other lymphocyte populations, where automated systems are starting to emerge as reference platforms, T_reg culture is to date carried out almost exclusively in TC Flasks and static plastic bags [122] or, to a lower extent, gas-permeable systems [123]. Although the translation to closed GMP-compliant systems is an important factor, most of the research is still focused on finding the best protocols in order to provide consistent T_{reg} expansion, both in terms of medium additives such as Rapamycin, Retinoic Acid, histone deacetylase and DNA methyltransferase inhibitors [124] and antigen presenting cells [125].

Natural Killer Cells

Natural Killer (NK) cells are innate lymphoid cells capable of mediating cytotoxicity against stressed cells such as tumors or viral-infected cells. Unlike other lymphocytes, NK activity does not require prior activation and does not rely on antigen presentation by MHC molecules, but is regulated by a tight balance between activating and inhibitory signals delivered on their surface [126]. Since NK cells do not rely on TCR recognition, they lack the potential to develop GVHD when used in an allogeneic setting, making NK cells a promising off-the-shelf therapy for cancer treatment [127]. The use of NK cells in the clinics has proven to be safe in both autologous and allogeneic settings, although the efficacy and *in vivo* persistence and efficacy was limited [127]. In case of autologous therapies, there is no consensus concerning the ideal dose for tumor relapse, although the use of higher cell doses is usually preferred, posing several issues concerning their manufacturing [128]. Early clinical trials involved the use of NK cells cultured only in the presence of cytokines (IL-2 and IL-15), resulting in low expansion rates compared to protocols involving the use of feeder cells. In this case, the expansion has been mainly carried out using stating systems such as multiwell plates, TC Flasks and gas-permeable systems [129]. For feeder-free conditions, wave bioreactors with adjusted feeding strategies have also been employed, resulting in total yields in the order of 10^{10} cells per run [130, 131]. To overcome many of the limitations posed by autologous and allogeneic therapies, immortalized NK-92 cells are being tested in the clinic as off-the shelf therapy for acute leukemic malignancies. NK-92 cells are capable of extensive replication *in vitro* in presence of soluble IL-2, providing more robustness and reproducibility in manufacturing. They have now been processed in GMP conditions using G-Rex systems with a median expansion time of 24 days to produce doses

of $1 - 3 \cdot 10^9$ cells/m^2 [132].

Dendritic Cells

Dendritic cells (DCs) are antigen-presenting cells (APCs) and function as initiators and modulators of the immune response (Banchereau and Steinman, 1998). DCs are used in immunotherapy as cancer vaccines to prevent a wide range of tumors, especially melanomas, prostate cancer, gliomas and renal cell cancers [133]. The therapeutic mechanism of cancer vaccines is based on the infusion of antigen-pulsed DCs, with the aim to expand existing tumor-specific cytotoxic lymphocytes to reduce the tumor mass and induce immunological memory [134]. Excluding the approaches that target DCs *in vivo*, which are beyond the scope of this review, *ex vivo* generation of DC cancer vaccines has been performed following two main routes. The first one is based on the isolation of circulated DCs by leukapheresis, followed by maturation, activation, antigen loading in specific cytokine cocktails and reinfusion back into the patient, where DCs migrate to lymphoid tissues [135]. Given the low frequency of circulating DCs, a more common approach for DC-based vaccines involves the generation of DCs form peripheral blood monocytes or hematopoietic progenitor cells after *in vitro* differentiation in presence of maturation factors [136]. This approach is used in the FDA-approved drug Provenge® (Sipuleucel-T). Provenge contains a mixture of PBMCs (including DCs), which are activated *ex vivo* in presence of a fusion protein consisting of granulocyte–macrophage colony-stimulating factor (GM-CSF) and prostatic acid phosphatase as tumor-associated antigen [137]. In this case, the cultivation time for the production of DC-based vaccines is significantly lower compared to other immune system cells due to the lack of a real expansion step and its substitution by differentiation and maturation, resulting in three to seven days cultures being the industrial standard [138].

2.4.4 Expansion Processes for High-Dosage Cell-Based Therapies

It is expected that high cell numbers ($> 10^{10}$) will be needed to promote regenerative processes of tissues and organs where the native population is either severely damaged or completely missing. The clinical translation of these CTPs is expected to be a major development in cell therapy and regenerative medicine, but current investigations are limited to smaller tissue grafts. For example, pluripotent stem cells derived cardiomyocytes have been administered at a very conservative mean dose of $8.2 \cdot 10^6$ cells

for ischemic left ventricular dysfunction to prove the safety of the treatment [139], although animal models suggested the use of more than $7 \cdot 10^8$ cells to restore function in infarcted hearts [140]. Manufacturing of these CTPs will most likely base their expansion protocols on scalable bioreactor technologies that can be integrated with the use of microcarriers in case of adherent cells.

Mesenchymal Stromal Cells

The concept of Mesenchymal Stromal Cells (MSCs) identifies a population of adherent cells with fibroblast-like morphology isolated from BM, adipose tissue (AT) and several other tissues [141]. Despite the efforts to define a standard set of criteria to identify MSCs [142], questions about their true identity [141, 143], stem cell nature and heterogeneity [144] still remain. Additionally, putative MSCs derived from different tissues are characterized by different marker expression, proliferation and differentiation potential [145]. Nevertheless, MSCs are the second most common cell type after hematopoietic cells for number of active clinical trials. MSCs are proposed to elicit their therapeutic efficacy through several mechanisms such as differentiation into distinct lineages (mainly adipose tissue, cartilage and bone), immunomodulatory properties, secretion of survival paracrine factors and homing to the sites of inflammation [146], and MSC transplantation has proved to be safe and tolerated even in allogeneic settings. These properties have made MSCs an attractive therapeutic modality for the treatment of several disease areas, including immune diseases, bone and cartilage reconstruction, myocardial injury and several others, as reviewed in [146, 147]. Interestingly, the majority of the clinical trials are currently carried out with allogenic cells [147], while all other somatic-cell based therapies favor the use of patient-derived material. Common dosages of MSCs range from $0.5 - 5 \cdot 10^6$ cells/kg, although up to $5 \cdot 10^7$ cells/kg cells can be infused without harm [148]. Manufacturing of MSCs depends on the source, isolation and culture protocols in terms of medium and setup. The process starts with the isolation of the stromal cells population from primary tissue biopsies. Although tissue processing is highly source-specific, the vast majority of MSC purification protocols relies on plastic adherence to exclude hematopoietic and other weakly adherent cells regardless of the tissue source. MSCs grow as anchorage dependent cells until confluency, and the final product yield is determined by the culture area occupied. The typical planar flask culture is still extensively used in clinical trials [149] and in commercial manufac-

turing of MSCs for GVHD [150]. On the other hand, the safety profile of allogeneic MSCs, together with their high *ex vivo* proliferative potential, prompted the interest of several research groups in developing scale-up strategies and devices for the expansion and manufacturing MSC-based off-the shelf products. In this respect, bioreactor technologies are gaining increased interest for clinical manufacturing of MSC-based therapies. Although some authors reported successful expansion of MSCs in fixed bed reactors based on hollow fibres [151] or packed beds [152], microcarrier cultivation in suspension systems is the most widely adopted technology for large-scale expansion of MSCs [59]. Microcarrier cultivation of MSCs has been performed in various stirred system and across different scales, ranging from the few mL of Ambr® bioreactors [153] to 50 L single use bioreactors [154] and, to a far lesser extent, rocking systems [155]. Typical cell densities achieved for microcarrier-based processes range from 0.5 to $2 \cdot 10^6$ cells/ml, therefore culture systems with working volumes in the range of 0.5 to 2 L are sufficient to produce the number of cells needed for clinically relevant doses. Perfusion for MSC microcarrier cultures has been mostly performed with batch-exchange strategies, where agitation is stopped to induce sedimentation of the beads, allowing the medium to be removed without loss of viable cells in the process. Alternatively, cell retention systems based on meshes can be employed, allowing for continuous perfusion to be implemented [63]. Fed-Batch like feeding strategies have also been investigated, resulting in improved medium utilization [156].

Pluripotent Stem Cells

Pluripotent stem cells (PSCs) are self-renewing stem cells with intrinsic differentiation potential for all adult somatic and germ cells (De Los Angeles et al., 2015). Although pluripotency *in vivo* is restricted only to the cells in the epiblast during the early stage of embryonic development, PSCs represent a stable state that can be established *in vitro* and maintained indefinitely [157]. PSCs can be derived from the inner cell mass of the blastocyst or from somatic cells that are induced in a stable pluripotent state either via somatic nuclear cell transfer (SNCT) or through transfection of specific transcription factors (iPSCs). Despite potential issues concerning these genetic reprogramming methods, the use of iPSCs in cell therapy has several advantages with respect to other pluripotent stem cells, as they do not involve destruction of embryos and do not require immune suppression after transplantation when derived from the patient itself. Moreover, gen-

eration and banking of iPSC from donors who are mono-allelic at their HLA loci could lead to the generation of semi-universal cell lines, which are tolerated by the immune system of large portions of population. When placed in culture, PSCs are able to maintain and undifferentiated phenotype in presence of basic fibroblast growth factor (FGF2) and transforming growth factor beta (TGF-β) or other cytokine combination [158]. Under these conditions, PSCs are characterized by an unlimited proliferative potential and the possibility to generate any somatic cell type, making their use extremely promising in cell therapy and regenerative medicine, especially for tissues where stem cells have not been identified or are extremely difficult to expand [17]. Human PSCs are adherent cells and grow as flat colonies on TC flasks when in presence of feeder cells, Matrigel® or other natural and synthetic substrates, and are routinely passaged chemically or enzymatically [159]. Although this strategy is sufficient for the production of small tissue grafts for age related macular degeneration [160], several attempts have been reported in literature to scale up the PSC expansion process to provide higher cell yields. The development of such processes would enable the translation of PSC-derived product to a clinical application in ischemic heart disease, amyotrophic lateral sclerosis, diabetes and other replacement therapies [161]. Similarly to MSCs, large-scale PSC expansion has transitioned to 3D suspension systems rather than scaling out planar systems, and thoroughly optimized with respect to important process conditions such as oxygen tension, feeding rates, agitation and inoculation density [55]. Suspension culture of PSCs has been initially performed using microcarriers in combination with spinner flasks and stirred tank bioreactors, resulting in similar expansion rates when compared to planar cultures, reviewed extensively by Adil & Schaffer [162]. However, the use of microcarriers necessitates optimization of cell adhesion and the implementation of harvesting procedures for cell detachment, which result in significant loss of yield and viability due to the sensitivity of PSCs to single-cell dissociation [163]. A more promising culture format for PSC expansion in suspension is based on the formation of small floating clusters of cells. PSCs cultured as aggregates can maintain their phenotype and their karyotype over several months [164], and have been successfully expanded in both spinner flasks and bioreactors at laboratory scale [162], achieving peak cell densities above 10^6 cells/mL [61]. For this culture method, the aggregate size represents a critical process parameter and must be tightly controlled to avoid unwanted differentiation or apoptosis due to mass transfer limitations for the innermost cells [165]. In this respect, microencapsulation techniques have been devised to prevent fusion of aggregates and reduce

the mechanical effects of shear on cultured PSCs, although they still require the implementation of harvesting steps to separate the cell from exogenous materials and increase the complexity of the entire system. While academic researchers are investigating the use of suspension systems, clinical translation of PSC-derived products is still relying on conventional planar cultures. Retinal pigment epithelium (RPE) cells derived from autologous PSCs are being tested in phase I and II clinical trials for macular degeneration. Starting from certified cell banks, PSCs are usually passaged and differentiated in TC flasks either spontaneously and then manyally dissected [166] or with the addition of exogenous factors [160]. PSC-derived cardiovascular progenitors have been tested for the treatment of ischemic heart disease in a phase I clinical trial (NCT02057900). The manufacturing process starts from a master cell banks and consists of two passages on feeder layers followed by a four days differentiation step to induce the desired phenotype of cells, which are then delivered within a fibrin patch. The product PEC-01 (ViaCyte, United States), consisting of allogeneic PSC-derived β-cell progenitors for the treatment of T1D is manufactured by expanding cGMP compliant PSCs for 15 days in TC flasks and then in a multitray system. Subsequently, the cells are aggregated and differentiated in a four-stage protocol using roller bottles. The product is then frozen, formulated and loaded in flat capsules to prevent immune rejection. The entire manufacturing process takes up to 20 days and has been reported to produce up to 10^{10} cells in a clean room environment [167].

2.5 Current Challenges and Future Directions

The clinical translation and commercialization of cell therapies faces several challenges connected to their manufacturing, as well as regulatory, logistic and economic aspects, which are unprecedented in the pharmaceutical industry. Within the complex manufacturing scheme of CTPs, the implementation of at least one expansion step is mandatory in the vast majority of the therapies to achieve clinically relevant numbers for the cell population of interest. On the other hand, cell expansion is widely regarded to as one of the main bottlenecks for CTP manufacturing. For example, 9% of the enrolled patients for the Kymriah™ pivotal trial were not treated due to the failures in producing sufficient number of cells [168]. Moreover, the number of cells infused per dose in all the approved therapies is relatively low, ranging from 10^5 cells per dose for small grafts to 10^9 T cells for CAR-T therapies (Table 2.1), which reflects the fact that the development

of CTPs with dosages higher than 10^9 cells/dose is still facing technological and/or biological challenges. The difficulties in the expansion of therapeutic cells are manifold and directly connected to their level of complexity. Compared to biological drug manufacturing, where sequential selection procedures are used to screen the most promising clones in terms of growth, productivity and product quality for a given platform, therapeutic cells are characterized by a significant intrinsic variability that deeply affects the consistency and reproducibility of the entire manufacturing process. This variability is often accompanied with the possibility for the cells of interest to undergo rapid aging upon prolonged expansion, progressively increasing their doubling time. In this respect, a deeper characterization of the starting material, together with the development of model-based processes that can compensate patient- and time-specific differences in terms of growth and phenotype could significantly accelerate the development of novel therapies. The expansion step must not only be designed with the aim of maximizing the final yield, but optimal operating conditions must be defined to ensure the obtainment of cells that match the desired quality target product profile in terms of viability, identity and potency [10]. Although not in the focus of this review, there are several safety aspects that need to be carefully assessed during CTP production, since extensive cell divisions *in vitro* are often associated with loss of function [169], senescence and alterations in phenotypes of the cultured cell population [170]. Long cultivation times are also correlated with increased risks of the acquisition of mutations and epigenetic or chromosomal instabilities, possibly resulting in malignant or tumorigenic transformations. It has recently been shown in the phase I trial for B cell leukaemia using CAR-T cells (NCT01626495) that the infusion of one single aberrant cell can result in the death of the patient [171]. Ultimately, process development in CTP production should also incorporate economic considerations to prevent the commercialization of overly expensive therapies, which can cause marketing failures due to the impossibility to access reimbursements [172].

Until recently, most of the technologies used for therapeutic cell expansion result from a direct translation of the platforms implemented in the biotech industry. While the transfer of this expertise can provide several benefits to allogeneic therapies, which follow a similar manufacturing scheme as biologics, the success of autologous therapies is likely to depend on the development of novel, tailored technologies. In this context, there is a need for closed single-use systems that can provide flexibility to accommodate for patient-specific differences in cell number and phenotype, integrate on-line process

analytical technology (PAT) and combine multiple unit operations to reduce the operator workload. Innovative all-in-one systems for manufacturing of cell-based therapies as the Cocoon™ (Octane Biotech, Canada) and CliniMACS Prodigy (Miltenyi Biotec, Germany) can integrate the entire processing described in Fig. 1 from cell isolation to formulation, providing the possibility of automated end-to end manufacturing of CTPs in a closed environment [34, 116]. Although their use is still limited and their impact in clinical trials is still to be assessed, they could promote the transition towards a decentralized model for the manufacturing of autologous therapies. Lastly, process intensification strategies involving the use of mathematical models and on-line analytical technologies, together with the implementation of more sophisticated operation modes such as continuous perfusion, could provide several benefits in improving the yield and controllability of both autologous and allogeneic CTP manufacturing.

Conclusion

Together with a deeper understanding of the biology and the therapeutic mechanisms of cells, the clinical translation and commercial success of cell-based therapies depends on further developments of reliable and scalable technologies for cell manipulation and expansion. Up until now, the efforts in the development of cell-based therapies, especially in academic institutions, have been mostly directed towards the product and its efficacy, without thoroughly considering the importance of the production process itself. This review discussed the strategies behind the expansion processes that are currently carried out to allow the clinical translation of cell-based therapies, highlighting the need for the development and optimization of novel technologies and processes for scalable and resource-efficient industrial manufacturing. From a process engineering perspective, it is likely that this need will drive the development of novel platforms based on automation and PAT for the autologous setting, while allogeneic therapies will require a transition from laboratory-scale cultures to large-scale systems to fully benefit from the economies of scale. Further steps in these directions will align the manufacturing of therapeutic cells to the production schemes of already established drug classes and will serve as the basis for the commercialization of safe and cost-effective cell therapies.

Chapter 3

Continuous Expansion of Human Induced Pluripotent Stem Cells in Perfusion Stirred Tank Bioreactors with Shear-Controlled Aggregate Size

3.1 Introduction

The potential to generate almost every adult cell type, coupled with the possibility for unlimited *in vitro* expansion, makes PSCs an extremely valuable platform for cell therapies and regenerative medicine, especially for tissues and organs where stem cells are either undiscovered or difficult to expand [17, 147]. In this context, a successful clinical translation of PSC-derived cell therapy products requires the development of scalable, robust and resource-efficient expansion processes [24]. Human PSCs are anchorage dependent cells that have routinely been expanded on two-dimensional culture systems in combination with either chemical or enzymatic passaging procedures [173]. The transition to scalable low-footprint suspension-based systems was initially demonstrated in several articles with the use of microcarriers (MCs) [174–178]. Despite the significant increase in surface area provided compared to planar culture systems and remarkable developments in chemically defined and fully synthetic coatings [159], MC-based systems require the implementation of additional downstream processing steps for cell detachment and MC removal, which are often responsible for a reduced yield as well as increased complexity and cost of the entire process [162]. Recent reports have highlighted the possibility for human PSCs to survive and expand in suspension for prolonged periods of time as floating clusters without the need for feeder cells or exogenous substrates [179, 180]. This strategy bypasses the need for external substrates and allows a direct integration of the expansion and differentiation steps by simply switching the medium composition [181]. Thanks to these advantages, suspension cultures of PSC aggregates have been increasingly used for the expansion of human PSCs at laboratory scale, in combination with Erlenmeyer flasks [164], spinner flasks [182, 183], and stirred tank bioreactors [184–187]. For this type of processes, the size of PSC aggregates represents a critical process parameter since it directly determines important product quality attributes such as cell viability [54] and growth rate [188], while playing an important role in influencing possible differentiation trajectories [189]. Preventing PSC aggregates to exceed a critical diameter represents one of the main technical challenges in PSC expansion. This critical value has been estimated to be around 250-350 μm to prevent mass transfer limitations for the innermost cells [54] or undesired reductions in pluripotency markers expression [188]. Until now, the main strategies to control the size of PSC aggregates involve the use of manual enzymatic or mechanical procedures, usually implemented through serial interruptions of the culture. Enzymatic strategies are based

on prolonged incubation with proteases [182, 190–193], which trigger cell dissociation through the cleavage of cell-cell and cell-extracellular matrix (ECM) interactions, and are often associated with low viable cell recovery efficiency due to the sensitivity of human PSCs for single-cell dissociation [163, 194]. Contrarily, mechanical methods cause the physical disruption of aggregates into smaller clumps through the use of meshes [184, 195], microfluidic devices [196] or prolonged pipetting [180, 197]. These manual procedures are labor intensive, inefficient, difficult to scale up and require the use of open systems. We report the development of a scalable stirred tank-based system for human PSC expansion, which implements a continuous on-line aggregate breakup strategy based on extensional flow through a contracting nozzle located in the perfusion loop. The exposure to well-defined pulses of hydrodynamic shear stress causes a continuous breakage of the biggest aggregates into smaller clumps without significantly affecting cell viability, maintaining a steady-state aggregate size distribution throughout the entire culture.

3.2 Experimental

3.2.1 Cell Culture

The following iPSC cell lines were used: cord blood CD34+ cells derived Gibco Human Episomal iPSC line (hereby themed hiPSC Line 1) (ThermoFisher, USA) and skin tissue-derived human induced pluripotent stem cells (hiPSCs) HPSI113i-podx_1 and HPSI1213i-xuja_2 (hereby themed hiPSC Line 2 and 3) (HipSci, UK). All cell lines were routinely cultivated on vitronectin-coated flasks at 37 °C, and 5% CO2 in a humidified incubator using StemFlex Medium (ThermoFisher). Upon reaching 80% confluency, cells were passaged using 50 mM EDTA according to previously described procedures (Beers et al., 2012). Single spheroids were cultivated in 96 ultra-low attachment plates (Corning, USA) in the same media and under the same environmental conditions.

3.2.2 Perfusion Bioreactor Design and Operation

The bioreactor design used is based on 1L DASGIP® bioreactor systems with flat bottom (Eppendorf AG, Switzerland). The cells were cultured at 37 °C, 15% dissolved

oxygen tension (DOT) and 7.2 pH. Oxygen and pH levels were maintained by controlling the fractional composition of O_2, N_2 and CO_2 in the inlet gas flow. Gas supply was performed through overhead aeration at a constant flow rate of 10 L/h (0.16 vvm), while mixing was ensured by a single 4.5 cm diameter 6-blade Rushton impeller. The stirring rate was kept constant at 120 rpm unless stated otherwise. Aggregate retention was performed using a single ATF2-MC screen filter module (Repligen, US), located inside a stainless-steel chamber mounted on top of the bioreactor. Media circulation between the culture vessel and the screen module was regulated by a diaphragm pump (Repligen), which periodically alternates the flow direction within the perfusion loop. The two units were connected with a stainless still tube of 1 cm inner diameter. Cells were inoculated at a nominal viable cell density (VCD) of $0.1 \cdot 10^6$ cells/mL in form of small clumps, obtained by EDTA passaging of human PSCs expanded in T flasks and cultivated in the same medium. The initial culture volume was 500 mL. Two days after inoculation the volume was increased to 1L and perfusion was initiated and maintained at 0.5 reactor volumes per day throughout the entire culture through the action of peristaltic pumps. The cultivation volume was kept constant by gravimetric measurements of the waste and fresh media bottles.

3.2.3 Shear Stress Calculation and Nozzle Design

The flow in the bioreactor and in the external perfusion loop were turbulent for all conditions tested (Table 3.1 and Table 3.2). The average impeller shear stress $\langle\tau\rangle$ (Pa) in the bioreactor was estimated from the volume average dissipation rate $\langle\epsilon\rangle$ (m^2s^{-3}) according to Equations 3.1 and 3.2 [198]:

$$\langle\tau\rangle = \sqrt{\mu\rho\langle\epsilon\rangle} \tag{3.1}$$

with

$$\langle\epsilon\rangle = \frac{N_p d_i^5 N^3}{V} \tag{3.2}$$

Where N_p is the impeller power number, assumed equal to 5 [199], d_i is the diameter of the impeller (m), N is the impeller rotation speed (s^{-1}) and V is the bioreactor volume (L), while ρ and μ indicate the density and the dynamic viscosity of the medium at 37 °C. For simplicity, the medium was assumed to have the same physical properties as pure water. The shear stress in the dip tube, which connects the culture vessel to the

cell retention device, was estimated from the data of Karst et. al [200]. To expose the cells to well defined, high levels of hydrodynamic shear stress, we connected a contracting nozzle with circular section at the liquid-submerged end of the dip tube. The nozzle design and dimensions are based on previous reports [201]. The shear intensity was modulated by varying either the nozzle internal diameter or the flow rate within the perfusion loop generated by the diaphragm pump. The magnitude of the maximum hydrodynamic shear stress generated was estimated through computational fluid dynamics (CFD) simulations as a function of both flow rate and internal nozzle diameter [201] and reported in Table 3.2.

3.2.4 Analytics

Offline Measurements

Cell density and viability were measured via trypan blue exclusion (Cedex HiRes, Roche Diagnostics, Switzerland) after enzymatic dissociation of the aggregates into single cells using TrypLE Select (Gibco). The aggregate diameter was determined by light microscopy imaging (Leica DM IL LED, Leica Microsystems, Germany) of freshly sampled aggregates combined with image analysis (ImageJ, NIH, USA).

Flow Cytometry

Cells from aggregates were dissociated with vigorous pipetting in 0.5 mM EDTA in PBS and washed with PBS +2% fetal bovine serum (FBS, Gibco, USA) as blocking buffer. Single-cell suspensions were stained with primary antibodies on ice for 30 min and analyzed on LSRFortessa (BD Bioscience, US). Sytox Blue (Thermofisher) was used as viability dye. Data analysis was performed on FlowJo (Tree Star, US). The following antibodies (purchased from BioLegend, US) were used: APC-conjugated mouse anti-human TRA-1-81, FITC -conjugated mouse anti-human TRA-1-60, PerCP-CY5.5-conjugated mouse anti human SSEA-4, PE-conjugated rat anti-human SSEA-3.

Immunocytochemistry

For pluripotency staining, PSC aggregates were harvested from the bioreactor, washed twice with PBS and fixed in 4% (v/v) paraformaldehyde in PBS for 30 min at room temperature. After permeabilization in 0.1% Triton X-100 in PBS for 30 min and block-

Table 3.1: Hydrodynamic shear stress values caused by impeller agitation estimated by using Eq. 3.1

Agitation rate (rpm)	Volume (mL)	$Re_{Impeller}$ (-)	$\langle\tau\rangle$ (Pa)
100	500	4850	0.004
200	500	9700	0.011
300	500	14550	0.018
400	500	19400	0.026

ing with 0.2% bovine serum albumin (BSA) in PBS, the aggregates were incubated overnight at 4°C with primary antibodies under shaking. After washing with PBS + 0.2% BSA, the aggregates were incubated overnight with the secondary antibody and for 4h in DAPI (Molecular Probes, USA). All images were acquired using a Leica SP8-AOBS confocal microscope. The following antibodies were used at 1:200 dilution: Polyclonal Antibody to Octamer Binding Transcription Factor 4 (OCT4) (Cloud-Clone, US), Purified anti-SOX2 Antibody (Biolegend), Anti-Human Nanog (Peprotech, US), Goat Anti-Rabbit Alexa Fluor 488 conjugate Antibody (MerckMillipore, Germany).

3.3 Results

Effect of Impeller Agitation on Human PSC Aggregate Size in Benchtop Bioreactors

PSC aggregation is a fast and spontaneous process, governed by homotypic interactions of various cell adhesion molecules [202], which allows PSC cultivation in suspension by preventing dissociation-induced apoptosis [163]. With the goal of designing a suspension-based process capable of expanding undifferentiated human PSCs while controlling the aggregate size below the critical threshold of 300 μm through the use of hydrodynamic shear stress, we first assessed the impact of the shear forces generated by the impeller rotation of benchtop stirred tank bioreactors in terms of aggregate size distribution and growth rate of PSCs. PSCs were inoculated as small aggregates (<200 μm) in stirred tank bioreactors and cultivated for 8 days in perfusion under different agitation rates. To isolate the effect of the fluidic shear forces generated by the impeller, perfusion was performed by incorporating a 30 μm mesh filter as cell retention device in a similar fashion as other reports [61, 203] (Figure B.1). Agitation rates ranging from

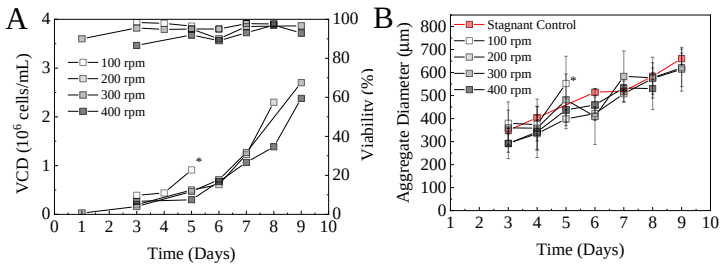

Figure 3.1: Viable cell density (A) and mean aggregate size (B) evolution of human PSCs cultured in perfusion under different impeller agitation speed. All cultures were performed using cell line 1.

100 to 400 rpm did not significantly affect the growth rate of the cells (Figure 3.1 A) nor the aggregate size distribution of PSCs (Figure 3.1 B), which continuously increased throughout the entire duration of the cultivation, reaching mean values above 600 μm after one week of culture. Of note, agitation at the slowest speed resulted in the formation of mm-sized clusters, most likely trough the fusion of multiple aggregates [188], which then sedimented at the bottom of the bioreactor. For this reason, the culture at 100 rpm was stopped after five days. We did not observe a significant difference in the growth profiles of aggregate size under impeller agitation at different speed with respect to single aggregates grown in stagnant conditions in single wells, where no breakage nor fusion can occur (Figure 3.1 B, red markers). We therefore conclude that although the use of an adequate stirring speed avoids the spontaneous fusion between aggregates, the shear forces generated by the impeller rotation are not sufficient to induce aggregate breakup in the conditions tested, leading overt time to the formation of large clumps due to cell mitosis. From a physical perspective, aggregate breakage occurs when the local hydrodynamic shear rate exceeds a critical value [204], which depends on the mechanical properties of the aggregate. For multicellular aggregates, the minimum shear stress required to dislodge cells from the outer layers of multicellular aggregates has been experimentally determined to be in the range of 0.65 – 1 Pa according to previous reports [205–207]. In stirred bioreactor systems, the maximum shear is localized in a narrow region near the impeller, whereas the rest of the culture volume is characterized by significantly lower hydrodynamic stress levels [60,208]. Using the empirical correlation of Huchet et. al [198], we estimated an average shear stress in the entire bioreactor volume in the order of 2-13 mPa (Table 3.1), confirming that, in the condition tested, the effect of agitation would not be sufficient to induce PSC aggregate breakup.

Table 3.2: Hydrodynamic shear stress for the loop and loop-nozzle systems in Fig. 3.2 using the characterization of Neunstoecklin *et al.* and Villiger *et al.*

d_n (mm)	Q_{max} (L/min)	Volume (mL)	Re_{Loop} (-)	τ_{max} (Pa)
No nozzle	2	1000	7300	15
6	2	1000	10200	21
4.5	2	1000	14000	33
3	1	1000	10200	41.5

Effect of Oscillating Shear Stress on Human PSC Aggregates

To achieve stress values sufficient to cause mechanical disruption of the aggregates, we modified the perfusion setup (Figure 3.2) to include an external loop composed of a dip tube (Figure 3.2 A) connected to a cell retention device (Figure 3.2 B). In this configuration, the culture broth is moved periodically between the vessel and the cell retention system through the action of a diaphragm pump, with a cycle time that depends upon flow rate [200]. The first part of the cycle, responsible for moving the fluid from the vessel to the diaphragm pump, was performed at a volumetric flow rate of 0.5 L/min, while the flow rate of the second part of the cycle was set to a higher value to avoid a possible accumulation of aggregates within the cell retention device (Table 3.2).

To test whether the magnitude of the hydrodynamic forces generated in this setup could induce aggregate breakup, we performed two perfusion runs at 2 L/min as maximum flow rates in the external loop using two different cell lines. Under these conditions, we estimated the maximum shear stress in the dip tube to be in the order of approximately 15 Pa, providing a significant increase with respect to the shear generated from the impeller agitation and lergely exceeding the previously reported threshold of 0.6-1 Pa for cell detachment. The corresponding cell culture data are presented in Figure 3.3 A-D. In both cases, viability remained high throughout the entire cultivation and the cells proliferated for over ten days, achieving total viable cell densities in the order of $3 \cdot 10^6$ cells/mL, indicating that the oscillating stress did not significantly impact PSC proliferation or viability in the conditions tested. Unlike the experiments performed without the perfusion loop, the PSC aggregate size distribution reached a steady state trend after an initial growth phase of five days and did not increase further, settling at a mean value of around 450 μm. Since the total number of cells increased continuously through the culture, while the dimension of PSC aggregates reached an equilibrium, we can hypothesize that once the aggregates reach a critical size, determined by the

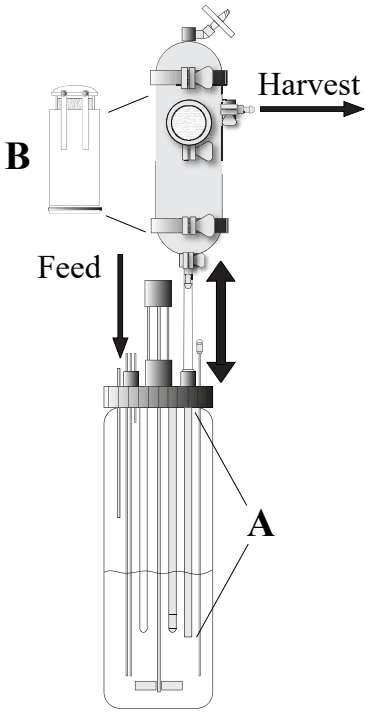

Figure 3.2: Schematic representation of the initial perfusion bioreactor setup used for human PSC cultivation with continuous, shear-driven aggregate breakup. Higher shear is generated in the dip tube (A) though the action of a diaphragm pump. (B) depicts the cell retention system used.

maximum shear of the system, they are mechanically disrupted into smaller clumps, in which the cells continue to proliferate. On the other hand, despite providing a mean to continuously breakup the stem cell aggregates without interrupting the culture, even at the maximum flow rate provided by the pump the diameter of most PSC aggregates in this configuration was still above the maximum desired value of 300 μm.

Optimized Bioreactor Design for Prolonged Human PSC Culture with Controllable Aggregate Size

To further increase the maximum hydrodynamic shear stress within the system, we connected a contracting nozzle at the entrance of the dip tube that connects to the cell retention device, whose inner section is smaller than the dip tube (Figure 3.4 4). This strategy allowed us to apply very brief pulses of high shear with a defined intensity to all PSC aggregates flowing through the perfusion loop [209].

Using the same cell line (hiPSC Cell Line 1), we performed three different bioreactor

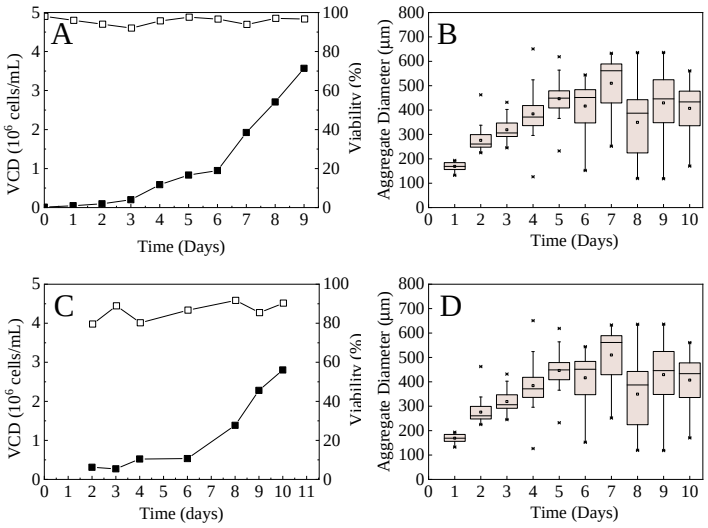

Figure 3.3: Viable cell density (black markers), viability (white markers) and aggregate size distribution profiles of cell line 1 (panels A-B) and cell line 2 (panels C-D) cultured under oscillating flow in the perfusion loop at 3 L/min maximum flow rate.

runs using nozzles of similar geometries but different internal diameter (d_n), allowing us to modulate the maximum shear intensity within the device (Table 3.2). PSCs cultured in perfusion proliferated up to 3.5 and $2.5 \cdot 10^6$ cells/mL while maintaining more than 90% viability in presence of nozzles with 6 or 4.5 mm d_n, respectively (Figure 3.5 A and C). On the other hand, PSC growth was drastically reduced when using a nozzle with 3 mm d_n (Figure 3.5 E). Interestingly, viability was not significantly affected in this condition, suggesting a growth-arrest mechanism rather than induction of cell death trough shear (Figure 3.5 E). Like the previous strategy, PSCs aggregate size distribution reached a steady state behavior after an initial phase, with the mean value scaling with the maximum shear (Figure 3.5 B-D-F). PSCs cultured in combination with the 4.5 mm d_n nozzle showed a narrow aggregate diameter distribution at steady-state, centered at approximately 250 μm, while using a 6 mm d_n nozzle resulted in a wider distribution of aggregate diameters, centered around 350 μm. Lastly, the 3 mm d_n nozzle provided the best control over the aggregate size, with an average diameter of 200 μm, although it severely limited cell proliferation, since the viable cell density did not exceed $1 \cdot 10^6$ cells/mL over the course of 10 days. Taken together, these results indicate an inverse correlation between aggregate size and PSC growth rate with the maximum hydrodynamic shear stress [188], highlighting the possibility to modulate the mean PSC

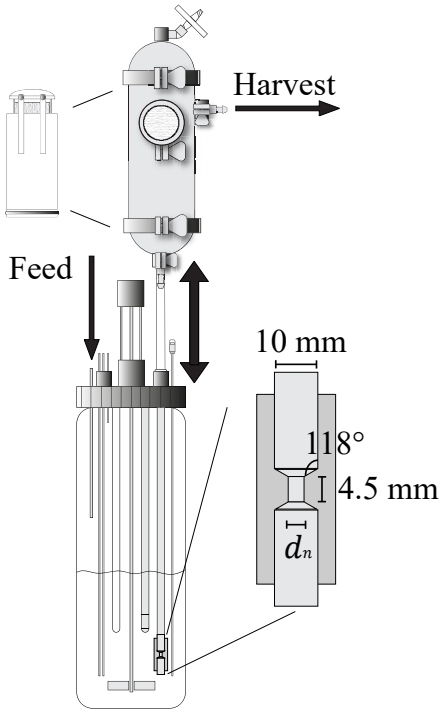

Figure 3.4: Modification of the perfusion setup to generate maximum higher shear stress values by the addition of a nozzle to the dip tube. The dimensions are indicated in the figure.

aggregate size with a single process parameter.

To prove the robustness of our approach, we performed a set of two biological replicates using two different human induced pluripotent stem cell lines. PSCs were cultured in the perfusion bioreactor platform shown in Figure 3.2 equipped with the 4.5 mm d_n nozzle due to its better trade-off between proliferation and aggregate size control of human PSCs. Both cultures revealed similar trends in terms of growth rate and steady-state aggregate size distributions, with final viable cell densities of 1.8 and $2.5 \cdot 10^6$ cells/mL after ten days of culture and a mean steady-state aggregate diameter around 250 μm (Figure B.2). Pluripotency was measured at the end of the culture and confirmed by flow cytometry for surface markers (Figure 3.6 A-D) and immunofluorescence images of PSC aggregates for intracellular markers (Figure 3.6 E-G). Moreover, after bioreactor expansion PSCs retained their morphology when transferred to vitronectin-coated culture plates (Figure 3.6 H).

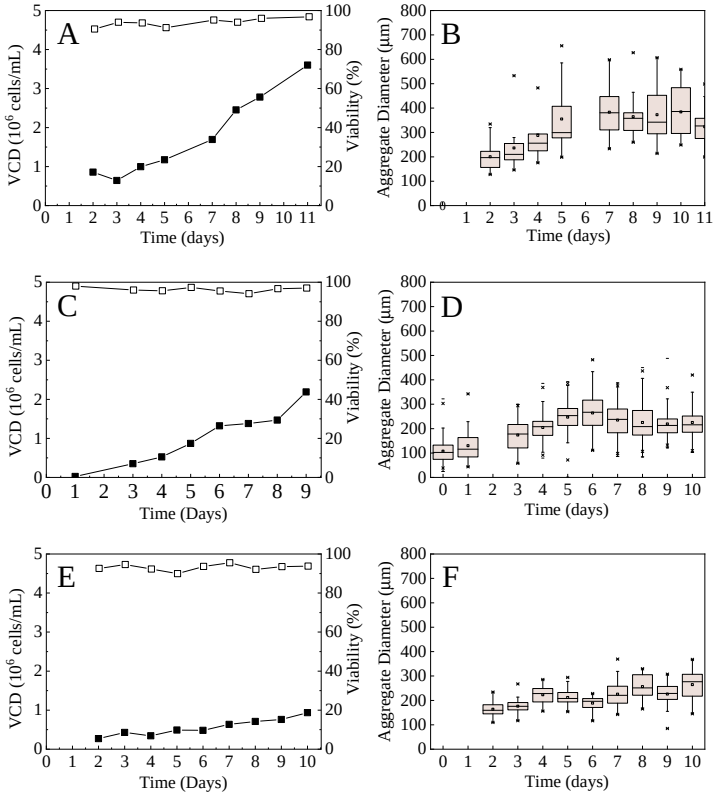

Figure 3.5: Viable cell density (black markers), viability (white markers) and aggregate size as a function of time for cell line 1 cultured in presence of a contracting nozzle in the perfusion loop with 6 (panels A-B) 4.5 (panels C-D) and 3 mm (panels E-F) internal diameter.

3.4 Discussion

The success of PSC-based therapies will depend on the development of scalable and cost-efficient expansion processes to produce enough cells with desired quality and safety profiles. This concept holds particularly true for regenerative medicine applications, where over 10^9-10^{10} cells are required to restore the function of a tissue or organ [210]. The use of PSC aggregates has allowed the transition from static, planar systems to scalable suspension processes. One of the main limitations posed by aggregate-based cultures is the control the dimension of cell aggregates below a critical size of 300 μm [54] to prevent undesired cell death or differentiation events due to nutrient or growth factor transfer limitations. To this end, several authors have investigated the use of serial mechanical or enzymatic passaging procedures, which have the drawback of requiring

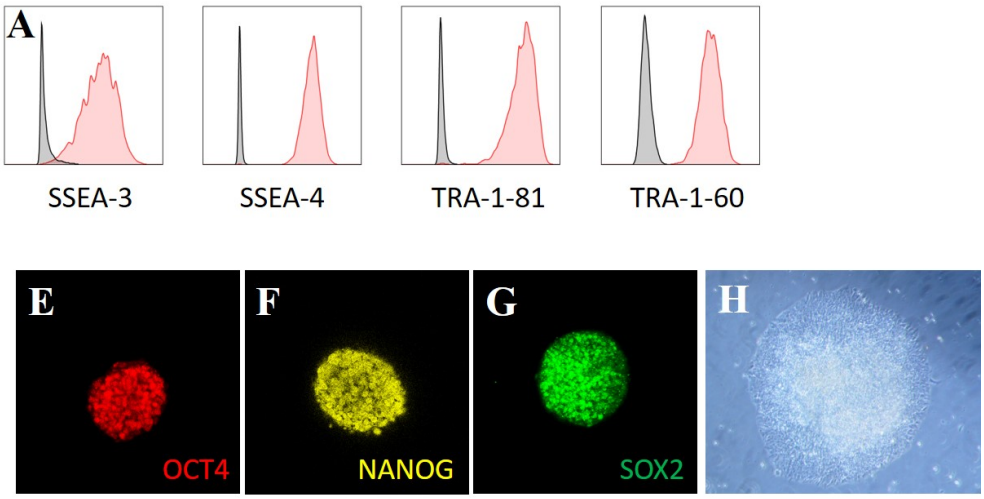

Figure 3.6: Phenotypic analysis of human PSCs after expansion under optimized conditions (4.5 mm internal diameter nozzle). Flow cytometry analysis (grey lines indicates isotype controls) of surface proteins SSEA-3, SSEA-4, TRA-1-81, TRA-1-60 (A-D). Immunostaining of aggregates for intracellular markers OCT4, Nanog and SOX2 (E-G). Morphology of bioreactor-expanded PSCs after transfer to vitronectin-coated flasks.

the interruption of the culture and the use of open systems [162]. Here, we demonstrate the development of a bioreactor-based platform with shear-driven aggregate breakup as a strategy for continuous expansion of human pluripotent stem cells. We first observed that, in benchtop bioreactors, the shear stress generated by the impeller rotation is not enough to induce the breakup of multicellular aggregates (Figure 3.1 B). Although it would be theoretically possible to reach a sufficient hydrodynamic stress by increasing the agitation speed, it would most likely lead to the formation of vortexes within the system, that would induce the formation of air bubbles within the culture broth, causing extensive cell damage [211]. Furthermore, process scale-up or transfer to another system would remain difficult as maximum shear stress depend on impeller and bioreactor dimensions. To expose the cell to higher, well-defined pulses of hydrodynamic shear stress, while maintaining a low impeller agitation, we embedded a contracting nozzle in the perfusion loop. We found that aggregate breakup occurred well above 1 Pa, in accordance with previous reports [205, 206], with significant growth reduction occurring only after exceeding 40 Pa of pulsed shear. Although particular mammalian cell lines have been reported to be able to withstand up to 30 Pa [209], other studies have reported nonlethal responses in the range of 1-10 Pa [211]. We observed the ability of aggregated

PSCs to survive and proliferate up to $2.5 \cdot 10^6$ cells/mL even when subjected to shear stresses in the order of 30 Pa. We believe that, since the residence time in the high shear region of the nozzle is extremely limited, it is reasonable to expect the flow through the restriction to not cause significant cell death even at high velocities due to the short exposure time for the cells, as noted by previous reports [208]. Our findings suggest that, within our system, PSC aggregates break up once they reach a critical diameter, whose value is determined by the maximum shear intensity experienced by the cells, continuously forming novel smaller aggregates. Overall, this strategy allows prolonged expansion of undifferentiated PSCs achieving final viable cell densities consistent with other reports [61,184] while preventing the need for manual passaging procedures. This process can be further optimized through several strategies. For example, recent studies suggested use of macromolecules to modulate the mechanical properties and size of PSC aggregates [165]. The combination of chemical and hydrodynamic strategies could possibly lead to a reduction in the shear needed to induce aggregate breakup, allowing the obtainment of smaller and more homogeneous PSC aggregate size distributions. Additionally, supplementation of small molecules and cytokines capable of modulating the pluripotent cell state [161, 212], together with the use of concentrated feeds and other process intensification strategies, could further improve the PSC expansion rates in suspension.

Chapter 4

Bioprocess Optimization for Memory T-Lymphocyte Expansion in Serum-Free Conditions

4.1 Introduction

Adoptive cell transfer (ACT) using human T lymphocytes has shown tremendous objective response rates for the treatment of therapy-resistant tumors and chronic infections [94] and is expected to enter mainstream clinical practice in the next future [107, 109]. Within the general scheme used in clinical trials for ACT manufacturing, a large part of the process is reserved for the expansion of the lymphocyte population of interest [96]. This step is necessary to achieve a clinically relevant dose of cells, which is in the order of 10^8 for Chimeric Antigen Receptor (CAR) T cells [108], between 10^{10} and 10^{11} for T Cell Receptor (TCR) engineered T cells [213], and over 10^{11} for Tumor Infiltrating Lymphocytes (TIL) [214, 215]. Contrary to standard biological drugs (*i.e.* recombinant proteins and vaccines), the processes and unit operations for T cell expansion for are not standardized, and often involve the use of open systems in combination with manual handling steps [110], hampering the industrialization and commercial-scale production of these therapies [216]. Besides the need for large numbers of cells, various pre-clinical and animal studies have associated the infusion of less differentiated lymphocyte subsets, including T stem cell memory (T_{SCM}) and T central memory cells (T_{CM}), to a significant improvement in anti-tumor activity [217]. This effect has been explained through several mechanisms, including a higher replicative capacity, longer *in vivo* persistence and a superior metabolic fitness of memory T cell populations compared to mature T effector cells (T_{EFF}) [218, 219]. The differentiation status of the adoptive lymphocytes is largely affected by the *in vitro* protocols used for their *in vitro* expansion, with prolonged culture times and repetitive activations inevitably resulting in differentiation towards short lived effector cells [96]. Within this trade-off between expansion rate and memory cell formation, most of the currently reported methods for T cell culture used in clinical trials tend to maximize the growth rate of the cells through high IL-2 supplementation, causing excessive cell stimulation and resulting in a vast differentiation towards short-lived effector cells [69, 220]. Several strategies have been proposed to reduce this progressive differentiation of T cells caused by *in vitro* culture, including the reduction of IL-2 concentration in the media [69], addition of cytokines such as IL-7, IL-15 and IL-21 [221, 222], metabolic limitation of glycolysis [219], pharmacological targeting of different molecular pathways through the supplementation of specific agonists or inhibitors [223–226], and modulation of mitochondrial dynamics [227]. Until now, the approaches for the generation and expansion of T lymphocyte populations with

functional properties related to early memory phenotypes have been developed using small scale open systems, such as tissue culture plates and gas-permeable bottles [228], in combination with serum-enriched media formulations. Furthermore, no real investigation with respect to key process parameters has been performed to improve the yield or scalability of T cell expansion processes. Given the limitations of the current strategies, we report the development and optimization of a scalable expansion process for the expansion in serum-free conditions of a T cell product with a significant fraction of early memory T cells. We first identified the critical medium components capable of substituting the addition of serum to support T cell proliferation. Secondly, we optimized the medium formulation in order to provide the best trade-off between growth and arrest of T cell differentiation. Lastly, we translated the expansion of memory T cells from tissue culture flasks to benchtop stirred tank bioreactors, implementing optimal process conditions previously determined in a small-scale investigation.

4.2 Experimental

4.2.1 Human T Cell Culture

Unfractionated CD3+ T cells harvested from healthy donors (Zenbio, USA) were used for all experiments. The cells were routinely cultivated at 37 °C, 90% humidity and 5% CO_2 in a humidified incubator in the indicated culture medium in 25 cm^2 or 75 cm^2 T-flasks and split every 4-5 days to maintain a viable cell density (VCD) below $2 \cdot 10^6$ cells/mL. T cells were activated every 7-10 days using magnetic CD3/CD28 coated beads (Dynabeads, ThermoFischer, Swtizerland). For shear-stress experiments, the cells were cultivated in 500 mL Erlenmeyer Flasks (Corning, USA) in a shaking incubator (Adolf Kuhner AG, Birsfelden, Switzerland), using static T75 Flasks as control.

4.2.2 Media and Reagents

RPMI 1640, GlutaMAX Supplement, HEPES (Invitrogen, USA), supplemented with 100 U/mL IL-2 (ProSpec, Israel) was used as basal medium for all the experiments. The medium was supplemented with either 10% v/v heat-inactivated fetal bovine serum (FBS) (Invitrogen, USA) or, for experiments in absence of serum, with a combination of the following components: recombinant human insulin (Sigma Aldrich, USA), human

transferrin (ProspecBio, Israel), Mdiv-1 (Sigma Aldrich, USA), M1 (Sigma Aldrich, USA), AKTi-1/2 (Tocris, UK), Metformin hydrochloride (Tocris, UK), PF-06409577 (Tocris, UK), Ethanolamine (Sigma Aldrich, USA), Oleic Acid (Sigma Aldrich, USA), Linoleic Acid (Sigma Aldrich, USA).

4.2.3 Bioreactor Culture

The bioreactor design is based on a DASGIP parallel bioreactor system with a working volume of 1L (DASGIP Technologies, Eppendorf, Switzerland). Bioreactors were equipped with a pitched-blade impeller, online pH-sensors (05-DPAS-SC-K8S pH Probe, Mettler Toledo, Switzerland), dissolved oxygen (DO)-sensors (InPro® 6820, Mettler Toledo, Switzerland), and temperature (T) sensors (Platinum RTD Temperature Sensor, Eppendorf, Switzerland). Temperature was set to 38 °C throughout the culture. DO was maintained to 30% of air saturation by applying an overhead gas flow rate of 15 L/h while controlling the inlet fractional composition of O_2, air and N_2. The pH was maintained at 7.1 trough on-demand supply of CO_2. The stirring speed was set to 120 rpm. Exponentially growing cells were inoculated at a seeding concentration of 0.2-0.4 $\cdot$ 10^6 cells/mL and conventional batch cultures were carried out for 7 to 9 days at 0.5 L working volume. Satellite control runs were performed with cells coming from the same expansion and cultured in static T-75 Flasks with the same seeding concentration at a working volume of 15 mL. Both bioreactor and control runs were performed in duplicates. Samples were taken daily for offline analysis of viable cell density and viability, while phenotype analysis was performed at the end of the culture.

4.2.4 Shear Stress estimation

The average shear stress $\langle\tau\rangle$ (Pa) in shaking Erlenmeyer flasks and stirred tank bioreactors was derived from the volume average dissipation rate $\langle\epsilon\rangle$ (m^2s^{-3}) according to Equation 4.1 [229]:

$$\langle\tau\rangle = \sqrt{\mu\rho\langle\epsilon\rangle} \tag{4.1}$$

where ρ and μ indicate the density and the dynamic viscosity of the cell suspension at 37 °C, which was assumed to behave like pure water. For Erlenmeyer flasks, the dissipation rate was calculated according to the correlations developed by Peter et. al for unbaffled shake flasks (Equations 4.2- 4.4) [230]:

$$\langle \epsilon \rangle = Ne' \cdot n^3 \cdot d^4 \cdot V^{-\frac{2}{3}} \tag{4.2}$$

$$Ne' = 75 \cdot Re^{-1} + 25 \cdot Re^{-0.6} + 1.5 \cdot Re^{-0.2} \tag{4.3}$$

$$Re = \frac{\rho \cdot n \cdot d^4}{\mu} \tag{4.4}$$

where Ne' and Re indicate the Newton number and Reynolds number for the system, n is the agitation rate (s^{-1}), d is the maximum diameter of the flask (m) and V is the culture volume (m^3). In case of the bioreactor, the following equation was used 4.5 [209]:

$$\langle \epsilon \rangle = \frac{N_p d_i^5 N^3}{V} \tag{4.5}$$

Where N_p indicates the impeller power number (assumed equal to 2.35), d_i is the diameter of the impeller (m), and N the impeller agitation rate (s^{-1}).

4.2.5 Analytics

Cell density and viability were measured via trypan blue exclusion (Cedex HiRes, Roche Diagnostics, Switzerland). For flow cytometry, the following antibodies were used (all from Biolgened, USA): FITC anti-human CD27, PE anti-human CD62L, PE-Cy7 anti-human CD127 (CCR7), PerCP/Cy5.5 anti-human CD8, APC anti-human CD279 (PD-1), APC anti-human CD57, PE-Cy5 anti-human CD4. All flow cytometry measurements were performed using LSRFortessa (BD Bioscience, US) and analysed with FlowJo (version 10, TreeStar, USA).

4.2.6 Statistical Analysis

For medium optimization studies, P values were calculating using Students t test. Statistical significance was considered for groups with $p<0.05$.

4.3 Results

4.3.1 Minimal Serum-Free Medium Composition for T Cell Culture

Human serum is a crucial raw material used in clinical T-cell-based therapies due to its beneficial effects in promoting proliferation, inhibiting proteases and protecting against shear stress, but its use is often associated with batch-to-batch variability, limitations in supply chain and risks of cross-contaminations or infections [231, 232]. Using RPMI-1640 supplemented with 5 mg/L Insulin and 100 U/mL IL-2 as basal media, we found that the combined addition of human serum albumin (2.5 g/L), human Transferrin (10 mg/L) and a combination of fatty acids (FA) was necessary to guarantee cell survival and minimal proliferation levels (Figure 4.1). Removal of albumin resulted in rapid cell death after cell thawing (Figure 4.1 A). Although albumin is known to bind toxic components and reduce shear stress-induced death, we found that the loss of viable cells was due to irreversible adhesion of lymphocytes to the bottom of the culture dish in absence of albumin (data not shown), in line with other reports [233]. Transferrin is a carrier protein which facilitates iron internalization and, promoting growth and, in case of T cells, contributes significantlyit is necessary for to their activation process [234]. As expected, removal of transferrin drastically reduced T cell proliferation (Figure 4.1 B). Although it has been reported that iron chelators such as ferric citrates can substitute the effect of transferrin [235], we found that the addition of ferric ammonium citrate (final concentration 2 mg/L) only partially rescued T cell growth, resulting in a significant increase in the cell doubling time compared to transferrin (Figure 4.1 B). Fatty acids are present in serum in form of protein-bound lipids and are essential components for the metabolism of several cell types, including T cells [236]. A mixture of oleic acid and linoleic acid was found to promote growth at a 1 mg/L concentration each with respect to a lipid-free condition (Figure 4.1 C). This effect was reversed by the addition of the fatty acid oxidation inhibitor Etomoxir (100 μM final concentration), which resulted in a severe growth impairment even in presence of exogenous fatty acids (Figure 4.1 C). To reduce the complexity of the final medium composition, we tested the individual contribution of the two fatty acids to T cell proliferation. Linoleic acid alone was found to support T cell growth better than oleic acid, and at a comparable level of the oleic-linoleic acid mixture (Figure 4.1 D). We therefore decided to remove oleic acid from the

final formulation and add linoleic acid at the concentration of 15 μm for optimal growth (Figure 4.1 E). Although the addition of insulin, transferrin, albumin and linoleic acid was sufficient to promote growth and survival of the cells, ethanolamine was included in the final formulation (20 μM) due to its well-reported growth-enhancing effect (Figure 4.1 E). The final medium formulation used in subsequent experiments is reported in Table 4.1.

Table 4.1: Minimal serum-free media composition for T cell culture.

Component	**Concentration**
Human Serum Albumin	2.5 g/L
Human Transferrin	10 mg/L
Human Insulin	10 mg/L
IL-2	$2 \cdot 10^5$ U/L
Linoleic Acid	15 μM
Ethanolamine	20 μM

4.3.2 Akt Inhibition Improves Memory T Cell Formation Without Compromising Growth in Presence of Allosteric AMPK Activation

To delay the differentiation into short-lived effector T cells caused by *ex vivo* cultivation, we first expanded T cells in serum-free conditions for seven days in presence of anti CD3/CD28 beads and previously reported pharmacological agents that are known to promote memory T cell formation. Compared to T cells expanded in the simple medium formulation previously developed, the growth rate was significantly reduced for all the additives tested (Fig. 2A), with an average 30% reduction in growth rate with the Akt inhibitor Akti (10 μM) [237], a 50% reduction with JQ1 addition (0.15 μM) [224], and a 70% reduction for T cells cultured in presence of Mdivi-1 (1 μM) and M1 (2 μM) [227]. Given that cell-based immunotherapies require T cell expansion to be performed in a limited timeframe, we sought to identify possible components that would inhibit effector T cell differentiation without significantly compromising T cell proliferation. The best results were achieved with the allosteric AMPK activator PF-06409577 (10 μM) [238], which had no direct negative effects on cell growth (Figure 4.2 A) but enhanced the expression of memory markers compared to DMSO

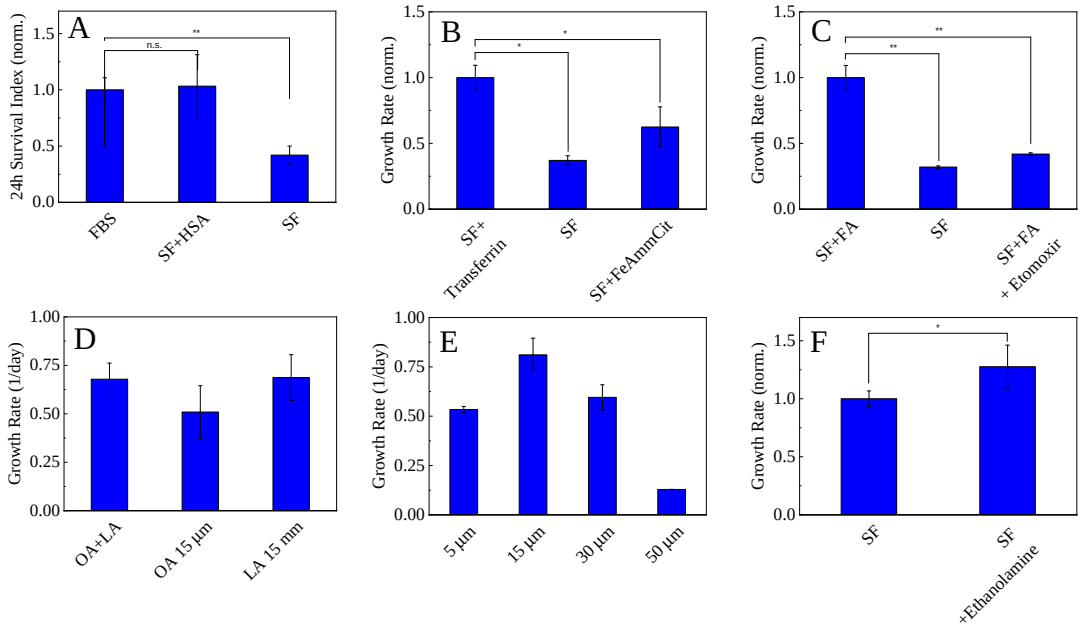

Figure 4.1: Effect of critical medium components for supporting survival and growth of human T cells as opposed to plain serum free (SF) conditions without the compound considered. All experiments were performed using cells from three different donors. Effect of human serum albumin (HSA) on T cell survival (A), defined as the ratio of surviving cells and seeded cells. Effect of transferrin and ferric ammonium citrate (B) and fatty acids (FA) (C) on T cell proliferation. Growth rate of T cells in presence of oleic (OA) and/or linoleic (LA) acids (D). Estimation of the optimal LA concentration for T cell proliferation (E). Effect of ethanolamine (F). For graphs A,B,C and F, the values are normalized with respect to the control condition. $*P < 0.05$, $**P < 0.01$.

addition (Figure 4.2 B-D). At the same time, we noted that the effect of PF-06409577 in upregulating the expression of CD62L, CCR7 and CD27 was lower than the well-established Akt inhibitor Akti [226, 239] (Figure 4.2 B-D). Surprisingly, PF-06409577 supplementation in conjunction with Akti significantly improved T cell growth under serum free conditions (Figure 4.2 E). AMPK activation has been reported to play a key role in the metabolic adaptation of lymphocytes and to promote survival under nutrient limitations [220, 240]. We therefore hypothesize that a direct AMPK activation reduces the environmental stress on T cells undergoing activation and expansion in serum-free conditions in presence of Akti, improving their proliferative potential. Of note, we observed this effect only through direct AMPK activation, since the addition of the indirect AMPK activator metformin (final concentration 1 mM) resulted in a severe growth inhibition (Figure 4.2 F). In terms of phenotype, combined addition of PF-06409577 and

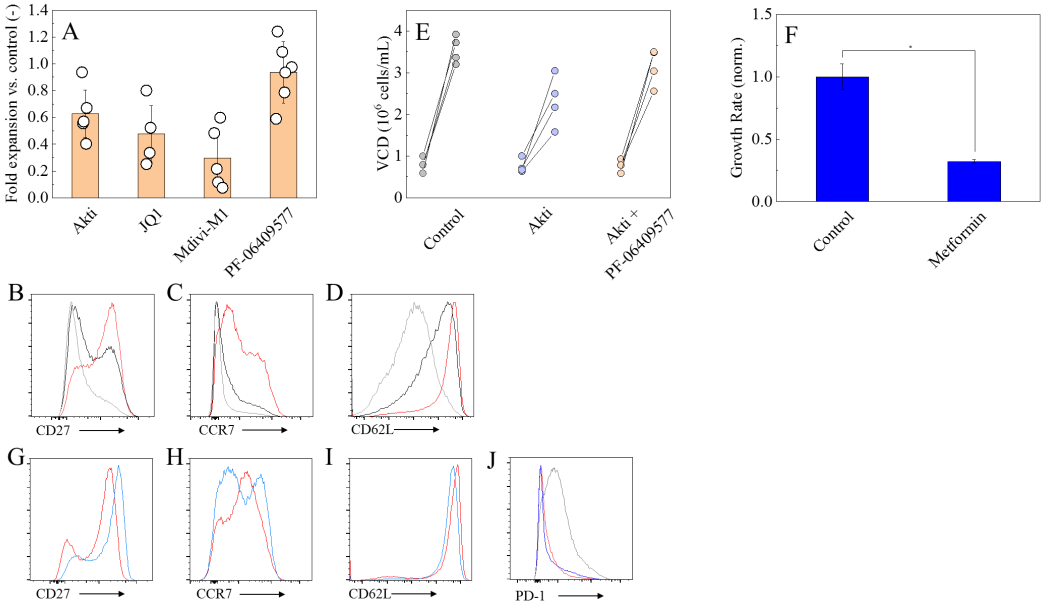

Figure 4.2: Effect of different pharmacological agents on T cell proliferation (n=5) (A). Phenotype of T cells cultured in presence of Akti (black line), PF-06409577 (red line) and no additives (grey line) (B-D). Viable cell density (VCD) increase after cultivation in presence of different compounds for three days (E). Growth inhibiting effect of metformin (F). Phenotype of T cells cultured in presence of Akti and PF-06409577 (blue line) or Akti alone (red line) (G-J).

Akti slightly improved the expression of T cell memory markers compared to the effect of single compounds (Figure 4.2 G-I), possibly because the two compounds activate two different pathways that support the formation of memory T cells. This was also confirmed by a reduced surface expression of the exhaustion marker PD-1 (Figure 4.2 J) compared to the control condition. Given that the addition of Akti and PF-06409577 did not provoke a significant reduction in cell proliferation, we decided to include both compounds in the medium formulation due to the improvement in the generation of cells expressing key markers that are characteristic of more potent T cell subsets for ACT.

4.3.3 Optimization of Physicochemical Variables for Memory T Cell Expansion

Scalable bioreactor systems based on rocking motion or impeller agitation provide the possibility to monitor and control important process parameters that can impact proliferation and viability of the cells such as temperature, pH, dissolved oxygen and carbon

dioxide tension, as well as hydrodynamic shear stress [39]. To estimate the optimal operating conditionsy for large-scale expansion of T lymphocytes, we performed a series of small-scale experiments using static T flasks or shake flasks. First, T cells were cultivated in serum-free media under static conditions at different temperatures. An increase in growth rate of approximately 20% was observed when cultivating T cells at 38 °C (Figure 4.3 A), with respect to the 37 °C control, in line with other reports [241, 242]. The stimulatory effect of temperature was lost above 39 °C, resulting in lower expansion rates. Conversely, temperatures lower than 37 °C provoked a temperature-dependent growth inhibition, a common behavior observed in several mammalian cells [243]. To evaluate the effect of pH, T cells were cultivated under static conditions at 37 °C and the media was equilibrated using concentrated NaOH or HCl solutions. The dependence of cell growth (measured after 48h) on pH showed a typical bell-shaped curve (Figure 4.3 B), with the optimal pH value being slightly more acidic (7.0-7.2) than the pH used during the control run (7.4). This optimal range of pH is also in agreement with previous investigations performed in serum-containing conditions both for growth [241, 244] and cytotoxicity [245] of human T lymphocytes. The maximum operating shear stress was determined by cultivating T cells for 7 days in Erlenmeyer flasks (100 mL working volume) in a shaking incubator without the addition of serum or other synthetic shear protectants. Under these conditions, human T lymphocytes were found to be extremely sensitive to shear, with a severe reduction in proliferation occurring above 0.1 Pa (Figure 4.3 C). This trend is similar to previous reports, which showed a better culture performance for lymphocytes cultured at lower agitation speeds [66, 244]. Cell viability remained above 90% in all conditions (Figure 4.3 D), indicating a non-lethal, growth inhibiting effect of shear on lymphocytes as opposed to induction of necrosis and apoptosis [246].

4.3.4 Scale-up of Memory T Cell Expansion in Stirred Tank Bioreactors

To develop a more resource-efficient and scalable process for T cell expansion, we investigated the possibility to translate T cell culture from static flasks to agitated stirred tank bioreactors. T lymphocytes from three different donors were cultivated at 0.5 L scale in benchtop bioreactors for 7-9 days, using standard T-Flasks as control runs. Both bioreactor and flask experiments were performed in duplicates for each donor. The pre-

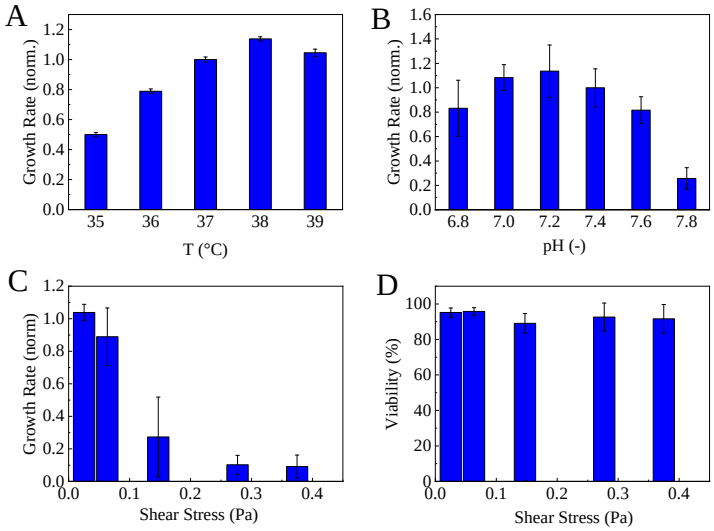

Figure 4.3: Small scale optimization of environmental variables on T cell proliferation and viability. Effect of temperature (A), pH (B) and hydrodynamic shear stress (C-D).

viously developed serum-free medium composition and optimized process parameters were implemented in both systems to support memory cell formation and at the same time provide the best conditions for cell proliferation. The agitation in the bioreactor was adjusted at 120 rpm, corresponding to an average shear stress in the vessel of $3 \cdot 10^{-3}$ Pa (Eq. 4.5), which is largely below the previously determined maximum operating value of about 0.1 Pa. The dissolved oxygen tension was maintained at 30% of air saturation to reproduce the physiological condition of the bone marrow [247]. T cells cultured in both bioreactor and T flasks proliferated over the entire course of the experiment, with final viable cell densities in the range of 1.5-2.5·10^6 cells/mL and viability constantly above 90% (Figure 4.4). The use of an agitated system was not associated to a decrease in T cell proliferation, and actually the growth curves show either equal or better performance for the bioreactor (Figure 4.4 B).

Flow cytometry analysis confirmed that T cells cultivated in both systems present comparable phenotypes (Figure 4.5), suggesting that agitation did not have an impact on T cell differentiation in the conditions tested. Despite the significant differences in marker expression between the three donors, more than 50% of the T cells after bioreactor expansion retained expression of memory markers such as CD27 and CD62L (Figure 4.5), while the exhaustion marker CD56 was detected at low levels (20%) only for one donor (Figure 4.5 F). These results indicate the validity of the approach to expand

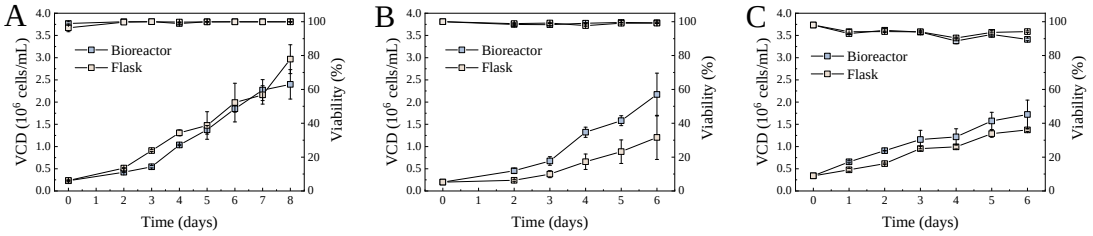

Figure 4.4: Viable cell density and viability profiles during bioreactor expansion for three different donors.

T cells in stirred tank bioreactors with a similar performance as conventional static systems but with much higher productivity and scalability potential.

4.4 Discussion

In the context of ACT, preclinical and animal studies have linked an increase in the cancer regression rate to the infusion of a higher number of T cells [248–251] and less differentiated T cell subsets [218]. With the aim of tackling both criticalities, this study reports the development of a scalable process for T cell expansion with an optimal trade-off between the yield (number of cells) and quality (phenotype) of the final T cell-based product. The first part of the work aimed at identifying the most critical compounds that support T cell survival and proliferation to develop a minimal serum-free medium composition for the expansion of T cells. We found that removal of albumin, transferrin and linoleic acid drastically reduced the culture performance (Figure 4.1). Together with the addition of ethanolamine, this formulation (Table 4.1) was able to support robust lymphocyte growth without the need for other additives besides insulin and IL-2. We then evaluated the addition of chemical inhibitors of T cell differentiation to limit the detrimental effects of *in vitro* cultivation. While many compounds that target pathways responsible for T cell development resulted in reduced proliferation when tested in serum-free conditions (Figure 4.2 A), the combination of Akti and PF-06409577 provided the best trade-off between T cell proliferation and expression of memory-associated surface markers. Akt inhibition is known to improve the formation of memory T cells by promoting nuclear translocation of FOXO1 [239, 252]. Although our data suggest a slight reduction in T cell proliferation following Akt inhibition, this result does not agree with previous studies, who reported no differences in

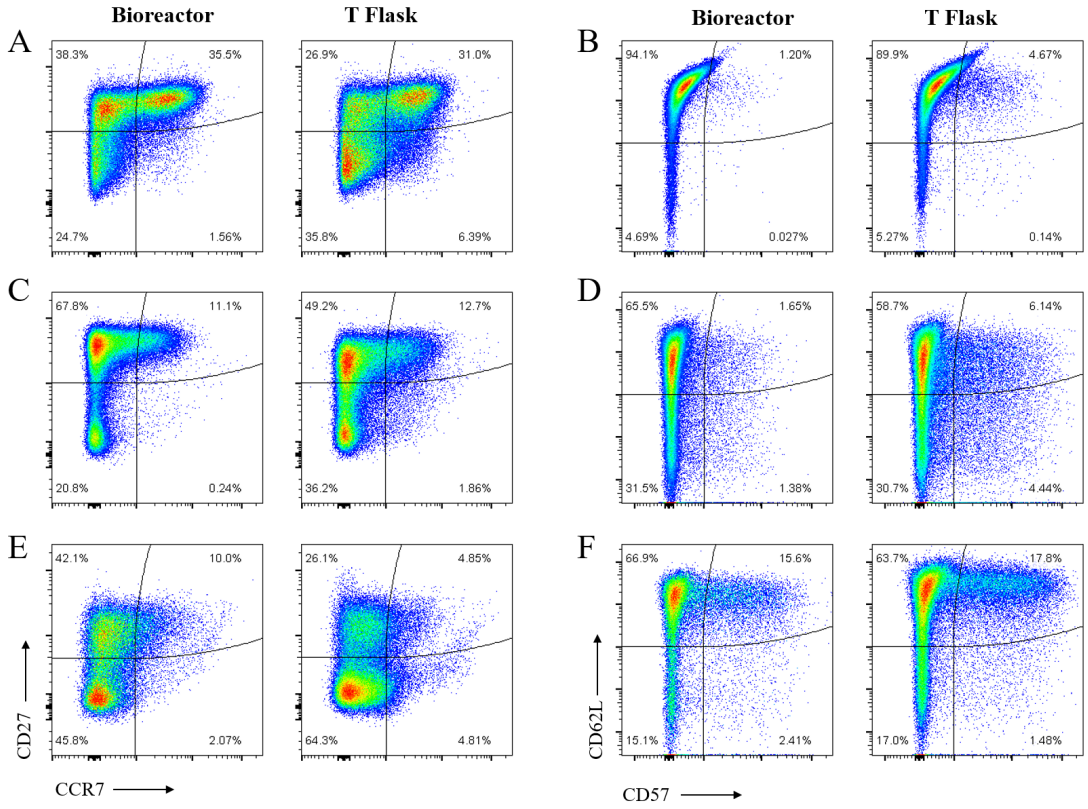

Figure 4.5: Marker expression for T cells expanded in bioreactor or T-Flasks from three different donors.

terms of growth upon Akti treatment [226, 239]. We believe that this is due to the different conditions used, since we performed this test in absence of serum, which is known to have strong growth-promoting effects [231]. AMPK activation has been proposed to promote CD8 T cell memory development by upregulating oxidative metabolism in the mitochondria [225, 236, 253]. Most of the studies involving AMPK activation in lymphocytes have been performed indirectly through the use of compounds like metformin [225], which blocks mitochondrial ATP synthesis by inhibiting the respiratory chain complex I [254], causing an almost complete growth arrest (Figure 4.2 F). On the other hand, allosteric activation of AMPK did not affect the proliferation of lymphocyte significantly (Figure 4.2 A). This discrepancy between the effect of direct and indirect activation of AMPK on cell cycle progression has also been documented by previous studies on cancer cells [255]. Lastly, we evaluated the possibility to expand T lymphocytes with the optimized medium formulation in a scalable bioreactor platform.

Compared to more conventional culture systems like T flasks and culture bags, stirred bioreactors are closed systems that provide a more efficient utilization of the culture volume, on-line monitoring and control of environmental variables, as well as the possibility to automate feeding strategies [38]. Most of the studies on T cell culture in bioreactors have been performed using rocking-motion systems [104, 256–258, 258], which provide efficient mixing in a low-shear environment [259]. Compared to rocking-motion systems, agitated bioreactors are the main industrial platform to produce recombinant proteins and have been extensively characterized with respect to operating conditions and scale-up criteria. Here, we show that by controlling the shear stress caused by mechanical agitation, T cells can be expanded to cell densities above $2.5 \cdot 10^6$ cells/mL in stirred tank bioreactors without significantly affecting the growth rate or the phenotype of the cells (Figure 4.5). Although our fold increase is lower compared to other studies on gas-permeable systems and culture bags [41,56,104,258], we did not perform bioreactor expansion in presence of feeder cells or anti-CD3 antibodies, which are strong growth promoters for lymphocytes. Moreover, we did not optimize our system with respect to critical parameters such as oxygen tension [260] and perfusion rate, which can provide additional strategies to further increase the performance of the system. The resulting T cell population showed high expression of memory markers such as CD27 and CD62L after bioreactor expansion. In particular, infusion of CD27+ cells has been recently correlated with sustained remission in a CD19 CAR-T cell therapy [261], indicating potential benefits for using the expansion strategy developed in this work for clinical applications.

4.5 Conclusion

Together with the identification of novel tumor markers, the reduction of the intrinsic toxicity and a deeper understanding of the factors that regulate the *in vivo* persistence, the success of T cell therapies will also rely on the ability to produce sufficient quantities of high-quality lymphocytes through robust and resource-efficient manufacturing processes. Our work reports the development of a bioprocessing framework to produce over $2 \cdot 10^9$ lymphocytes with a significant fraction of CD27+ cells in a single scalable, closed system in serum-free conditions. Although we did not work with genetically-modified T cells, this strategy can be readily applied to produce CAR or TCR-engineered cells introducing an additional processing step for T cell transfection. Our results represent

an attractive strategy to expand T cells with improved quality attributes for cancer treatment.

Chapter 5

Influence of Protein/Glycan Interaction on Site-Specific Glycan Heterogeneity

This chapter is based on the following publication: ME. Losfeld, E. Scibona, CW. Lin, TK. Villiger, R. Gauss, M. Morbidelli, and M. Aebi *Influence of protein/glycan interaction on site-specific glycan heterogeneity*, The FASEB Journal, **2017**, 31, 4623-4635.

The author of this thesis contributed in designing the glycosylation network, developing the model, performing the simulations and participated in the data representation and the writing of the manuscript.

For the experimental section of this chapter, all credit goes to ME. Losfeld and CW. Lin. For details, and please refer to Appendix C.

5.1 Introduction

N-glycosylation is a major post-translational modification of proteins that modulates folding, maturation, trafficking, secretion, as well as specific protein functions [262–264]. Contrary to many other post-translational modifications, N-glycans are composed of many different monosaccharide units, creating a large diversity of glycan structures [265, 266]. In eukaryotic cells, the N-glycosylation occurs in the endoplasmic reticulum (ER) after a conserved pathway. The oligosaccharide $Glc_3Man_9GlcNAc_2$ is assembled on the lipid dolicholpyrophosphate at the membrane of the ER and then is covalently linked to the side-chain amide of the asparagine residue in the sequon N-X-S/T by oligosaccharyltransferase (OST) [262, 267, 268]. Multiple sites on one glycoprotein can be modified by the OST complex and with the increasing complexity of multicellular organism, an increasing number of N-glycosylation sites in the glycoproteome are observed. It is estimated that up to 6000 different sites are modified by OST in mammalian cells [269]. In the second phase of the N-glycosylation pathway, the protein-linked glycan is trimmed by glucosidases and mannosidases [262, 270] and it is subsequently modified by different glycosyltransferases, spatially distributed along the secretory pathway. N-glycan processing enzymes have defined substrate specificities and locations in the secretory pathway [270, 271], and their expression level can be regulated upon internal and external signals. Glycan maturation in the secretory pathway is not a template-driven process. The hallmark of the N-glycosylation pathway is the generation of a heterogeneous population of N-glycoproteins: N-glycans differ at a given N-glycosylation site (microheterogeneity) [272, 273] and the composition of the N-glycan population can differ between N-glycosylation sites on a protein (site-specific microheterogeneity). Microheterogeneity is viewed as the result of competing alternative processing pathways and the incomplete processing by hydrolases, glycosyltransferases, or both. This incomplete processing can therefore be modulated by altering the reaction-limiting parameters, such as enzyme and substrate concentrations, enzyme-substrate exposure time, and substrate affinities [274–276]. In addition, properties of the N-glycoprotein itself, such as accessibility of the N-glycan to the processing machinery can result in differential site-specific glycan structures [277, 278]. Site-specific glycan structures are widely known and, for some of them, a specific biologic function has been identified. Prime examples are the N-glycan structure of the Fc-domain glycan in IgG molecules [279] or the high mannose structure on gp120 of HIV as part of the

epitope of neutralizing antibodies [280]. Recently, glycan microheterogeneity has become a major hindrance in the production of glycoproteins [281–283]. Chinese hamster ovary (CHO) cells are a mammalian cell line frequently used to produce recombinant glycoprotein [275, 284, 285]. Glycosylation in CHO cells has been thoroughly studied [286, 287], and the glycan structures found are essentially composed of mannose, N-acetylglucosamine, galactose, fucose, and sialic acid, differently assembled and generating four main classes of glycans: oligomannose, hybrid, complex, and fucosylated complex [287, 288] as summarized in Figure 5.1.

Altering glycostructures in production processes is mostly done by varying the culture conditions or by changing the activity level of specific glycosyltransferases and glycosyl hydrolases, with most of the studies being performed on glycoproteins with a single N-glycosylation site such as mAbs [283, 289–293]. The analysis of site-specific microheterogeneity on a protein with multiple N-glycosylation sites in cell or tissue-derived extracts requires more elaborate analytical methods that have become available only recently [277, 278, 294–296]. Few studies have shown the relation between protein primary sequence and the observed glycan profile. For example, Yu et al. [297] showed that in IgG replacing a phenylalanine residue that interacts with the non-reducing end GlcNAc and the b-Man of the N-glycan core $Man_3GlcNAc_2$ by alanine results in increased N-glycan processing. Chen et al. [298] introduced a phenylalanine residue into the IgG CH2 domain, which interacts with the reducing end GlcNAc of the chitobiose core. This stabilized the protein and resulted in an alteration of N-glycan processing. To determine the role of the glycan–protein interaction on site-specific glycan processing in the ER and Golgi of mammalian CHO cells in a more systematic manner, we expressed protein disulfide isomerase (PDI), carrying five N-linked glycans, as model protein. We directed the localization of the model protein (retained in the ER or secreted to the medium) and quantified the site-specific glycan structure produced. We then combined the analysis of the site-specific glycan profile of various point mutants with enzymatic flux analysis. This combined approach allowed us to determine the site-specific bottlenecks in the processing pathway. We showed that by altering the primary sequence of the protein, it is possible to modulate site-specific glycan processing, showing the importance of the direct interaction between N-glycans and amino acids of the glycoprotein on the processing in the ER and the Golgi. We showed that, depending on its side chain, each amino acid induced a different and specific change in the glycan profile. We demonstrated that this modification of site-specific N-glycan profile is the

result of modified associated enzymatic fluxes.

5.2 Mathematical Modeling

5.2.1 Glycosylation Flux Analysis of PDI Glycosylation in CHO Cells

Flux analysis was used to identify the presence of limiting steps in the biosynthesis of different structures for each site of PDI (16). Glycans are connected by fluxes (v), according to the stoichiometry of the network presented in Figure C.3, with the addition of one exchange flux per structure to represent its potential secretion from the Golgi compartment. The glycan processing pathway model was assumed to start in the ER with the M9 structure [299] and included 62 species connected by 74 reactions. Structures and enzymes were connected according to the following rules: 1) the presence of galactose prevents the attachment of additional branching N-acetylglucosamine monomers onto the mannose of the glycan core; 2) stereoisomers are not distinguished (i.e., they are grouped into single entities); 3) fucose addition is possible only before the addition of the fifth N-acetylglucosamine; 4) removal of the 2 mannose sugars by mannosidase II is grouped into a single reaction [300]. Fluxes were considered time invariant [277]. In addition, a pseudo steady state was assumed for structures within the Golgi, given that the protein residence time in the Golgi (20–40 min) is much shorter than any observed change in protein glycosylation, which is on the order of days [11, 299]. The balance of the fluxes between the different glycan structures within the glycosylation network can therefore be written as 5.1:

$$S\,v = 0 \tag{5.1}$$

To evaluate internal fluxes (*i.e.*, the fluxes within the glycosylation network), the vector v was divided into two components, v_i and v_e, representing the unknown internal and the measured exchange fluxes (*i.e.*, the rates of secretion of the glycans), respectively. The latter correspond numerically to the measured glycan fractions and were therefore used as inputs into the model. Similarly, the stoichiometric matrix was split into an internal stoichiometric matrix S_i and a stoichiometric matrix of the exchange fluxes S_e, such that Eq. 5.1 can be written as (Eq. 5.2):

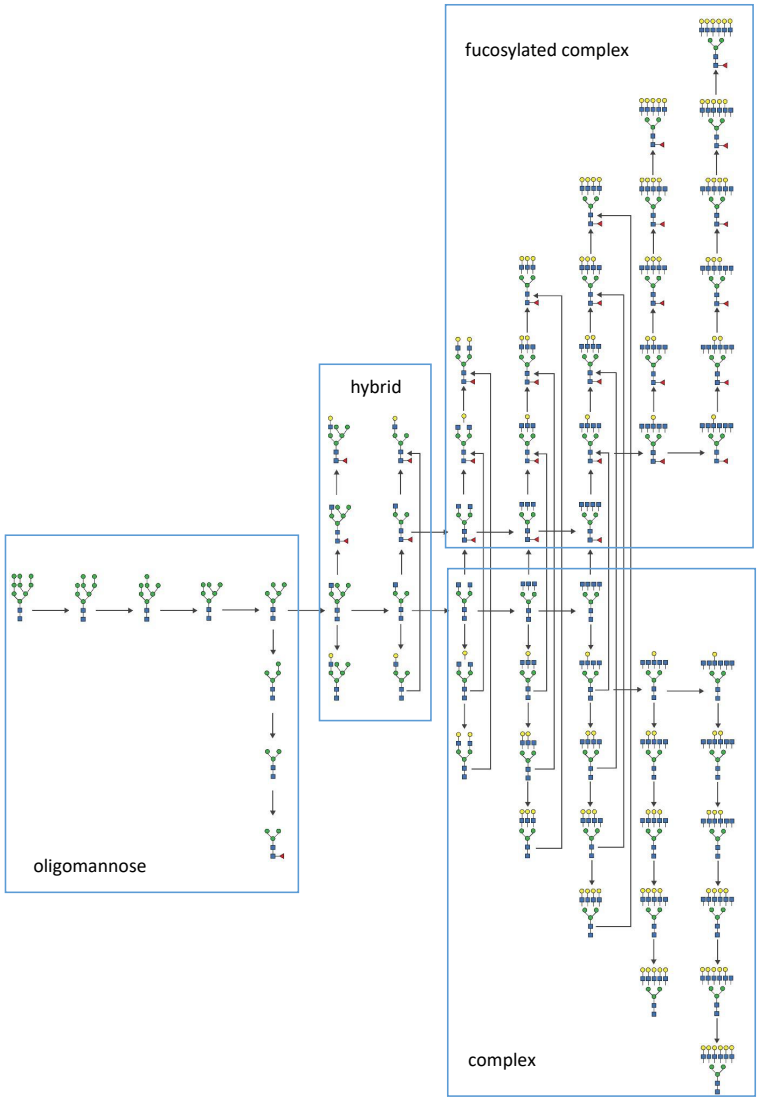

Figure 5.1: Representation of the nonsialylated glycan structures and glycosylation network in CHO-S cells.

$$S_i v_i + S_e v_e = 0 \tag{5.2}$$

For the network studied, the number of reactions exceeds the number of structures measured because of the branching and converging of many pathways (i.e., at least one glycan structure can be synthesized in two or more different ways). This disparity results in an under-determined problem with multiple flux distributions as a solution that can fit the data equally well. To obtain a fully determined system with a unique solution, converging pathways were constrained to be equal, which can be formulated as a linear constraint (5.3):

$$Q v_i = 0 \tag{5.3}$$

This allows matrix inversion of the matrix composed by S_i and Q (5.4):

$$\begin{bmatrix} S_i \\ Q \end{bmatrix} \tag{5.4}$$

Equation 5.2 can be solved to find vi using the fixed network structure and the measured exchange fluxes as only inputs into the model (Eq. 5.5):

$$v_i = -\begin{bmatrix} S_i \\ Q \end{bmatrix}^{-1} S_e V_e \tag{5.5}$$

Fluxes define the rate at which a species is processed within a given pathway. Because rates depend on substrate availability, fluxes do not provide any direct information about enzyme activity. We therefore calculated the conversion of each enzymatic step by normalizing the corresponding flux with respect to the sum of all fluxes leading up to the glycan structure that is being consumed in the reaction under investigation (Eq. 5.6):

$$\xi_i = \frac{v_i}{\sum v^{in}} \tag{5.6}$$

All computations were performed in Matlab R2014a (Mathworks, Natick, MA, USA).

5.3 Results

5.3.1 PDI Expression

PDI contains 5 N-glycosylation sites (N82/N117/N155/N174/N425, numbered according to full-length PDI protein) [301]. We transiently expressed secreted (without HDEL retrieval sequence) and the ER-retained form of PDI (with the HDEL retrieval sequence), respectively, called secreted Sec-PDI and ER-PDI [277], in Freestyle CHO-S cells. Recombinant N-terminally His10-tagged PDI proteins were purified via Ni-NTA affinity chromatography. After purification and concentration, proteins were reduced, alkylated, and digested by trypsin. For the secreted protein, samples were digested by neuraminidase to remove terminal sialic acids residues. A list containing the calculated m/z of the 5 PDI glycosites bearing 62 potential glycan structures of the canonical N-glycosylation pathway of mammalian cells was created Figures C.1 and C.2 , and relative quantification of these glycopeptides was performed as described elsewhere [277]. For the subsequent analysis, the structures experimentally detected were organized and grouped according to the network presented in Figure 5.1. For each structure, the relative abundance on each site was calculated by normalizing the absolute value measured to the sum of all the structures detected at the same site. For a simplified analysis, we grouped the glycostructures in oligomannose, hybrid, complex, and fucosylated complex, as depicted in Figure 5.1.

5.3.2 Site-Specific N-glycan Processing in the ER and in the Golgi

As expected, because of the lack of Golgi processing, ER-retained PDI contained primarily high mannose structures, which differed in the number of hexose units. We did not observe glycan structures that were modified by GlcNAc transferase I (GnT I) but the occurrence of a diverse set of high-mannose structures showed an exposure of the model protein to a set of mannosidases. Processing of the N-glycans by mannosidases was found to be site specific (Figure 5.2). Sites 1, 2, 3, and 5 carried primarily $Man_6GlcNAc_2$ and $Man_5GlcNAc_2$ glycans, whereas site 4 contained mainly $Man_9GlcNAc_2$ oligosaccharides, but further processed forms were also present. Site-specific glycan processing was also observed for the secreted form of PDI. Grouping the N-linked glycans into four major classes (oligomannose, hybrid, complex, and fu-

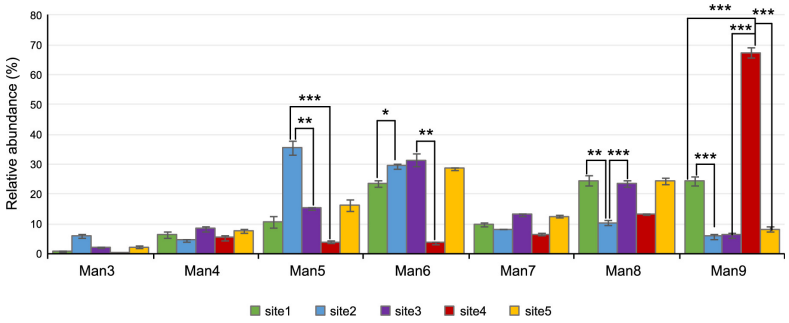

Figure 5.2: Site-specific glycosylation profile of ER-retained PDI in CHO-S cells. Relative abundances of the different glycoforms were calculated for each site. Data represent the average of 3 biologic replicates, for each of which 3 technical replicates were processed. Error bars denote sd.*P < 0.05; **P < 0.01; ***P < 0.001 (paired Student's t test).

cosylated complex) revealed major differences among the different sites (Figure 5.3). A more detailed representation of the quantitative site-specific glycosylation profile, displayed in connection with the processing pathway, revealed a site-specific glycosignature (Figure 5.4). Exposed to the same processing machinery at the same concentration, each glycosylation site leaves the secretory pathway with a highly reproducible, site-specific microheterogeneity. We note that the global trend was similar to the one observed for the same protein (yeast PDI) when expressed in insect cells [277]: elaborate processing of N-glycan at positions 1 and 3, strongly reduced processing at position 4. We concluded that this protein-specific position effect represents a major determinant of N-glycan processing; however, the processing machinery of the cell line used for expression determined the glycosylation space of the process.

5.3.3 Site-specific Flux Analysis

To evaluate the differences in the activity of the ER- and Golgi resident enzymes on the 5 glycosylation sites, we calculated the flux rates of the individual glycan-processing steps (glycosylation flux analysis) according to the stoichiometry defined by the network in Figure 5.1 and Figure C.3. We observed that site-specific microheterogeneity was the result of directed fluxes and resulted in a site-specific clustering of glycostructures (Figure C.4). Fluxes were generally found to be larger for the first stage of reactions, corresponding to the trimming of mannose residues by the mannosidase I and II enzymes and N-acetylglucosamine addition by GnT I (Figure 5.4). Fluxes downstream in the network showed diverging characteristics to reflect the microheterogeneity mea-

sured in the 5 PDI glycosylation sites. For example, fluxes connected to fucose addition were substantially lower in sites 3 and 4 when compared to the other sites, reflecting the lower levels of fucosylation measured by glycopeptide analysis.

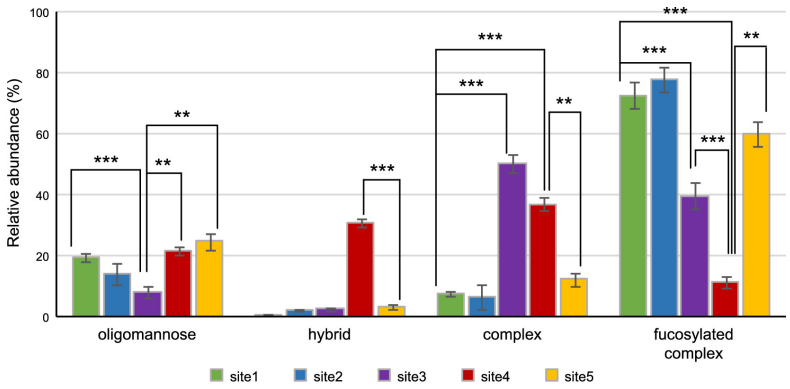

Figure 5.3: Site-specific relative abundance of glycans on secreted PDI. Relative glycan abundances were calculated for each site, then grouped according to glycan types corresponding with oligomannose, hybrid, complex, and fucosylated complex types. Data represent the average of 3 biologic replicates, for each of which 3 technical replicates were processed. Error bars denote sd.*P < 0.05; **P < 0.01; ***P < 0.001 (paired Student's t test).

5.3.4 Altering Site-Specific N-Glycan Processing by PDI point Mutations

To address the role of the primary sequence of PDI on N-glycan processing, we relied on the previously published molecular dynamic simulations of the $Man_9GlcNAc_2$ oligosaccharides interactions with the protein surface [277]. We identified potentially interacting residues and performed site-directed mutagenesis to determine their impact on the glycan heterogeneity.

First, we focused on tyrosine residue 178, located on the α helix of the glycosylated sequon at site 4. This residue, 1 turn from the glycosylated Asn (+4 AA), appears to interact with the hydrophobic site of the reducing end GlcNAc of the N−glycan (Figure 5.5 A). When mutated to an alanine, both the ER retained and the secreted proteins (ER−Y178A and Sec−Y178A) presented an altered processing specifically on site 4 as compared to the wild−type PDI. Processing of the other N−glycosides was not affected (Figure 5.5 B). We measured a higher degree of site 4 processing: more trimming of the high−mannose oligosaccharide in case of the ER−retained PDI and a strong shift toward the synthesis of fucosylated complex type glycans in the secreted protein was

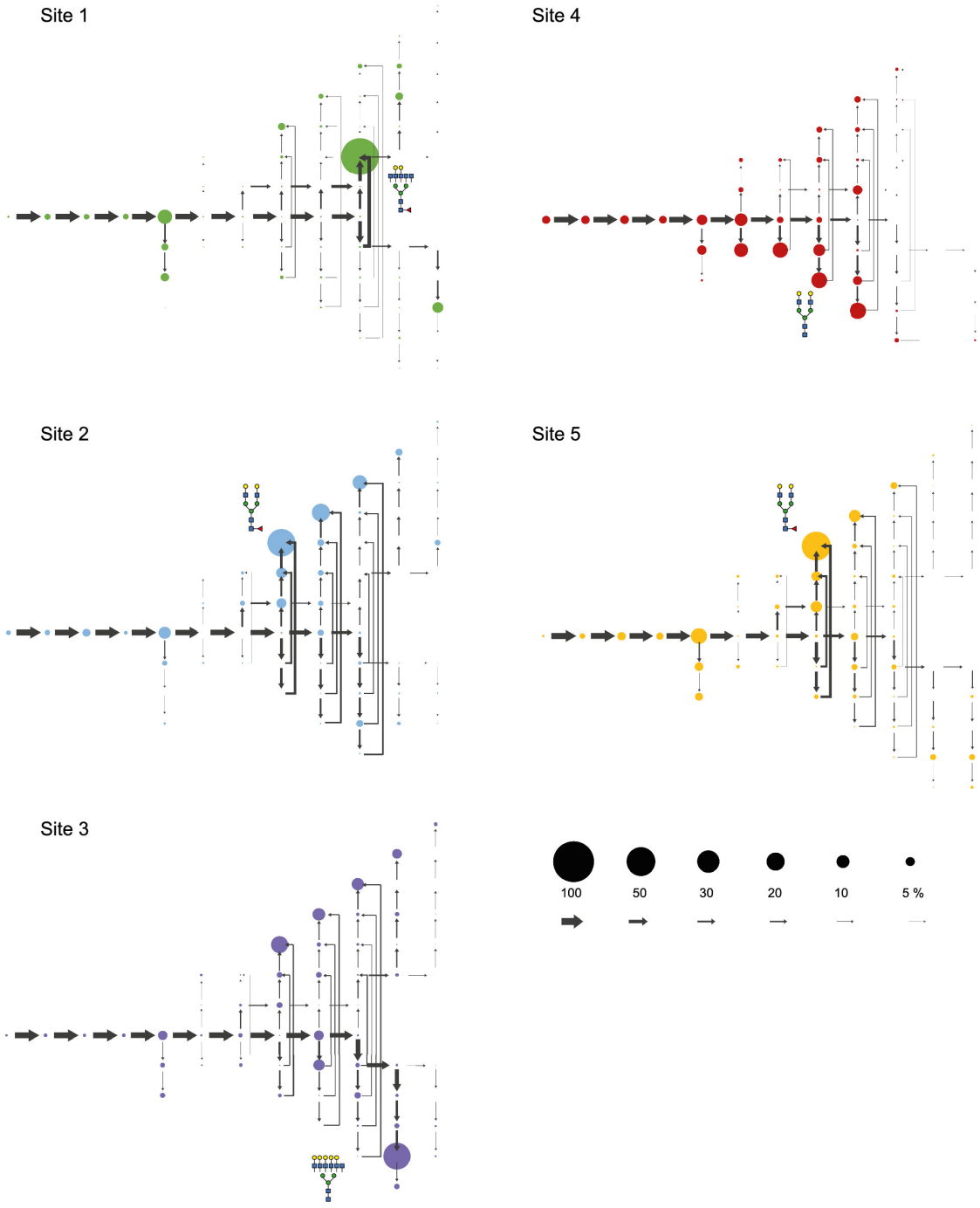

Figure 5.4: The relative abundance of each glycan is represented by dots of proportional sizes and ordered according to the glycosylation network presented in Figure 5.3. Proportional arrows: enzymatic fluxes calculated with the glycosylation flux analysis.

observed. It is worth noting that site 4 of Y178A PDI presented a heterogeneity signature profile similar to those of sites 2 and 5 in the wild−type (Figure 5.6 A Figure 5.7 B).

We then evaluated additional mutations that changed Y178 to threonine (Y178T), histidine (Y178H), or phenylalanine (Y178F). Processing in the ER was increased for ER-Y178T and ER-Y178H on site 4 only as was the case for ER-Y178A (Figure 5.5 C-D). The level of $Man_9GlcNAc_2$ was intermediate in ER-Y178H, suggesting a role of the π stacking in the modulation of processing. Indeed, no change in mannose trimming was observed on ER-Y178F, as compared to wild-type (Figure 5.5 E). In contrast, Sec-Y178F presented a significant increase in oligomannose structures and a decrease in complex structures on site 4 when compared to the wild-type (Figure 5.5 B and Figure 5.7 C).

To further test our hypothesis that glycan–protein interaction is a major determinant of site-specific processing, we took advantage of the fact that both sites 3 and 5 are also located in an α helix (as it is the case for site 4) and exchanged the D421 and A151, both located 1 turn (+4 AA) from the glycosylated asparagine, into a tyrosine residue. The effect of these mutations on site-specific processing was less pronounced, as compared to the mutations at position 4 of PDI. The microheterogeneity of the site 5 glycan was altered in the D421Y mutant, with an increase of oligomannose structures (Figure 5.8). Of further note, a small effect on site 4 was also observed. For the A151Y mutant, no change was observed relative to the wild-type in neither the ER nor the secreted form (data not shown).

5.3.5 Site-Specific Heterogeneity can be Reconstructed by Flux Analysis

To estimate changes in enzyme activity on the site-specific N-glycan processing, we calculated the conversion rate of the enzymes acting on each structure by normalizing the outgoing fluxes of that glycan structure with respect to the sum of all incoming fluxes to that structure. This analysis revealed that in wild-type PDI, mannosidase I and especially mannosidase II enzymes presented a lower conversion rate for site 4, compared with the other sites (Figure 5.9 A and C). This difference explains the high levels of hybrid structures measured for site 4 on secreted PDI. The same calculation, applied to the heterogeneous output of the Y178A mutant, showed a large and site-

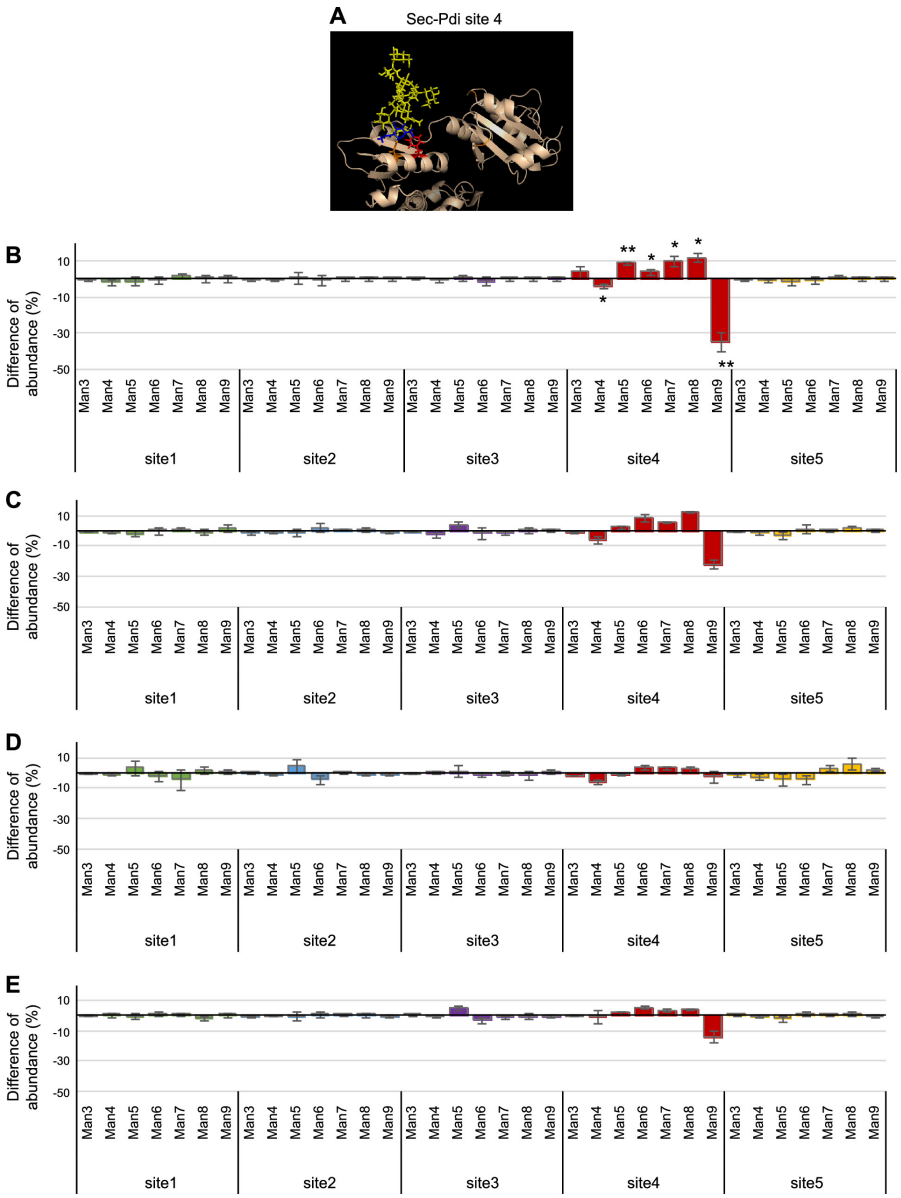

Figure 5.5: Alteration of the ER-retained PDI glycan profile on site 4. A) Truncated PDI structure simulation representing the respective position of the glycan anchor in red and the targeted amino acid in orange. B–D) Histograms represent the difference of glycan abundance between ER-retained wild-type PDI and Y178 for ER-Y178A PDI (B), ER-Y178T (C), ER-Y178H (D), and ER-Y178F (E). Glycan relative abundance was calculated for each site, and the wild-type control level was deducted from mutant levels. Data represent the average of 3 biologic replicates. Error bars denote sd. *P < 0.05; **P < 0.01; ***P < 0.001 (paired Student's t test).

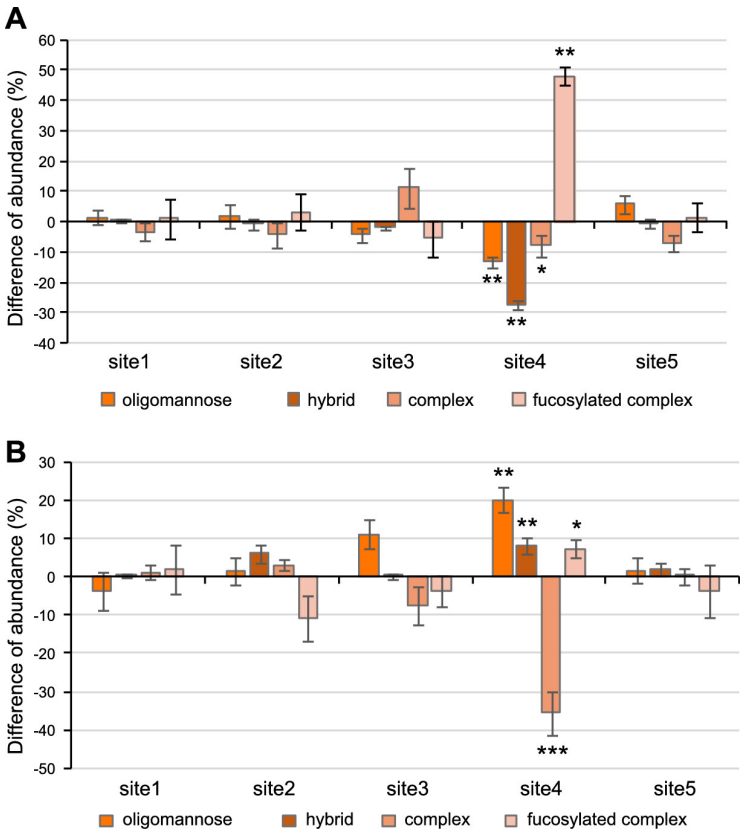

Figure 5.6: Alteration of the secreted PDI glycan profile on site 4. Histograms represent the difference in glycan abundance between secreted wild-type PDI and Y178 mutants respectively for Sec-Y178A PDI (A) and Sec-Y178F PDI (B). Relative abundance of glycans was calculated for each site, and the level of wild-type control was deducted from mutant levels. Data represent the average of 3 biologic replicates. Error bars denote sd. *P < 0.05; **P < 0.01; ***P < 0.001 (paired Student's t test).

specific increase in α-mannosidase II activity on site 4 (Figure 5.9 C), indicating the loss of the bottleneck in the processing of mutant glycoprotein. For Sec-Y178F, we found that the altered processing was explained by a decreased α-mannosidase I conversion rate, resulting in the accumulation of oligomannose structures (Figure 5.9 A). Finally, for Sec-D421Y flux analyses showed that GnT1 rate was decreased by 15% on site 5 in this mutant (Figure 5.9 B), but remained stable for the other sites.

In summary, our results revealed that site-specific glycosylation is strongly influenced by the interaction of the oligosaccharide with the surface of the glycoprotein and that a single mutation can alter this interaction significantly. We noted that the monosaccharide involved in this interaction (e.g., GlcNAc residue), which is not directly affected

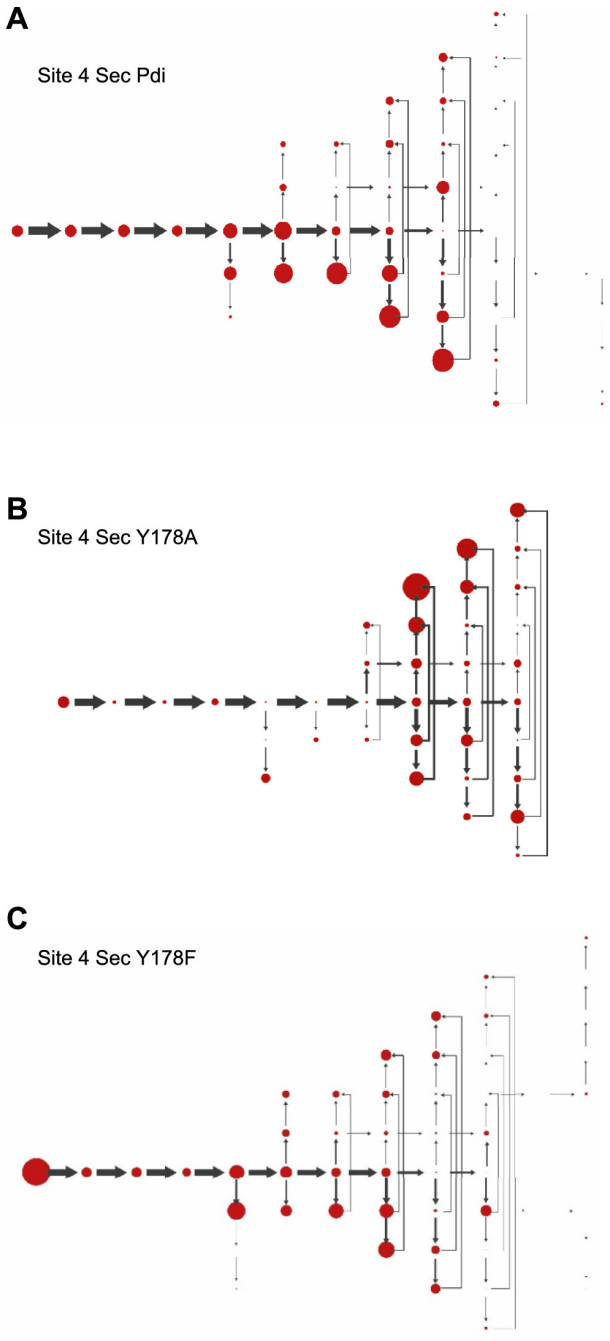

Figure 5.7: Relative abundance of glycans on site 4 of Sec-Y178 mutants and corresponding enzymatic flux. A) Glycan profile of site 4 in Sec-PDI. B) Glycan profile of site 4 in Sec-Y178A mutant. C) Glycan profile of site 4 in Sec-Y178F mutant. Relative abundance of each glycan is represented by different dots ordered according to the glycosylation network presented in Figure 5.1. Proportional arrows denote enzymatic fluxes.

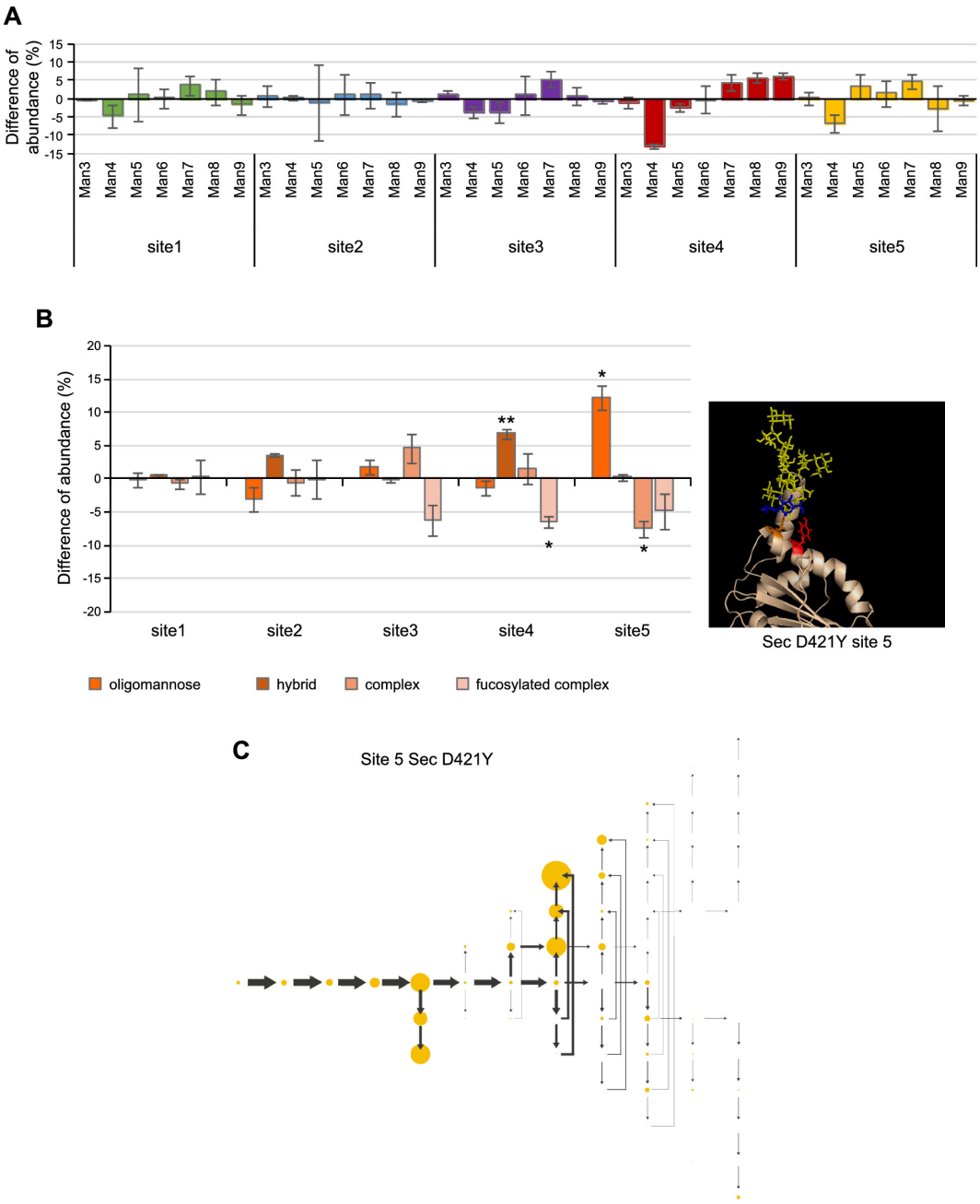

Figure 5.8: A) ER-D421Ycompared to ER- PDI. B) Sec-D421Y compared to Sec-PDI. Right: simulated truncated PDI structure; red, respective position of the glycan anchor; orange, targeted amino acid. C) Glycan profile of site 5 in the Sec-D421Y mutant. Relative abundance of each glycan is represented by dots ordered according to the glycosylation network presented in Figure 5.1 Proportional arrows denote enzymatic fluxes. Relative abundances were calculated for each site and represent the average of 3 biologic replicates. Error bars denote sd. *P < 0.05; **P < 0.01; ***P < 0.001 (paired Student's t test).

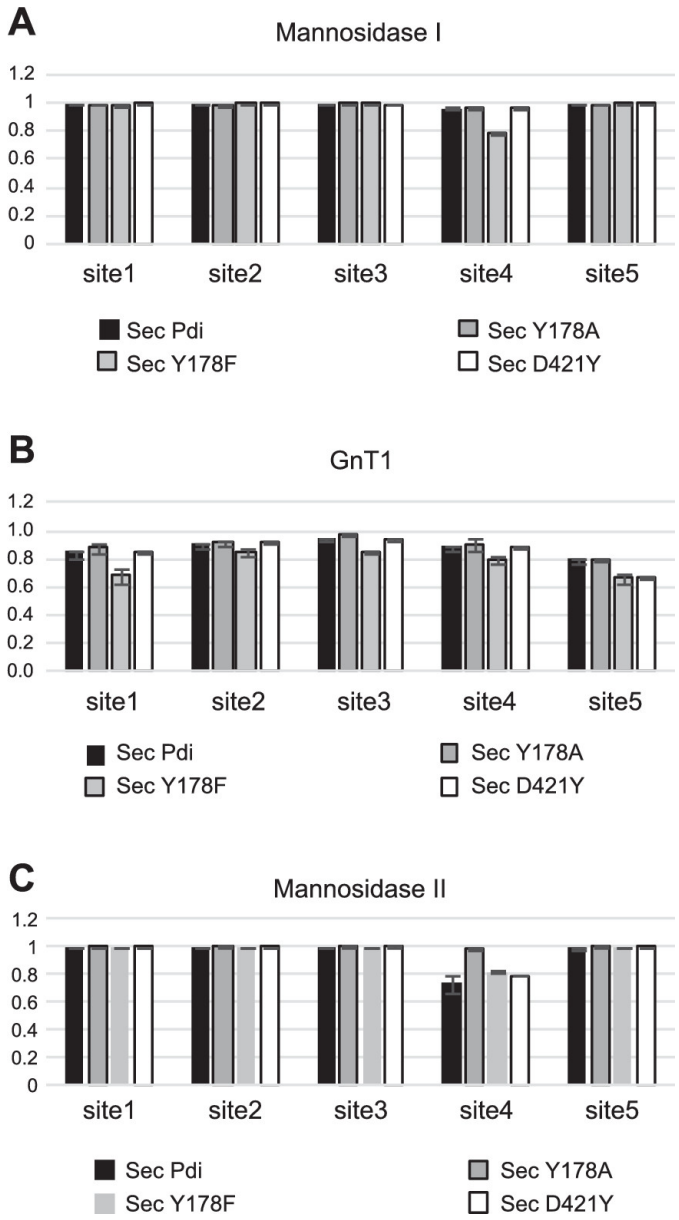

Figure 5.9: Influence of mutations on specific enzyme conversion rates. The site-specific conversion rates calculated for mannosidase I (A), GnT1 (B), and mannosidase II (C) of Sec-PDI, Sec-Y178A, Sec-Y178F, and Sec-D421Y. Error bars denote sd.

in the processing step (*i.e.*, not trimmed or elongated), could have an effect on the interaction equilibrium of the whole glycan with the protein surface, resulting in an apparent alteration of substrate concentration or accessibility.

5.4 Discussion

In this study we expressed in mammalian cells the ER-retained and secreted forms of PDI carrying point mutations in the vicinity of the glycosylation sites, and monitored the resulting changes in the heterogeneity of glycan structures on the 5 sites of glycosylation, both in terms of relative abundance and in the enzymatic fluxes. Other studies have hypothesized the role of the protein's tridimensional structure in glycan processing [277, 302, 303]. Hang et al. [277] demonstrated the importance of the domain a of PDI in the trimming of site 4, by deleting the whole domain, and thus removing the potential interaction of this domain with glycan antennae. We showed that this influence is most likely not caused by a steric hindrance caused by the protein structure surrounding the glycan, which could reduce its accessibility to the processing enzyme, but by direct interactions of specific amino acids with the glycan structure. Indeed, molecular dynamics analyses on our model protein had suggested a direct interaction of the glycan with surrounding amino acids [277] and recent studies characterized the CH-π interaction between the CH groups of the first GlcNAc of the glycan core and aromatic amino acid side chains of the glycoproteins [304]. The presence of phenylalanine at the -2 position of the N-glycosylation sequon localized in a reverse turn increases the stability of the protein, but also of glycan homogeneity [305–307]. We thus hypothesized that, in PDI, the glycan structures observed on site 4 are the result of the change in the glycan torsion caused by the interaction of the core GlcNAc with the tyrosine, itself favoring the interaction of the whole glycan with the protein surface and the domain a of PDI. Flux analysis and calculation of enzymatic conversion rate allowed us to pinpoint mannosidase II activity as the limiting step of the site 4 glycan processing in PDI. We also demonstrated that it is possible to modulate the degree of processing by selectively modifying the interacting amino acid residue: phenylalanine reduced the degree of processing, whereas nonaromatic side chains shifted Golgi processing toward a more default value represented by site 2 and 5 structural microheterogeneity. This concept was not limited to a specific site, because the introduction of a tyrosine one turn away in the α helix on the site 5 sequon resulted in decreased glycan processing, although to a lesser extent than

at site 4. In this case, we identified GnT I activity as being modulated, showing that not only trimming, but also the initial part of the elongation is affected by surface glycan interaction, in line with other reports that suggested the effect of N-glycan–carbohydrate interaction on glycan processing and protein structure [302, 303, 308]. For example, studies performed on antibodies showed the role of a phenylalanine on the IgG glycan distribution by modifying the protein stability [297, 298].

We used a model glycoprotein with multiple glycosylation sites that revealed site-specific microheterogeneity. For sites 2 and 5, our quantitative analysis revealed an almost identical glycan pattern. We propose that this glycan distribution is the optimal output of a processing system, where most of the enzymatic reactions do not go to completion (as visualized by the calculated conversion rates). For N-glycans 2 and 5, this processing was not affected by additional factors, such as glycan–protein interaction, that reduce the apparent substrate concentration for specific modification reactions. The relative effect on the processing is therefore given by the strength of the interaction, determined by the glycan structure and the structure of the protein. Within the framework of our hypothesis, it is the primary structure of the protein that determines site-specific glycan structures in a given N-glycan processing setting, and individual point mutations can result in different glycan structure alterations. Accordingly, site-specific microheterogeneity becomes a property that can be selected at the primary genetic level. An alternative explanation of site-specific processing is a steric hindrance of access for the processing enzymes by the glycoprotein substrate itself. For the experimental system described in this study, we consider this hypothesis to be unlikely. The specific point mutations introduced in the immediate vicinity of the N-glycosidic linkage affect primarily the processing of nonreducing end mannoses, far away from the mutated amino acid residues. In addition, the replacement of tyrosine with the less bulky phenylalanine reduces the N-glycan processing, which is compatible with the increased stacking potential of phenylalanine vs. tyrosine, but not explained by a steric hindrance model. On the other hand, it is evident that reduced accessibility of N-glycans to the processing enzymes related to steric hindrance is a determining factor in glycan remodeling of many other N-linked glycoproteins.

Protein-directed site-specific glycosylation requires a network where individual reactions do not go to completion; otherwise, the transient, noncovalent interaction of the N-linked glycan with the protein surface (or reduced accessibility due to steric hindrance) would not yield site-specific processing. Accordingly, the organization of the

secretory pathway in eukaryotic cells evolved for this purpose; limited exposure time of glycoprotein substrates to processing enzymes because of defined localization of enzymes in Golgi stacks, limiting enzyme, or substrate concentrations are properties that are the prerequisite for primary sequence-directed glycan maturation. The structural organization of the secretory pathway in eukaryotic cells therefore follows the functionality of site-specific glycan processing, generating novel properties mediated by site-specific structures [105, 279, 309, 310].

It is evident that for biotechnological application, the route of primary sequence-directed site-specific glycan processing offers unique opportunities to provide novel functionalities to proteins. However, it is also apparent that small changes in the glycomachinery settings of glycoprotein expression can have strong effects on site-specific glycan structures, a fact well known in the field of glycoprotein production [311].

Most of the presently available glycoengineering techniques address and alter the processing machinery by knocking down, inhibiting, or overexpressing glycosylation enzymes [283, 285, 291, 292, 312, 313] and thus are designed to modify simultaneously all the glycans carried by a given protein. Combining site-directed glycoprotein mutagenesis and classic glycoengineering techniques toward the limiting enzymes, as determined by flux analysis, can yield specific and targeted distributions of glycan on a single site. Acquisition of such defined glycan profiles may be a great plus for novel application of recombinant glycoproteins.

The notion of site-specific microheterogeneity of glycans as a functional output of the eukaryotic secretory apparatus asks for more precise analytical approaches to address glycoprotein function. Mass spectrometry-based glycoproteomics technologies will be essential in meeting this requirement.

Chapter 6

Mechanistic Reconstruction of Glycoprotein Secretion Through Monitoring of Intracellular N-Glycan Processing

This chapter is based on the following publication: I. Arigoni-Affolter, E. Scibona, CW. Lin, D. Bruehlmann, J. Souquet, H. Broly and M. Aebi, *submitted*.

The author of this thesis contributed in designing the mathematical model, performing the simulations and participated in the data representation and the writing of the manuscript.

For the experimental section of this chapter, all credit goes to I. Arigoni-Affolter and CW. Lin. For details, please refer to Appendix D.

6.1 Introduction

N-linked protein glycosylation involves the attachment and modification of a complex carbohydrate to the amide nitrogen of asparagine residues in the Asn-X-Ser/Thr* consensus sequence of newly synthesize proteins. This post-translational modification is present in all domains of life [314], and plays a major role in protein folding, quality control, degradation and receptor signaling [262]. In contrast to nucleic acids and peptides, the synthesis of N-Glycans is a non-template driven process, which results from a complex biosynthetic pathway comprising many compartmentalized reactions [315]. The process begins at the cytoplasmic face of the ER of eukaryotic cells with the synthesis of a membrane-bound dolichol-linked precursor oligosaccharide ($Glc_3Man_9GlcNAc_2$), which is transferred *en bloc* to nascent polypeptides bearing an accessible consensus sequence by the oligosaccharyltransferase (OST) enzyme [316]. Glycosyl hydrolases that are part of the glycan-directed folding and quality control machinery of the ER trim three glucoses and up to four mannose residues from the initial $Glc_3Man_9GlcNAc_2$ glycan [317]. The properly folded glycoproteins are encapsulated inside lipid vesicles and transported to the Golgi apparatus [318], where multiple enzymes trim and elongate the N-glycan to yield the secreted glycoprotein. Despite starting from a defined oligosaccharide ($Glc_3Man_9GlcNAc_2$), the subsequent steps of N-glycan processing are usually not carried out at 100% efficiency, resulting in the generation of species-, cell- and site-specific heterogeneous mixture of N-linked glycans. This heterogeneity is determined by several factors, including the activities and localization of processing enzymes, the availability of nucleotide sugar donors, the culture conditions and the structure of the glycoprotein itself [271, 272]. N-glycan heterogeneity is tolerated by regulatory agencies, but poses a great challenge for the development of biosimilars and biobetters due to its significant impact on the biological activity of therapeutic proteins [319].

Current knowledge about the N-glycosylation reaction machinery relies on a) in vitro experiments that determine the activity and substrate specificity of various glycosyl transferase and hydrolases [320–324], and b) on microscopy and biochemistry data that provide the localization of the different enzymes and substrates within the ER and the Golgi [266, 325–329]. Although metabolic studies and mathematical models have contributed in providing possible descriptions of the N-glycosylation process [11, 330],

*Asn=Asparagine, Thr=Threonine, Ser=Serine, X=any amino acid except Proline.

they most often assumed and oversimplified the organization of the N-glycosylation machinery, since they have been developed with the aim of predicting the only the distribution of secreted oligosaccharides [11, 275, 331, 332]. This chapter presents a novel experimental approach for the characterization of the secretory pathway in mammalian cells, which is based on the monitoring and quantification of intracellular N-glycan processing. The methodology used combines PRM (parallel reaction monitoring), a quantitative targeted MS approach to quantify glycopeptides, with dynamic SILAC [333], a protein labelling technique to follow the kinetics of protein-bound glycans. The experimental data were used to formulate a kinetic model for intracellular glycoprotein processing, the retrieval of activity-based localization profiles as well as relative kinetic parameters of glycosyl transferases and hydrolases in the N-glycosylation reaction network. Thr results confirm and refine concepts on glycoprotein processing in the ER and the Golgi, suggesting an additional pathway for the export of folding intermediates from the ER directly to the lysosome.

6.2 Mathematical Modeling

A mechanistic model was developed to describe the time-dependent formation of the different oligosaccharide structures and reveal the kinetic informations of the various processing steps throughout the entire pathway. Compared to previous modeling works [11, 190, 299], this model takes into account the processing steps in the ER, considers different conformational configurations of the model protein, provides a solution for the localization of Golgi-resident enzymes which is not derived only by the information concerning the secreted structures and is able to describe the intracellular kinetics of the system. The following section provides information concerning all the theory and assumptions behind the model.

6.2.1 Modelling of the N-Glycan Pathway in the ER

After addition of the isotopic tracers in the medium, the incorporation of heavy labelled amino acids (H-AAs) on peptides occurs in the cytoplasm during RNA translation. Although the extracellular AA composition switch is very rapid, assuming an instantaneous switch from 100% L to 100% H-labeled peptides production leads to inaccurate predictions for the kinetics of the ER species in the model (data not shown). This is

probably due to the presence of an intracellular pool of L-AAs with a delayed consumption kinetic. To account for this, we assumed that the production of H-labeled HCs (q_p^H) follows a first order kinetic behavior (Eq. 6.1).

$$q_p^H = q_p^{max} - q_p^{max} e^{-t/\tau} \tag{6.1}$$

Where q_p^{max} the maximum cell productivity at steady state and $/tau$ is the time constant representing the delay in the turnover of intracellular H-AAs. This time constant was arbitrarily set to 10 minutes as measured by ^{13}C flux analysis on CHO cells [334]. The N-glycosylation pathway starts in the endoplasmic reticulum (ER) with the attachment of the $Glc_3Man_9GlcNAc_2$ glycan on the HC N-S-T motif catalyzed by the oligosaccharyltransferase (OST) enzyme. For the sake of simplicity, this step was assumed to occur co-translationally with the peptide synthesis, so that the production of the H-$Glc_3Man_9GlcNAc_2$ glycan is equal to q_p^H. The $Glc_3Man_9GlcNAc_2$-bearing HC is a transient species where the peptide is in a linear chain conformation deriving from the translocation into the ER. Since the purification method used (protein A affinity capture) requires the initial folding of the CH2 and CH3 domains of the HC [335], the detection of $Glc_3Man_9GlcNAc_2$ glycopeptides is possibly biased, since it can be attributed not only to the action of the OST, but also to the folding of the aforementioned domains. For this reason, the species $Glc_{1-3}Man_9GlcNAc_2$ (generated by ER Glucosidase I and II) were excluded from the model, and the kinetic constants relative to ER Glucosidase I and II set to be 100 times faster than the cell specific productivity q_p^{max}, due to the impossibility of correctly identify their values. After glucose trimming, we assume the HCs to reach a partially folded, protein A-binding state, represented by the $Man_9GlcNAc_2$ structure. This structure can either enter the quality control machinery of the ER (and lose mannose residues due to the action of EDEMs), or it can fold correctly and become available for translocation to the Golgi. It is important to mention that the folding step included in the model lumps together a series of transitions which include HC folding, LC folding, HC-LC dimerization and disulfide bond formation, which are indistinguishable from an N-glycosylation point of view. For the sake of simplicity, the reaction rate representing the single-step transition from partially to completely folded is assumed to follow a first order kinetic (Eq. 6.2) [336] and to share the same kinetic constant $k_{folding}$ for all the partially folded glycoprotein isoforms in the ER (denoted by the term S^{NF}).

$$r_{folding} = k_{folding} S^{NF} \tag{6.2}$$

The transport to the Golgi apparatus was assumed to be selective for all correctly folded species S^F (this is mathematically equivalent to assuming a perfect recycling of non-folded species) and to follow first order kinetics (with constant $k^{Golgi}_{Transport}$), similarly to folding (Eq. 6.3). To prevent parameter unidentifiability, the transport from ER to Golgi was assumed to be much faster than the folding step, and $k^{Golgi}_{Transport}$ was constrained to be 10^4 times $k_{folding}$.

$$R^{Golgi}_{Transport} = k^{Golgi}_{Transport} S^F \tag{6.3}$$

Non-correctly folded species in the ER can enter two different degradation pathways: the ERAD pathway, leading to cytosolic degradation, and a secondary pathway, leading to lysosomal transport and degradation. The lysosomal degradation pathway leads to the formation of the $Man_4GlcNAc_2$ glycan. From a kinetic standpoint, the appearance of this species is best explained by assuming its generation deriving solely from Glc_1Man_9. This species undergoes a transition to a terminally misfolded state, possibly linked to aggregation, with kinetic constant k_{agg}. Due to lack of information concerning lysosomal transport, this step is assumed to be instantaneous and to follow a first order mechanism (Eq. 6.4). After lysosomal translocation, the Glc_1Man_9 glycan is assumed to be trimmed down to a terminal $Man_4GlcNAc_2$ species (k^{Lys}_{Man}, Eq. 6.5), which is then degraded together with its protein backbone (k^{Lys}_{Deg}, Eq. 6.6). Since the parameter k^{Lys}_{Man} not be uniquely identified by the model, and given that $Man_4GlcNAc_2$ appearance is very fast compared to most of the species detected, we assumed aggregation and lysosomal transport to be the limiting steps in this process, and therefore set k^{Lys}_{Man} 100 faster than k_{agg}.

$$r^{Lys}_{T} = k_{agg} Man_9Glc_1 \tag{6.4}$$

$$r^{Lys}_{Man} = k^{Lys}_{Man} Man_9Glc^{Lys}_1 \tag{6.5}$$

$$r^{Lys}_{Deg} = k^{Lys}_{Deg} Man^{Lys}_4 \tag{6.6}$$

The ERAD degradation pathway is glycan-specific, since it is triggered by the exposure of terminal α1,6 mannose [337]. This was implemented in the model by including first a transport term to the cytosol for $Man_{7-5}GlcNAc_2$ bearing non-folded glycopro-

teins with first order kinetics with respect to substrate concentration (k_T^{Cyt}, Eq. 6.7), and subsequent degradation (k_{Deg}^{Cyt}, Eq. 6.8).

$$r_T^{Cyt} = k_T^{Cyt} Man_{7-5}GlcNAc_2^{NF} \tag{6.7}$$

$$r_{Deg}^{Cyt} = k_{Deg}^{Cyt} Man_{7-5}GlcNAc_2^{Cyt} \tag{6.8}$$

6.2.2 Modelling of the N-Glycan Pathway in the Golgi Apparatus

After translocation from the ER, folded Glycoproteins (i.e., correctly folded and dimerized mAbs) travel through the various stacks of the Golgi, where the N-glycans are modified by the action of several compartmentalized enzymes, before being secreted to the extracellular environment. The transport through the Golgi apparatus is assumed to occur at a constant linear velocity (the residence time in the Golgi was fixed at 20 min according to the secretion data) and are secreted only after they reach the end of the entire system. Like all other reaction rates considered, the action of glycosyltransferases is assumed to follow first order kinetics with respect to the substrate concentration. To correctly represent the spatial compartmentalization of the different enzymes, the kinetic parameters for Golgi resident enzyme-catalyzed reactions were assumed to vary with respect to the position along the Golgi stacks (represented by the coordinate z). Although this behavior can in principle be modeled using any continuous function, we decided to define the window of activity of all Golgi resident enzymes using normal Gaussian distributions (Eq. 6.9).

$$k_i(z) = E_{i,max} e^{\left(-\frac{z-z_{i,max}}{2\omega_i}\right)^2} \tag{6.9}$$

Where $k_i(z)$ refers to the value of the kinetic constant for the reaction catalyzed by Golgi enzyme i at position z, and $E_{i,max}$, $z_{i,max}$ and ω_i represent the peak height, the peak position and the width of the enzymatic window of activity, respectively. The peak height and the width of the distribution are highly correlated in defining the total window of activity (*i.e.*, the area under the curve for a given enzymes). For example, the area under the curve remains the same if the peak height decreases and the width increases by a certain amount. For this reason, the parameter ω_i was constrained to take the same value for all Golgi resident enzymes to prevent a priori parameter unidentifiability.

6.2.3 Material Balances

The mass balance for the species S in the ER (either folded or unfolded) assumes homogeneous distribution of both enzymes and substrates (perfect mixing) and perfect selectivity for transport (*i.e.*, only folded proteins move to the Golgi and only non-folded proteins are degraded). Mathematically, this translates as follows (Eq. 6.10):

$$\frac{dS_i}{dt} = q_i n - \sum_{j-1}^{N.R.} v_i r_j - q_{out} \tag{6.10}$$

The terms q_{in} and q_{out} represent transport in and out of the ER compartment, respectively. Inward transport is zero for all species except for $Glc_3Man_9GlcNAc_2$ bearing peptides, where it equals q_p^H, while outward transport depends on the folding and glycosylation processing as previously discussed. The term $\sum_{j=1}^{N.R} v_i r_j$ accounts for all the reactions described in the ER network. In this term, the indexes i and j are used for counting substrates and reactions respectively, such that i v is the stoichiometric coefficient for substrate i in reaction j (with sign -1 for reactants and +1 for products) and r is the corresponding reaction rate. Contrary to the ER, glycoproteins in the Golgi are not homogeneously distributed but vary in concentration along the entire apparatus. To account for this, the material balances includes a term to represent the special distribution of species S_i as presented in Eq. 6.11.

$$\frac{\partial S_i}{\partial dt} = -\frac{z_{Golgi}}{\tau_{Golgi}} \frac{\partial S_i}{\partial z} - \sum_{j-1}^{N.R.} v_i r_j \tag{6.11}$$

The terms z_{Golgi} and τ_{Golgi} represent the length and residence time in the Golgi, respectively, and their ratio defines the velocity of glycoprotein transport in the Golgi. The Golgi length was normalized to 1 and Golgi τ_{Golgi} was assumed to be 20 min, independently of the glycan or the position of the mAb. Please note that Eq. 6.11 corresponds to a model of cisternal maturation for the Golgi apparatus [299]. The mass balances for both ER and Golgi were solved for heavy labeled species, starting from the initial condition of 100% light-labeled species in the ER. For the Golgi, the initial condition $S_{i,Golgi}$ was set as non-zero only for the $Man_{9-5}GlcNAc_2$ glycoproteins (ER transport), and equal to (Eq. 6.12) at each time point and at $z = 0$.

$$S_{i,Golgi}(t) = \int_{t}^{t+dt} k_{Transport}^{Golgi} S_{i,ER}^{F}(t)\, dt \tag{6.12}$$

6.2.4 Model Construction and Parameter Estimation

system of ordinary differential equations (ODEs) of the ER was solved in MATLAB R2017a (The Mathworks, Natick, MA) using the built-in ODE15s solver. The system of partial differential equations of the Golgi was computed in FORTRAN using the solver DLSODES from ODEPACK. The solution was discretized along the Golgi axis z using first-order central finite differences (50 grid points). The entire system was numerically solved from 0 to 500 min after the L-H switch with a resolution of 5 minutes. Parameter optimization was performed using the genetic algorithm function of MATLAB, initialized with a latin hypercube sampling technique. The objective function was defined as the sum of least square errors between experimental data and the model output for ratios, intracellular fractions and secreted fractions of every species, except for $Glc_3Man_9GlcNAc_2$ and $Glc_1Man_9GlcNAc_2$. The error in the calculation of intracellular and secreted fractions was normalized with respect to the abundancy of each fraction. Evaluation of confidence intervals was performed with the *nlparci* function of MATLAB. The complete list of optimized parameters, together with their confidence intervals, is presented in Tables D.1 and D.2. Please note that all the kinetic parameters are normalized with respect to q_p^{max}, which was arbitrarily set equal to 1. Every parameter was identifiable in the control condition (i.e., the confidence intervals for the parameter do not include 0). Parameters that include 0 in their confidence interval were set to 0. Parameters that are related to reactions that do not occur due to inhibitions in the formation of one or more precursors were excluded from the calculation due to a priori unidentifiability.

6.3 Results

6.3.1 SILAC Coupled with Nano-UPLC-PRM Allows for Reliable Quantification of Glycopeptides from Intracellular and Secreted Recombinant IgG

IgGs containing a single N-glycosylation site at each heavy chain (HC), were purified from CHO cell extracts or culture supernatant via protein-A-capture. Glycoproteomics analysis was performed after tryptic digestion and reverse phase chromatography separation. For all detectable IgG tryptic glycopeptides, we performed data-dependent acquisition (DDA) with higher-energy C-trap dissociation (HCD) as described previously [277]. DDA data were used to generate the 30 target list for PRM analysis. Solutions containing different concentration of (glyco)peptides from secreted IgG samples were tested (10 μM to 200 pM, equivalent to 100 pmole to 1 fmole glycopeptides per analysis). Whereas the most abundant glycopeptides were still detectable at 200 pM (data not shown), less abundant ones, such as the sialylated glycopeptides, had a signal-to-noise ratio that prevented 35 quantification at concentrations below 100 nM total IgG (Figure D.1). The limit of detection (200 pM of IgG) was comparable to values obtained in previous studies [338]. Nevertheless, for a complete glycopeptide quantification, the limit of quantification was set at 100 nM IgG. To obtain the best fragmentation into Y ions (intact peptide with fragmentation at the glycan level), we tested different normalized collision energies (NCE). NCE=16 %, as opposed to NCE= 22 %, 40 gave the best fragmentation pattern: it led to decreased abundancy of the dominant Y1 ion (peptide with one N-Acetylglucosamine residue) and the oxonium ions (N-acetylglucosamine ions and disaccharide ions), and increased the abundancy of characteristic Y ions and unfragmented precursor ion (Figure D.2) [339].

As opposed to canonical tandem MS methods, where the precursor isolation window (Q1) is maintained as low as possible [340], we adjusted the analytical procedure and increased the Q1 isolation window to 6 Th, so that both heavy and light glycopeptides precursors were simultaneously isolated and fragmented (Figure 6.1 A). To evaluate the consistency of MS2-level quantification among all the different glycoforms, we analyzed different mixing ratios of heavy and light IgG and compared peak area- or height-based quantification. The ratio of all glycoforms was consistent with the original

IgG mixture (Figure 6.1 B and data not shown). The peak height-based quantification resolved into a more robust analysis for low-abundant glycoforms, so that we kept peak-height based quantification throughout the whole study. We compared the N-glycan distribution of secreted and intracellular IgG gained with MS1 quantification [277] with the MS2 quantification method described above (Figure 6.1 C). For both MS1 and MS2-based quantification, the N-glycan profile of secreted IgGs consisted of 80% complex N-glycan, whereas the intracellular IgGs presented 80% of high mannose N-glycan structures. The consistency between MS1 and MS2 based quantification, and the agreement with precedent studies on secreted or intracellular IgG glycan profiling using different MS approaches [331, 341] proved the suitability of the PRM-methodology for N-glycan profiling. To monitor intracellular IgG glycan processing, we coupled the PRM-based analytical setup to a dynamic SILAC regime. We purified IgGs from cell extracts that were lysed at different time points after switching to heavy SILAC medium. The fractional labeling of the different tryptic glycopeptides is reported in Figure 6.2 A. Labeled IgG glycopeptides bearing intermediates synthetized early in the N-glycosylation/secretory trajectory were detected shortly after the pulse (i.e. high mannose structures detected already after 10 minutes). In contrast, more complex, such as Golgi-derived fucosylated, galactosylated or sialylated N-glycopeptides appeared only after 20-60 minutes (Figure 6.2 A), indicating delayed accumulation/synthesis of the corresponding intracellular glycoform [327–329].

6.3.2 Mathematical Modeling enables the Derivation of Quantitative Kinetic Information of the Canonical N-Glycosylation Network

The fractional labeling data provided information about the turnover rates of the intracellular pools of defined IgG-bound glycans but cannot directly reveal the kinetic information and enzymatic activity windows along the secretory pathway. Therefore, we developed a mathematical model (detailed in the supplementary materials). The best fitting of the turnover reactions (Figure 6.2 A), the intracellular steady state N-glycan distribution (Figure D.3 A) and the final secreted N-glycan profiles (Figure D.4 A) were produced with the ER and Golgi networks presented in Figure 6.2 B-C. Importantly, a simple N-glycosylation model assuming a bare sequential order of glycosylation reactions did not fit the data successfully (data not shown). To correctly reproduce the

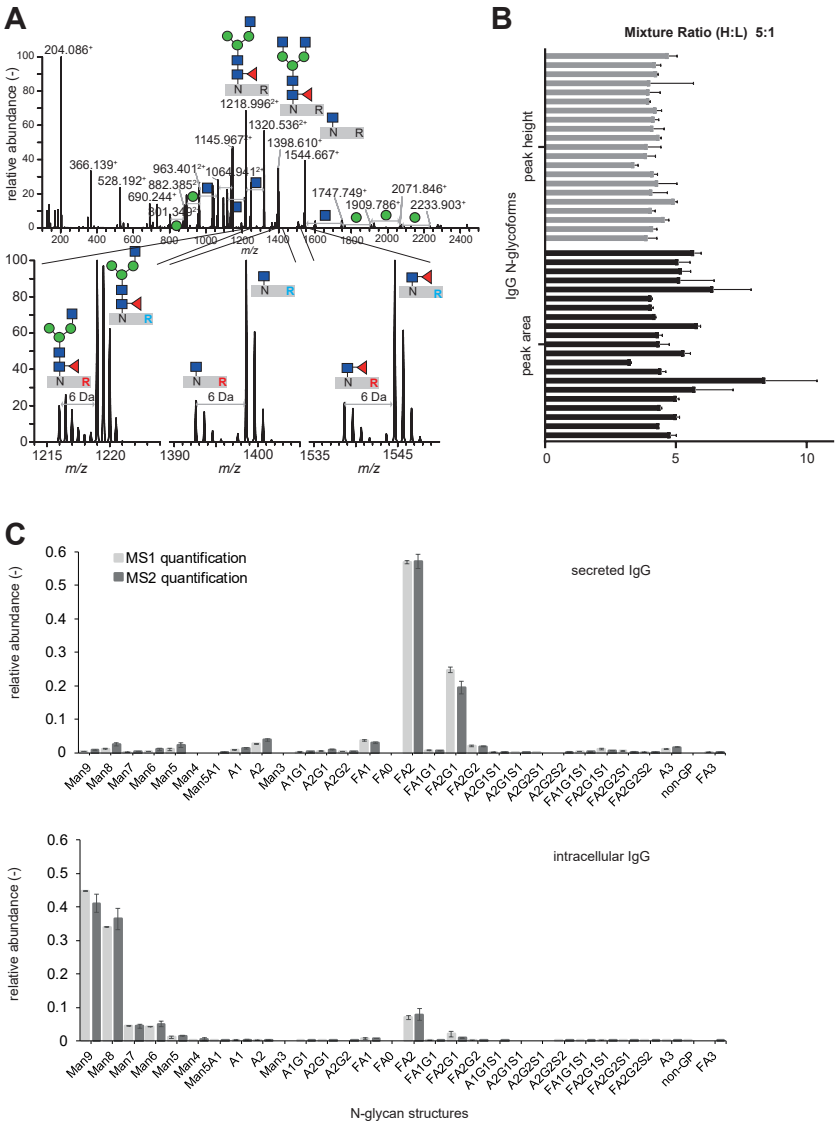

Figure 6.1: (A) Typical MS2 spectrum of an IgG glycopeptide obtained during SILAC-PRM acquisition to achieve glycan-level fragmentation of light and heavy glycopeptides simultaneously at 1:5 ratio. (B) SILAC-PRM data acquisition of 100% heavy and 100% light IgG glycopeptides mixed in a 5:1 ratio prior to MS-injection. Quantification was conducted by averaging the peak area (black bars) or peak height (gray bars) of defined glyco-transitions (n=3). (C) N-glycan profiling analysis of purified intracellular and secreted IgG on MS1 level (light gray), by averaging the intensity of the extracted ion chromatograms, and on MS2 level, by averaging the intensity of defined glyco-transitions (dark gray) (n=3). The relative abundance of each N-glycoform for secreted (top) and intracellular (bottom) IgG.

experimental data, it was necessary to include spatially separated pools of intracellular IgGs that carry the same high mannose (Man_{9-5}) glycans. The different pools are related because a high mannose-bearing IgG can be found in both the ER or in the cis-Golgi, and, within the ER, high mannose isoforms can account for different folding states of the protein. In the ER, high mannose structures are generated by the collaborative action of ER-localized alpha-mannosidases (ER-mannosidase I and/or EDEMs) implicated in the build-up of the degradation signal present on not properly folded glycoproteins (32-34). In contrast, a distinct Golgi-localized pool of $Man_{9-5}GlcNAc_2$ structures is generated by the Golgi-mannosidases I that trims $Man_9GlcNAc_2$ to $Man_5GlcNAc_2$ with slightly different specificities [342].

The obtained data implied a faster turnover of the Golgi-generated structures as compared to the oligomannose structures in the ER (Figure 6.2 A). Mechanistically, the fast turnover of Golgi species can be explained by a short residence time of glycoproteins in the Golgi cisternae. Conversely, slow ER turnover can be attributed to a slow export to the Golgi or the cytosol. This was also confirmed by the model, which, on one side predicted slower kinetic parameters for the formation and degradation of the $Man_{7-5}GlcNAc_2$ structures (D.2), and on the other side predicted a bigger IgG pool for folding intermediates in the ER (and ERAD) as compared to the pool of folded IgG in the Golgi (Figure D.5). Surprisingly, we observed a $Man_4GlcNAc_2$ glycan with an early onset and fast turnover. This structure has not been characterized in detail and there are controversial opinions regarding its generation either by Golgi α-mannosidases [343, 344] or by lysosomal mannosidases [294]. Importantly, neither ER mannosidases nor Golgi-mannosidase I can trim further than Man_5 due to their α-1,2 specificity [320]. Interestingly, it has been reported that protein aggregates, generated in the ER, are cleared from the ER and transported in single-membrane vesicles directly to the lysosome [345, 346]. Thus, we hypothesized the $Man_4GlcNAc_2$ structure to be generated by the action of a lysosomal mannosidase, on IgGs HC that are cleared from the ER in a pathway that differs from the well characterized ERAD pathway (represented by the collaborative action of ER-Mannosidase I and EDEMs). The integration of this pathway into the model allowed for an accurate fitting of the $Man_4GlcNAc_2$ kinetics (Figure 6.2 A). Moreover, the addition of MG132, a potent inhibitor of the proteasome 26S complex, showed a drastic accumulation of ERAD-relevant $Man_{7-5}GlcNAc_2$ species, without affecting the $Man_4GlcNAc_2$ turnover (Figure D.6 A), thereby excluding it as an ERAD intermediate. The mathematical model was used to calculate the trajec-

tory of IgGs through the entire N-glycosylation network (Figure 6.2 B-C). The model predicted the distribution of the activity profiles of the main Golgi enzymes (Figure 6.3 A) and the distribution of the respective N-glycan substrates abundance (Figure 6.3 B) along the Golgi compartment. On one side, the agreement with enzymes localizations resolved by microscopy [325, 327–329] was appreciated; on the other side, our data provided experimental support for inferred mathematical model outputs [11, 275, 332].

6.3.3 The Refined N-Glycosylation Network Correctly Predicts the Effect of N-glycan Processing Inhibitors

To evaluate the robustness of the model, we perturbed the system by the addition of well defined processing inhibitors and monitored the effect on the intracellular N-glycan processing and the IgG N-glycan profiling. Upon swainsonine (SWA) addition, a potent inhibitor of the Golgi-localized α-mannosidase II, N-glycan processing in the ER remained almost unchanged, whereas the N-glycan synthesis in the Golgi shifted completely toward hybrid N-glycan species (Figure 6.4 A-B and Figure D.3 B, Figure D.4 B, Figure D.6 B). The relative distribution of the activity profiles of the main Golgi enzymes and the distribution of the respective N-glycan substrates abundance showed only small shifts along both the Golgi- and enzymatic activity/abundance-axis (Figure 6.4 C-D) as compared to the untreated cells (Figure 6.3 A-B). Conversely, kifunensine (KIF), an inhibitor of α-1,2-mannosidases, significantly affected both the flux and the N-glycan processing in both the ER and Golgi (Figure 6.4 E-F, Figure D.3 C, Figure D.4 C, Figure D.6 C). Of note, neither SWA nor KIF addition affected the turnover kinetics of the $Man_4GlcNAc_2$ glycoprotein, confirming a processing pathway independent of ER- or Golgi-localized mannosidases (Figure D.7 A). To test this hypothesis, we treated cells with bafalomycin (BAF), a substance known to affect pH homeostasis in the lysosome and to reduce lysosomal hydrolases activity. Indeed, BAF treatment had a single effect on the turnover of the $Man_4GlcNAc_2$, strongly reducing its turnover (Figure D.7 B), whereas ER- (Figure D.7 C) or Golgi-synthetized N-glycan (Figure D.7 D) did not show significant deviations compared to the control turnover data (Figure 6.2 A). These data supported the hypothesis of a direct export the ER to the lysosome.

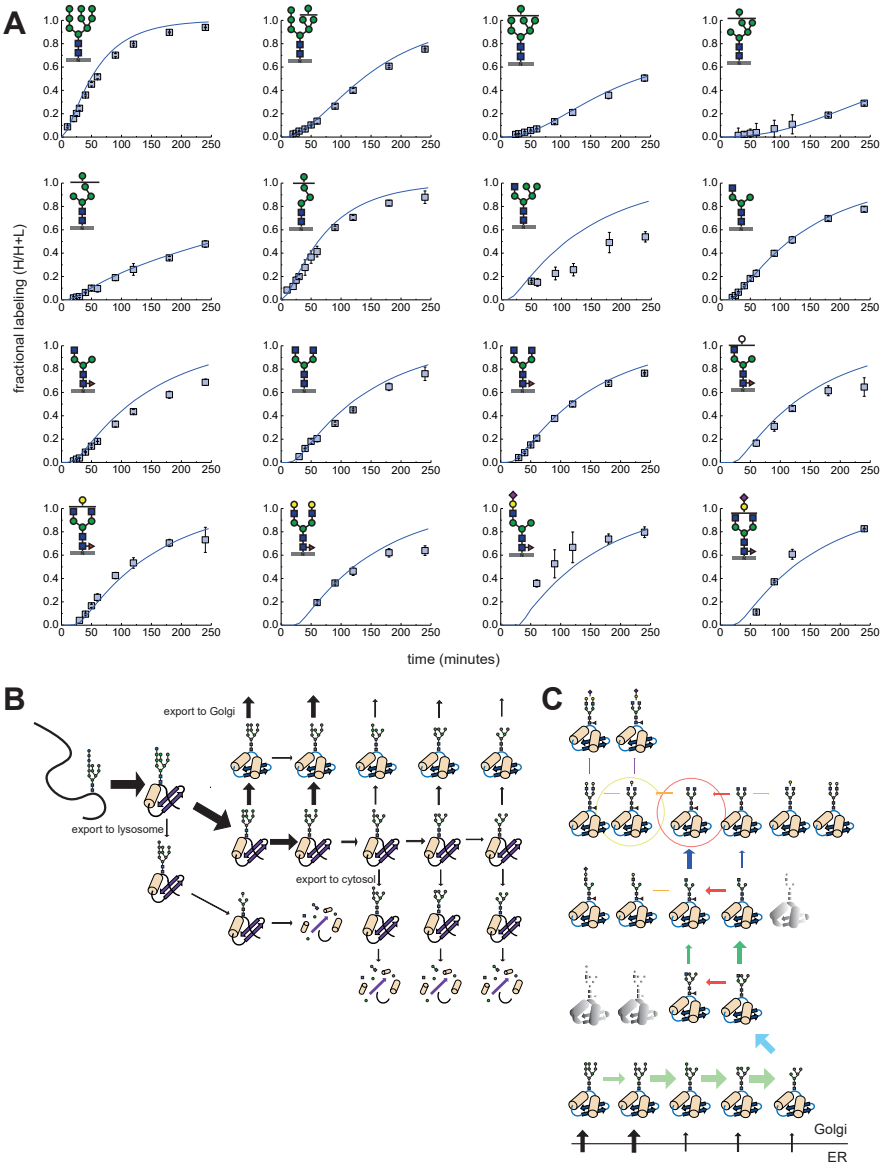

Figure 6.2: (A) Fractional labeling (y-axis) of intracellular pools of IgG peptides bearing different N-glycan intermediates (n=3, except for complex sialylated structures n=2). The modeled turnover kinetics are shown as curves. (B) IgG fluxes through the ER processing pathway calculated by the model. Blue proteins refer to folded, purple proteins indicate partially folded IgGs. (C) IgG flux through the Golgi N-glycan processing pathway. The colors of the arrows indicate the different enzymes catalyzing the reaction. Circles highlight the major glycoforms found on secreted IgGs.

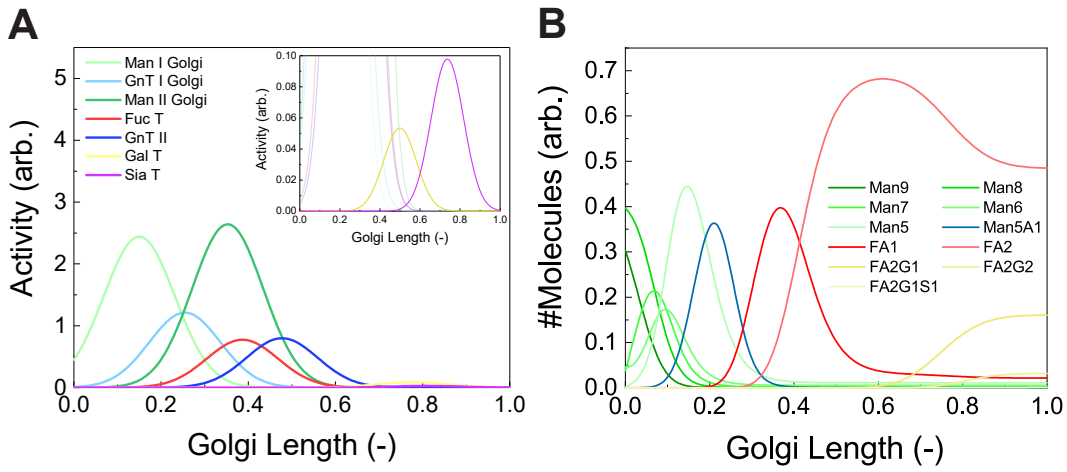

Figure 6.3: (A) Apparent activity of the different Golgi resident enzymes calculated by the model. (B) Intracellular distribution of the different N-glycoforms of IgG calculated by the model.

6.4 Discussion

We monitored the intracellular N-glycan processing of IgGs. The experimental data were used to develop a mathematical model for N-glycoprotein processing in CHO cells. The model was based on the current knowledge the N-glycosylation pathway in mammalian cells [271] and upon refinement of the canonical network, we were able to deduce a robust mathematical description of the process. In the ER, N-glycan processing is primarily involved in the folding and quality control process that ensures the exit of correctly folded protein from the ER. In contrast, Golgi processing is characterized by spatial separation of enzymes and a continuous flow of the substrate through the organelle.

The correct reproduction of the $Man_4GlcNAc_2$ kinetic was only possible with the incorporation of an additional degradation pathway that directly connects the ER to the lysosome. Based on previous ER-phagy studies [347] and recent descriptions of a vesicular transport from the ER to the lysosome [346], we propose that mannose trimming to $Man_4GlcNAc_2$ (and possibly further, to not protein-A-capture purifiable glycopeptides), reflects the quality control process involved in protein aggregate clearance from the ER, referred to as ERLAD [346]. Our glycoproteomics approach clearly differentiates this pathway from ERAD, which can be accurately followed by N-glycan processing down to $Man_5GlcNAc_2$ (Figure 6.2 A, Figure D.7 A). From our data, ERLAD acts

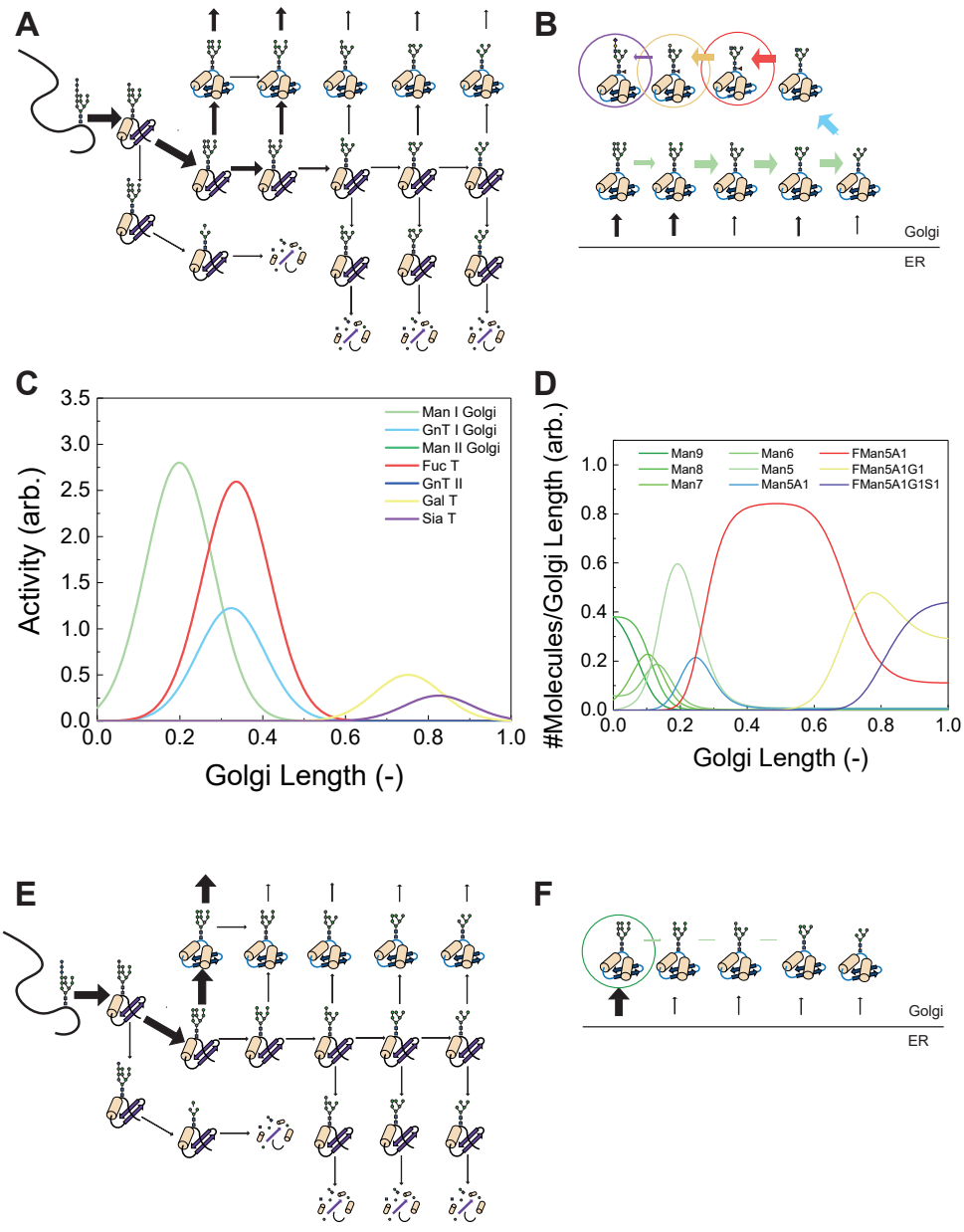

Figure 6.4: Fluxes through ER (A) and Golgi (B) under SWA treatment as calculated by the model. The major products in the presence of the inhibitors are circled. (C) Calculated activity of the different glycosyl hydrolases and transferases along Golgi and (D) intracellular distribution of N-glycan intermediates under SWA.Fluxes through ER (E) and Golgi (F) under KIF treatment as calculated by the model.

much more rapidly than ERAD, indicating a much longer half-life for ERAD-substrates as compared to their ERLAD counterpart. This observation is in line with previously described models, where a stochastic association of unfolded protein and chaperones with the signal-generating EDEMs determines half-life of ERAD substrates [348]. In contrast, glycoprotein aggregates interacting with calnexin (through $Glc_1Man_9GlcNAc_2$ N-glycans) are selected for export to the lysosome [346]. Based on the kinetic data and the model predictions, we propose that aggregation of polypeptides occurs after translocation into the ER lumen, where nascent polypeptides miss to associate with folding chaperones. They are characterized by $Glc_1Man_9GlcNAc_2$ glycan structures.

The SILAC-PRM methodology allowed us to follow the N-glycan maturation along the entire secretory pathway with a spatial-temporal resolution and the mathematical model estimated the *in vivo* kinetic relative information for many enzymes along the N-glycosylation network. Based on product formation, we obtained a functional map of enzyme activity distribution along the Golgi and noted a full agreement of the spatial localization of the enzymes determined by microscopy experiments [327–329]. Importantly, the measured Golgi enzymes activity in the experimental setup reflected a combination of multiple factors (catalytic activity of the enzyme, enzyme concentration exposure time and glycan substrate accessibility) rendering the model cell-, protein- and even glycosylation-site specific. An example of this specificity was evident in the SWA inhibition experiment (Figure 6.4 C-D) where the activity-based model output increased the activity of GalT and SiaT. This difference was due to an increased accessibility of the glycan substrate to the enzymes. In this respect, Crispin and colleagues showed that the protein-glycan interaction in the Fc region of IgG is reduced for hybrid- as compared to complex N-glycans [349], allowing better galactosylation of hybrid glycan structures.

This methodology and the new insights presented here allow for the calculation of the effects of 5 altered processing enzyme level or of changed enzyme localization on site-specific N-glycan composition. This is relevant to assess the quality of recombinant glycoproteins production in cell culture. On the other side, it offers a more reliable basis for the implementation and optimization of mathematical models used in product design of glycoproteins as biopharmaceuticals.

Chapter 7

Concluding Remarks

7.1 Conclusions

The production of biopharmaceuticals is a delicate task that involves several technological and biological challenges. Within the complex manufacturing scheme of these products, cell culture processes play a fundamental role in determining both the quantity and the quality of the main active pharmaceutical ingredient. While recombinant proteins are produced through established platform systems in large-scale facilities, most of the cell therapy products under clinical testing are manufactured using conventional cell culture techniques that do not consider critical industrial aspects such as scalability, robustness and reproducibility. The first part of this thesis aimed at developing optimized processes for the expansion of T cells and pluripotent stem cells. For the latter, a process was developed to allow prolonged expansion in form of aggregates without the need for manual passaging procedures. This was accomplished through the optimization of the maximum hydrodynamic shear in the system, allowing the control of the aggregate size throughout the entire expansion. In the case of T cells, a bioprocessing framework to produce billions of lymphocytes expressing memory-related markers in a single scalable, closed system in serum-free conditions was developed by combining medium optimization studies with process optimization studies. Both works represent improved strategies to expand cells of therapeutic interest with suitable quality attributes compared to the protocols that are currently implemented in clinical trials.
The second section of this thesis aimed at describing the N-glycosylation processing of proteins produced in mammalian cells through mechanistic mathematical models. This methodology and the obtained results provided a rigorous and quantitative description of the intracellular phenomena governing glycoprotein synthesis, maturation and secretion. The modeling framework described in this thesis can be used as a tool to identify bottlenecks in glycan processing and provide a solid basis for predicting the effect of different strategies, such overexpression or spacial relocation of enzymes, to produce specific oligosaccharides.

7.2 Future Directions

Like many other scientific fields, most of the progresses in bioprocessing will arise at the interaction between several areas, including chemistry, material science, biology and engineering. For cell therapies, the initial efforts will be focused on solving the

safety concerns that arise upon the transplantation of cultured cells. The introduction of safety switches that can trigger apoptosis is the main strategy currently investigated to prevent the occurrence of adverse effects such as malignant transformations of transplanted cells. Another area of great interest involves the generation of universal, allogeneic cell lines for off-the-shelf cell therapies. Such a platform can bring the benefits of the economy of scale and overcome many of the limitations of autologous cell therapies, including the variability of starting materials, limitations in supply chain, the impossibility to stockpile doses of drugs. A possible strategy to implement this feature is based on the elimination of the expression of HLA molecules on the surface of the cells to partially remove the donor specificity [350]. In the next future, genetic engineering and synthetic biology techniques will also be used to introduce novel functionalities, such as on-demand production of paracrine factors, redirection of cell migration, or enhancement of specific functionalities [15]. From the engineering side, the production of novel polymeric substrates capable to support the expansion of cells and stem cells could lead to a significant cost reduction and improvement of reproducibility for large-scale culture of cells compared to current undefined substrates such as Matrigel® [159]. Advances in material sciences will also aid the formulation of cell-based drugs by developing injectable scaffolds to deliver viable cells *in situ* without significant losses [351]. Lastly, cell-specific bioprocess intensification strategies (such as medium screening, platform development and operation mode) will be ultimately needed to improve the yield and quality of cell therapy products, while reducing their manufacturing costs. In this context, the implementation of PAT and automation will be of paramount importance to reduce the operator workload for manufacturing lots of autologous cell therapies. One possible application of great industrial relevance would be the development of an expansion platform that is able to correct the variability in starting material in terms of growth rate and phenotype by regulating the supplementation of different compounds.
Similarly, N-glycosylation modeling will vastly benefit from interdisciplinary efforts to dissect and identify as many mechanisms as possible in the cell machinery. First, the development of more precise analytical techniques could provide currently unaccessible information concerning the intracellular localization of glycoproteins with respect to their conformational state and folding status. This would confirm the validity of specific assumptions concerning the generation of non-canonocial oligosaccharides and their function *in vivo*. On the biological side, the use of specific knockout cell lines can improve the estimation of certain kinetic parameters that cannot be uniquely identi-

fied by mathematical modeling techniques (e.g., the generation of high mannose species through the action of different hydrolases). From the modeling side, the development of a kinetic model for a protein with multiple glycosylation sites would confirm many of the findings derived from the analysis of mAbs.

Appendix A

Appendix to Chapter 2

Table A.1: Approved products for Cord Blood storage.

Product	Cell Type	Indication	Manufacturer
Allocord	HPC	Hematopoietic reconstitution	SSM Cardinal Glennon Children's Medical Center
Clevercord	HPC	Hematopoietic reconstitution	Cleveland Cord Blood Center
Hemacord	HPC	Hematopoietic reconstitution	New York Blood Center, Inc
Ducord	HPC	Hematopoietic reconstitution	Duke University School of Medicine
HPC, Cord Blood*	HPC	Hematopoietic reconstitution	Clinimmune Labs
HPC, Cord Blood - LifeSouth	HPC	Hematopoietic reconstitution	LifeSouth Community Blood Centers, Inc.
HPC, Cord Blood - LifeSouth	HPC	Hematopoietic reconstitution	Bloodworks

Table A.2: Approved virus-based products for in vivo gene editing. Therapies withdrawn from the market are indicated with the symbol *.

Product	Virus Type	Indication	Manufacturer
Glybera*	Adenovirus	Lipoprotein lipase deficiency	uniQure N.V.
Luxturna	Adenovirus	Leber's congenital amaurosis	Spark Therapeutics, Inc
IMLYGIC	Herpes virus	Melanoma	Amgen

Appendix B

Appendix to Chapter 3

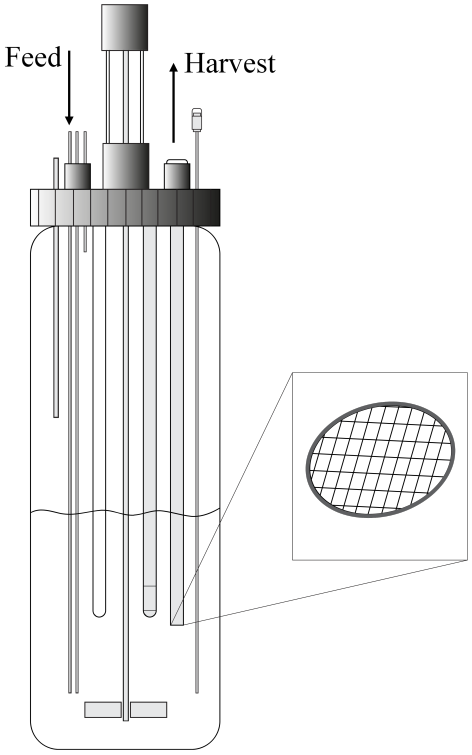

Figure B.1: Schematic representation of the perfusion system used to evaluate the impact of impeller agitation on PSC aggregates.

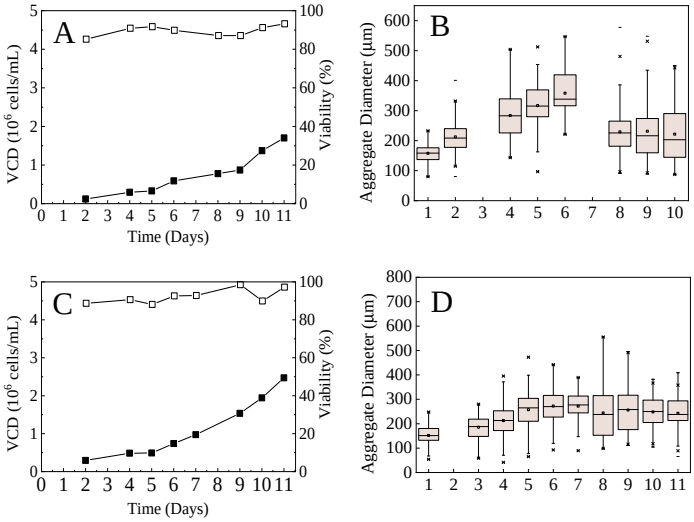

Figure B.2: Viable cell density (black markers), viability (white markers) and aggregate size distribution profiles of cell lines 2 (A-B) and 3 (C-D) cultured in presence of a 4.5 mm internal diameter contracting nozzle in the perfusion loop.

Appendix C

Appendix to Chapter 5

C.1 Experimental

C.1.1 Constructs

All the expression cassettes were cloned into the pcDNA3.1 vector under the control of the CMV promoter (Thermo Fisher Scientific,Waltham,MA,USA) using standard cloning protocols. pcDNA-His-ER-PDI and pcDNA-His-Sec-PDI were obtained by PCR amplification of the signal peptide, the His-tag and PDI gene from pRG85 and pRG105 respectively, omitting the HDELLE sequence of pRG105 [277] using ER-PDI_Fwd/ER-PDI Rev and Sec-PDI_Fwd/Sec-PDI Rev primers (Supplemental Table 1). PCR products were then cloned into the BamH1 and EcoR1 sites of pcDNA 3.1. pcDNA-His-ER-PDI and pcDNA-His-Sec-PDI point mutants were obtained after the Phusion site-directed mutagenesis (Thermo Fisher Scientific), by introducing a mismatch in the middle of the forward primer. PCR was performed with Phusion polymerase with phosphorylated primers, and PCR products were ligated afterward by the T4 ligase. Ligation products were then transformed into DH5a Escherichia coli bacteria. Positive constructs were confirmed by DNA sequencing.

C.1.2 Expression of PDI in CHO Cells

Recombinant expression of PDI was performed in Freestyle CHO cells (CHO-S; Thermo Fisher Scientific). The cells were first expanded as adherent cultures in standard polystyrene flasks (TPP; Millipore-Sigma, Darmstadt, Germany) in RPMI medium (Thermo Fisher Scientific) supplemented with 10% fetal bovine serum (PanBiotech, Aidenbach, Germany) and 1% penicillin-streptomycin (Thermo Fisher Scientific). For suspension culture, the cells were maintained at a density of 10^6 cells/ml in PowerCHO-2CD medium supplemented by sodium hypoxanthine-thymidine supplement (Thermo Fisher Scientific), 2 mM ultraglutamine, and 1% penicillin-streptomycin (all from Thermo Fisher Scientific). For the transfection, cells were transferred at a density of $2 \cdot 10^6$ cells/ml into ProCHO-4 supplement with hypoxanthine-thymidine supplement, 2 mM ultraglutamine, and 1% penicillin-streptomycin, and constructs were transfected using polyethylenimine (Polysciences, Warrington, PA, USA). After 4 h at 37 °C, PowerCHO-2CD was added at a 1:1 ratio to the transfection, and the cells were incubated for up to 5 days for transient expression at 31 °C and shaken at 160 rpm. When producing PDI mutants,

a corresponding wild-type PDI was simultaneously produced to account for potential batch-to-batch variation of glycosylation efficiency.

C.1.3 Purification of PDI

After expression, cells and culture medium were collected by centrifugation for 5 min at 200 rcf. For purification of the ER-retained proteins, the cells were lysed in a Tris/Cl 62.5 mM buffer at pH 6.8, supplemented with 3% Triton-100 and 1x protease inhibitor cocktail (Roche, Basel, Switzerland), sonicated for 1 min and centrifuged at 3500 rcf for 10 min. After centrifugation, the soluble fraction was diluted 4 times in PBS. For purification of the secreted proteins, the culture medium was diluted 2 times in PBS. The diluted fractions containing the recombinant proteins were incubated with Protino Ni-NTA beads (Macherey-Nagel, Duren, Germany) equilibrated in PBS on a rotating wheel for 4 h at 4 °C. Purification was performed on a gravity flow column. After binding, the beads were washed by 15 column volumes of 25 mM imidazole in PBS, and bound proteins were eluted by 4 column volumes of 250 mM imidazole in PBS. Eluted proteins were concentrated with the Amicon YM-30 filtering device (Millipore-Sigma), and buffer was exchanged to PBS. The purified proteins were then stored at −20 °C before further analyses.

C.1.4 Mass Spectrometry Sample Preparation and Analysis

Samples were prepared and analyzed as published (16, 39). In brief, 50 μg of proteins was applied onto an Amicon YM-30 filter device, reduced for 1 h at 37 °C by 50 mM DTT in 50 mM ammonium bicarbonate, alkylated by 65 mM iodoacetamide in 50 mM ammonium bicarbonate for 1 h at 37°C, then washed 3 times by 50 mM ammonium bicarbonate and digested by trypsin (Promega, Madison, WI, USA) overnight at 37 °C. Digested peptides were collected by centrifugation and dried. Peptides were desalted by zip-tip C18 (Millipore-Sigma). For each sample, 3 separate biologic replicates were analyzed. Samples were analyzed on an LTQ-Orbitrap Velos mass spectrometer (Thermo Fisher Scientific) coupled to a Nano-HPLC system (Eksigent Technologies, Dublin, CA, USA). Spectra obtained were analyzed with XCalibur 2.2 sp1.48 (Thermo Fisher Scientific).

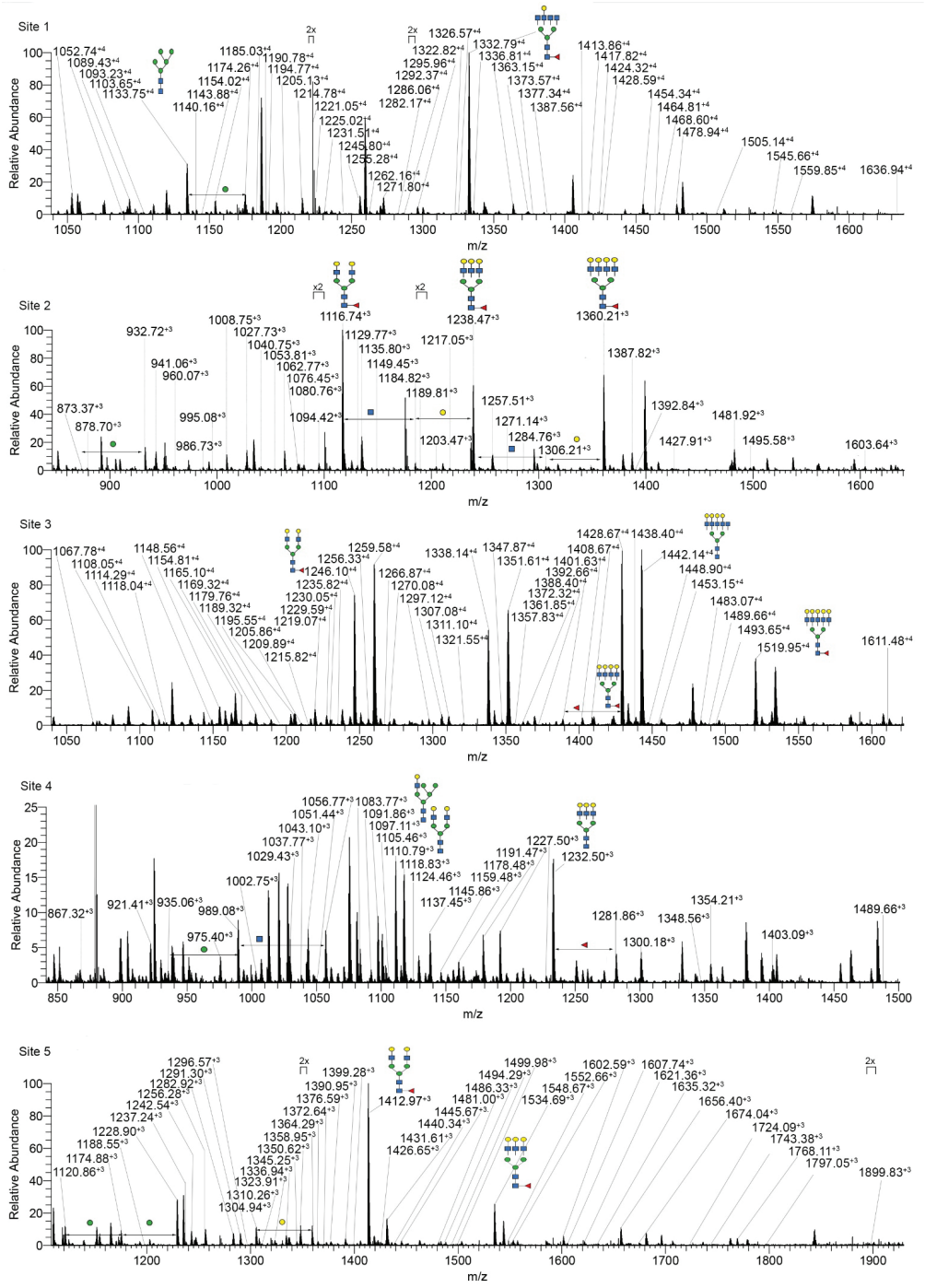

Figure C.1: MS spectra showing glycopeptides heterogeneity of Sec-Pdi glycosites.

	m/z					Average (%)					SD				
	Site 1 +4	Site 2 +3	Site 3 +4	Site 4 +3	Site 5 +3	Site 1	Site 2	Site 3	Site 4	Site 5	Site 1	Site 2	Site 3	Site 4	Site 5
(HexNAc2 Hex3)Hex6	1295.80	1148.79	1270.10	1191.48	1444.97	0.20	1.02	0.26	2.90	0.29	0.03	0.31	0.12	0.45	0.08
(HexNAc2 Hex3)Hex5	1255.28	1094.77	1229.59	1137.46	1390.96	1.62	1.33	0.60	3.21	1.32	0.82	0.35	0.21	0.29	0.29
(HexNAc2 Hex3)Hex4	1214.77	1040.75	1189.08	1083.44	1336.94	1.40	2.64	0.45	3.36	2.95	0.38	3.41	0.77	0.29	0.04
(HexNAc2 Hex3)Hex3	1174.26	986.73	1148.56	1029.43	1282.92	1.49	0.64	0.56	2.70	2.31	0.21	0.11	0.95	0.10	0.26
(HexNAc2 Hex3)Hex2	1133.74	932.72	1108.05	975.41	1228.91	9.39	6.73	3.97	4.96	11.49	0.80	0.51	1.22	0.29	0.67
(HexNAc2 Hex3)Hex	1093.23	878.70	1067.53	921.39	1174.88	2.23	1.17	0.94	3.89	3.41	0.33	0.35	0.19	0.97	0.51
(HexNAc2 Hex3)	1052.73	824.70	1027.02	867.39	1120.88	3.14	0.00	1.10	0.24	2.83	0.66	0.00	0.45	0.41	2.41
(HexNAc2 Hex3)Hex2HexNAc	1184.51	1000.41	1209.59	1043.10	1296.59	0.11	0.00	0.23	8.34	0.11	0.04	0.00	0.05	0.29	0.01
(HexNAc2 Hex3)Hex2(HexNAcHex)	1225.02	1054.42	1199.57	1097.11	1350.61	0.03	0.16	0.11	7.18	0.60	0.06	0.02	0.05	0.08	0.78
(HexNAc2 Hex3)HexNAc	1103.48	892.35	1118.29	935.06	1188.55	0.11	0.00	0.77	1.91	0.38	0.10	0.00	0.10	0.14	0.03
(HexNAc2 Hex3)(HexNAcHex)1	1143.99	946.39	1118.54	989.08	1242.57	0.12	0.21	0.53	10.27	0.17	0.07	0.07	0.09	0.14	0.04
(HexNAc2 Hex3)HexNAc2	1154.25	960.07	1169.07	1002.76	1256.25	0.05	0.14	0.06	1.53	0.39	0.05	0.09	0.02	0.11	0.09
(HexNAc2 Hex3)(HexNAcHex)HexNAc	1194.77	1014.09	1169.32	1056.78	1364.29	0.07	0.00	0.06	6.21	0.11	0.07	0.00	0.11	0.37	0.08
(HexNAc2 Hex3)(HexNAcHex)2	1235.29	1068.11	1209.84	1110.80	1310.27	0.59	0.00	0.62	11.26	0.90	0.35	0.00	0.18	1.19	0.12
(HexNAc2 Hex3)HexNAc3	1205.00	1027.73	1179.30	1070.42	1323.91	0.08	1.73	4.31	0.06	2.50	0.02	0.82	0.56	0.11	0.27
(HexNAc2 Hex3)(HexNAcHex)HexNAc2	1245.52	1081.76	1219.82	1124.45	1376.94	0.09	0.07	5.47	0.25	1.56	0.08	0.06	1.22	0.22	0.74
(HexNAc2 Hex3)(HexNAcHex)2HexNAc	1286.06	1135.80	1260.35	1178.49	1431.99	0.24	0.05	0.05	3.65	0.66	0.13	0.08	0.05	0.29	0.70
(HexNAc2 Hex3)(HexNAcHex)3	1326.57	1189.82	1300.87	1232.51	1486.00	0.16	0.08	0.00	12.16	0.07	0.08	0.14	0.00	1.54	0.08
(HexNAc2 Hex3)HexNAc4	1255.75	1095.40	1230.05	1138.09	1391.58	0.14	0.33	0.20	0.00	0.23	0.11	0.29	0.28	0.00	0.13
(HexNAc2 Hex3)(HexNAcHex)HexNAc3	1296.27	1149.43	1270.57	1192.12	1445.61	0.19	0.56	0.79	0.00	1.11	0.33	0.21	0.69	0.00	0.82
(HexNAc2 Hex3)(HexNAcHex)2HexNAc2	1336.81	1203.47	1311.10	1246.16	1499.65	0.17	0.31	1.87	0.00	0.10	0.19	0.54	0.31	0.00	0.08
(HexNAc2 Hex3)(HexNAcHex)3HexNAc	1377.34	1257.51	1351.63	1300.20	1553.69	0.03	2.14	0.16	0.27	0.22	0.05	3.70	0.04	0.13	0.27
(HexNAc2 Hex3)(HexNAcHex)4	1417.85	1311.53	1392.15	1354.22	1607.71	0.06	0.08	0.03	0.87	0.10	0.10	0.05	0.05	0.76	0.05
(HexNAc2 Hex3)(HexNAcHex)5	1509.10	1433.20	1483.40	1475.89	1729.38	0.04	0.00	1.34	0.00	0.06	0.04	0.00	0.63	0.00	0.05
(HexNAc2 Hex3)(HexNAcHex)HexNAc4	1347.02	1217.09	1321.32	1259.78	1513.27	0.00	0.08	0.27	0.00	0.00	0.00	0.14	0.28	0.00	0.00
(HexNAc2 Hex3)(HexNAcHex)2HexNAc3	1387.56	1271.14	1361.85	1313.83	1567.32	0.11	0.15	0.47	0.00	0.00	0.07	0.13	0.41	0.00	0.00
(HexNAc2 Hex3)(HexNAcHex)3HexNAc2	1428.09	1325.18	1402.38	1367.87	1621.36	0.04	0.56	1.10	0.00	0.20	0.04	0.74	0.22	0.00	0.27
(HexNAc2 Hex3)(HexNAcHex)4HexNAc	1468.60	1379.20	1442.90	1421.89	1675.38	0.20	0.00	32.99	0.00	1.55	0.10	0.00	2.32	0.00	0.62
(HexNAc2 Hex3)(HexNAcHex)6	1600.35	1554.86	1574.65	1597.55	1851.05	0.00	0.00	0.00	0.00	0.00	0.00	0.00	0.00	0.00	0.00
(HexNAc2 Hex3)(HexNAcHex)HexNAc5	1397.77	1284.76	1372.07	1327.45	1580.94	0.00	0.01	0.03	0.00	0.00	0.00	0.02	0.06	0.00	0.00
(HexNAc2 Hex3)(HexNAcHex)2HexNAc4	1438.31	1338.80	1412.60	1381.49	1634.99	0.00	0.08	0.00	0.00	0.41	0.00	0.14	0.00	0.00	0.57
(HexNAc2 Hex3)(HexNAcHex)3HexNAc3	1478.84	1392.84	1453.13	1435.53	1689.03	5.25	0.07	0.19	0.00	0.00	0.45	0.12	0.17	0.00	0.00
(HexNAc2 Hex3)(HexNAcHex)4HexNAc2	1519.35	1446.86	1493.65	1489.55	1743.05	0.00	0.00	0.17	0.19	1.55	0.00	0.00	0.29	0.16	1.34
(HexNAc2 Hex3)(HexNAcHex)5HexNAc	1559.85	1500.86	1534.15	1543.55	1797.05	0.03	0.00	0.00	0.00	0.40	0.06	0.00	0.00	0.00	0.35
(HexNAc2 Hex3)Fuc	1089.23	873.37	1063.53	916.06	1169.55	0.01	0.27	0.00	0.00	0.00	0.01	0.29	0.00	0.00	0.00
(HexNAc2 Hex3)FucHex(HexNAcHex)	1221.03	1049.10	1195.32	1091.78	1345.25	0.04	0.14	0.03	1.22	0.13	0.08	0.03	0.02	0.72	0.12
(HexNAc2 Hex3)FucHex2(HexNAcHex)	1261.53	1103.10	1235.82	1145.79	1399.28	0.04	0.00	0.29	0.79	0.31	0.07	0.00	0.44	0.69	0.30
(HexNAc2 Hex3)FucHexNAc	1140.00	941.06	1114.29	983.75	1237.25	0.04	1.10	0.33	0.07	0.98	0.04	0.26	0.14	0.06	0.21
(HexNAc2 Hex3)Fuc(HexNAcHex)1	1170.51	995.08	1154.81	1037.77	1291.26	0.00	0.42	0.07	0.62	0.51	0.00	0.06	0.06	0.54	0.44
(HexNAc2 Hex3)FucHexNAc2	1190.77	1008.75	1165.08	1051.45	1304.94	0.07	4.45	1.58	0.15	5.72	0.13	0.17	1.17	0.14	2.07
(HexNAc2 Hex3)Fuc(HexNAcHex)HexNAc	1231.28	1062.77	1205.59	1105.46	1358.96	0.43	5.23	1.43	1.60	4.40	0.11	0.39	0.35	0.50	0.85
(HexNAc2 Hex3)Fuc(HexNAcHex)2	1271.80	1116.79	1246.10	1159.48	1412.98	2.39	35.05	12.91	1.61	37.82	0.35	1.33	2.18	0.34	3.18
(HexNAc2 Hex3)FucHexNAc3	1241.54	1076.45	1215.84	1119.14	1372.64	0.00	1.19	0.04	3.85	0.58	0.00	0.13	0.07	1.28	0.16
(HexNAc2 Hex3)Fuc(HexNAcHex)HexNAc2	1282.04	1130.44	1256.33	1173.13	1426.63	0.01	1.48	1.48	0.35	0.22	0.02	0.02	0.33	0.60	0.11
(HexNAc2 Hex3)Fuc(HexNAcHex)2HexNAc	1322.82	1184.82	1297.12	1227.18	1481.00	0.31	1.99	0.84	1.12	1.02	0.12	0.27	0.60	0.88	0.17
(HexNAc2 Hex3)Fuc(HexNAcHex)3	1363.08	1238.51	1337.39	1281.19	1534.68	1.12	14.46	7.12	1.85	6.88	0.16	0.85	0.20	0.17	0.37
(HexNAc2 Hex3)FucHexNAc4	1292.32	1144.16	1266.62	1186.85	1440.34	0.05	0.00	0.01	0.00	0.33	0.09	0.00	0.02	0.00	0.30
(HexNAc2 Hex3)Fuc(HexNAcHex)HexNAc3	1332.79	1198.11	1307.08	1240.80	1494.29	63.05	0.00	0.15	0.00	0.42	3.67	0.00	0.14	0.00	0.64
(HexNAc2 Hex3)Fuc(HexNAcHex)2HexNAc2	1373.57	1252.49	1347.87	1295.18	1548.67	0.04	0.00	0.35	0.00	0.05	0.07	0.00	0.55	0.00	0.09
(HexNAc2 Hex3)Fuc(HexNAcHex)3HexNAc	1413.86	1306.20	1388.16	1348.89	1602.39	0.05	0.35	0.50	0.07	0.10	0.02	0.05	0.47	0.02	0.03
(HexNAc2 Hex3)Fuc(HexNAcHex)4	1454.37	1360.21	1428.67	1402.91	1656.40	1.01	9.49	6.83	0.48	2.18	0.25	2.72	1.63	0.27	0.06
(HexNAc2 Hex3)Fuc(HexNAcHex)5	1545.41	1481.92	1519.96	1524.29	1777.79	0.07	2.11	4.14	0.00	0.18	0.08	0.94	2.53	0.00	0.06
(HexNAc2 Hex3)Fuc(HexNAcHex)HexNAc4	1383.54	1265.78	1357.83	1308.47	1561.96	0.00	0.00	0.52	0.00	0.00	0.00	0.00	0.62	0.00	0.00
(HexNAc2 Hex3)Fuc(HexNAcHex)2HexNAc3	1424.32	1320.16	1398.62	1362.85	1616.34	0.11	0.00	0.04	0.00	0.00	0.19	0.00	0.04	0.00	0.00
(HexNAc2 Hex3)Fuc(HexNAcHex)3HexNAc2	1464.61	1373.88	1438.91	1416.57	1670.06	2.61	0.00	0.82	0.00	0.00	2.23	0.00	0.73	0.00	0.00
(HexNAc2 Hex3)Fuc(HexNAcHex)4HexNAc	1505.14	1427.91	1479.44	1470.60	1724.09	1.12	0.10	0.00	0.00	0.02	0.94	0.08	0.00	0.00	0.03
(HexNAc2 Hex3)Fuc(HexNAcHex)6	1636.94	1603.64	1611.23	1646.33	1899.83	0.05	0.22	0.67	0.00	0.04	0.05	0.13	0.13	0.00	0.03
(HexNAc2 Hex3)Fuc(HexNAcHex)HexNAc5	1434.29	1333.44	1408.58	1376.13	1629.63	0.00	0.00	0.01	0.00	0.00	0.00	0.00	0.02	0.00	0.00
(HexNAc2 Hex3)Fuc(HexNAcHex)2HexNAc4	1475.07	1387.82	1449.37	1430.51	1684.00	0.00	1.42	0.03	0.00	0.00	0.00	2.34	0.05	0.00	0.00
(HexNAc2 Hex3)Fuc(HexNAcHex)3HexNAc3	1515.36	1441.54	1489.66	1484.23	1737.72	0.00	0.01	0.03	0.00	0.00	0.00	0.02	0.05	0.00	0.00
(HexNAc2 Hex3)Fuc(HexNAcHex)4HexNAc2	1555.89	1495.58	1530.19	1538.27	1791.76	0.00	0.10	0.00	0.00	0.00	0.00	0.04	0.00	0.00	0.00
(HexNAc2 Hex3)Fuc(HexNAcHex)5HexNAc	1596.16	1549.27	1570.45	1591.96	1845.45	0.00	0.00	0.00	0.00	0.00	0.00	0.00	0.00	0.00	0.00

Figure C.2: Table of the relative abundances of every glycan structures on each sites of Sec-Pdi.

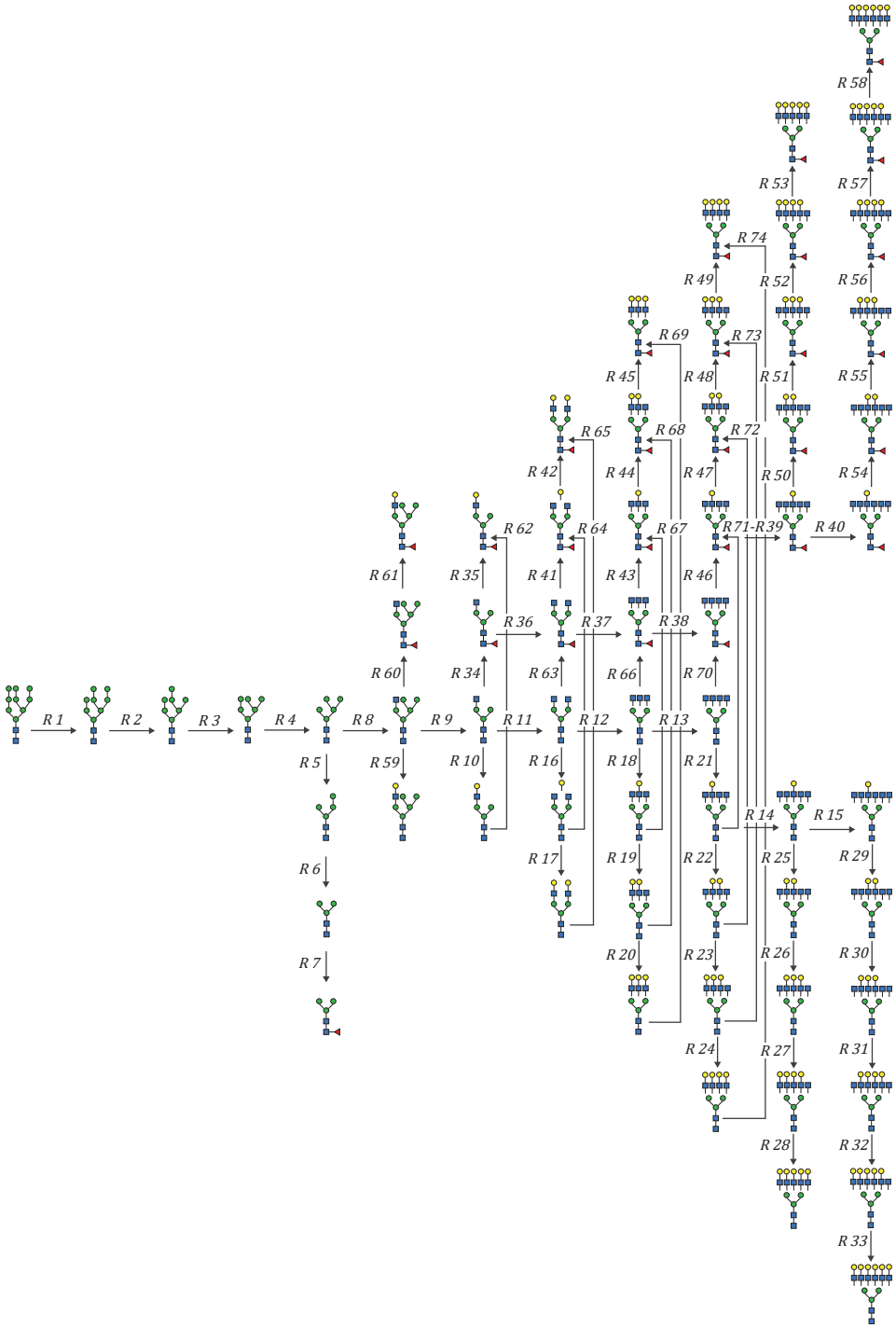

Figure C.3: Full network of Pdi with numbering.

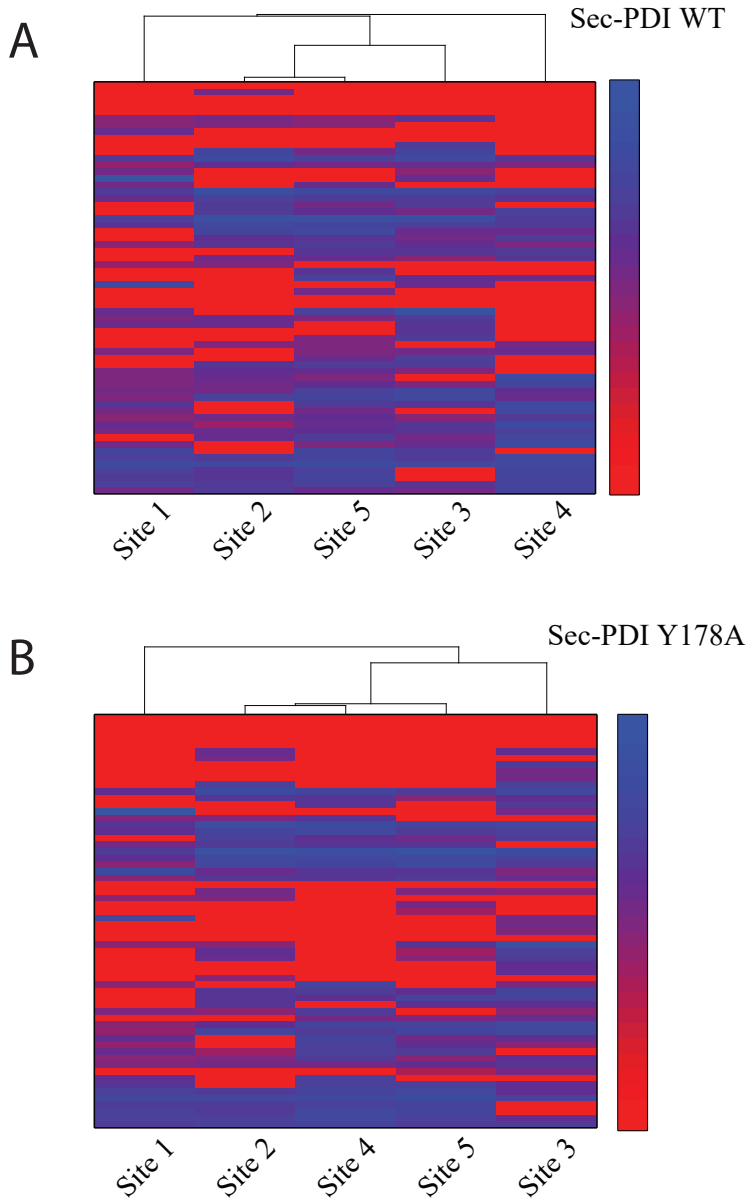

Figure C.4: Hierarchical clustering of the 5 sites based on Euclidean distance for A. Sec-Pdi and B. Sec-Y178A. The colors represent the relative abundance of the species (color bar in log scale). The structures are listed in the opposite order of Figure C.2.

Appendix D

Appendix to Chapter 6

D.1 Experimental

D.1.1 Preparation and Purification of Heavy and Light-Labeled Human IgG

CHO-S cells stably expressing IgG (provided by Biopharma Merck AG, Switzerland) were cultivated in suspension in expansion medium (customized medium by Biopharma Merck AG) at 320 rpm, 37 °C, 5% CO2 in a shaking incubator (Adolf Kuhner AG, Birsfelden, Switzerland). For the SILAC labeling, cells were centrifuged for 3 min at 300 rcf and resuspended at $5 \cdot 10^5$ cells/mL either in light or in heavy SILAC medium (containing light L-arginine and L-lysine or 13C-arginine and 13C, 15N-lysine, respectively). Cells were subcultured in SILAC medium every two days for 6 days to reach complete heavy isotope labelling. $5 \cdot 10^7$ cells from light or heavy culture were collected after centrifugation and lysed with 10 mL lysis buffer (3% Triton X-100, 110 mM KAc, 20 mM HEPES, 2mM MgCl2, pH 7.2, 1X complete EDTA-free protease inhibitor cocktail Roche). Protease inhibitor cocktails tablets (complete EDTA-free protease inhibitor cocktail tablets, Roche) were added to the cleared supernatants. The IgGs were purified via Protein-A-capture by adding 200 μL of Protein A Sepharose 4 Fast Flow beads (GE Healthcare Life Science) to the cell lysates and culture supernatants solutions. Batch binding was performed under continuous rotation for 3 h. Beads were then washed by centrifugation with 10 mL 0.02 M sodium phosphate buffer. IgGs were eluted by shaking the beads for 10 min in 800 μL 0.1 M citric acid in 1.5-mL Eppendorf. Eluates were placed onto 30K-cut off Micro filter (Millipore) and washed three times with water.

D.1.2 SILAC Labeling

CHO-S cells growing in expansion medium were transferred to light SILAC medium as described above and subcultured every two days for 6 days. For the last subculturing prior to the experiment, the cell were seeded to a cell density of $1 \cdot 10^6$ cells/mL. On the day of heavy chase experiment, cells (at concentration $5 \cdot 10^6$ cells/mL) were resuspended in heavy SILAC medium (hereby referred to as time 0, t0). Then, cells were incubated at 320 rpm, 37 °C, 5% CO2 for 4 hours. At different time points, 8 mL of culture (corresponding to roughly $5 \cdot 10^7$ cells) were sampled and subjected to centrifugation for 3 min at 300 rcf. Cell pellets and supernatants were flash frozen with

liquid nitrogen and kept at -20 °C prior to protein purification. For protein-A-capture, the cells were lysed with 10 mL lysis buffer and protease inhibitor cocktail tablets were also added to the cleared supernatants. The IgGs were purified as described above.

D.1.3 Cell Culture with Inhibitors of Glycosylation-Processing Enzymes

Cells were pre-treated in SILAC light medium with swainsonine (SWA) at 20 μM final concentration [349] for 2h. At time point t0, the cells were switched to the SILAC heavy medium containing 13C-arginine and 13C,15N-lysine and 20 μM swainsonine was added, to maintain the swainsonine concentration. $5 \cdot 10^7$cells were collected at different points (0, 10, 20, 30, 60, 90, 120, 180, 240 min). IgGs were purified via protein-A-capture and subjected to SILAC-PRM analysis. The same procedure was followed for kifunensine treatment, using 10 μM final concentration [349]. For bafalomycin and MG132 treatment, 100nM and 80 μM final concentrations were used, respectively (48, 49).

D.1.4 Sample Preparation for Mass Spectrometry Analysis

IgGs were further processed according to the FASP (filter-aided sample preparation) procedure modified from Wisniewski et al. [352]. Shortly, 25-100 μg IgGs were reduced with 100 mM DTT in 50mM ABC buffer (ammonium bicarbonate) pH 8.5 for 30 min at 37°C and alkylated with 130 mM iodacetamide (IAA) in 50mM ABC buffer for 25 min at 37 °C. Sequencing Grade Trypsin (Promega) was used to digest proteins at the ratio of 1:80 over night at 37°C. Peptides were collected by centrifugation and the filters were washed once with water and once with 10% acetonitrile in ddH2O. All flow through fractions were pooled and dried via SpeedVac centrifugation (Thermo Fischer). All samples were desalted by C18-ZipTip (Millipore) prior to MS analysis.

D.1.5 NanoUPLC-DDA and NanoUPLC-PRM for Glycopeptide Identification and Quantification

The discovery of all glycoforms were first performed on LTQ-Orbitrap Velos (Thermo Fisher Scientific) as previously described [277]. All quantitative experiments were performed with the nanoACQUITY UPLC system (Waters), coupled online to a calibrated

Q Exactive HF mass spectrometer (Thermo Fischer Scientific) with a PicoviewTM nanospray source 500 model (New Objective). The tryptic samples were dissolved in 2% acetonitrile/0.1% formic acid, loaded onto a nanoACQUITY UPLC 2G C18 trap column (180 μm × 20 mm, 100 Å, 5 μm particle size) and separated on a nanoACQUITY UPLC BEH130 C18 column (75 μm × 250 mm, 130 Å, 1.7 μm particle size), at a constant flow rate of 300 nL/min, with a column temperature of 50 °C and a linear gradient of 1 to 35% acetonitrile/0.1% formic acid in 42 min, followed by a sharp increase to 98% acetonitrile in 2 min and then held isocratically for another 10 min. For DDA analysis, one scan cycle comprised of a full scan MS survey spectrum, followed by up to 10 sequential HCD scans based on the intensity. Full-scan MS spectra (800–2000 m/z, for inhibitory experiments 500-2000 m/z) were acquired in the FT-Orbitrap at a resolution of 60,000 at 400 m/z, while HCD MS/MS spectra were recorded in the FT-Orbitrap at a resolution of 30,000 at 400 m/z. HCD MS/MS spectra were performed with a target value of $5 \cdot 10 \cdot 5$ by the collision energy setup at a normalized collision energy (NCE) of 22%. For PRM analysis, one scan cycle comprised a full scan MS survey spectrum, followed by 10 sequential PRM scans based on the inclusion list. Full-scan MS spectra (800–2000 m/z) were acquired in the FT-Orbitrap at a resolution of 60,000 at 400 m/z, while PRM MS/MS spectra were recorded in the FT-Orbitrap at a resolution of 60,000 at 400 m/z. PRM MS/MS spectra were performed with a target value of $5 \cdot 10^5$ by the collision energy setup at a NCE either of 22% or 16%. Automatic gain control (AGC) target values were $3 \cdot 10^6$ for full FTMS. The setup of each precursor ion was the average of observed light labelled glycopeptides from Velos measurement and their theoretical corresponding heavy-labelled m/z. The quadrupole isolation window for each precursor was 6 m/z.

D.1.6 Data Analysis and SILAC-nano-HPLC-PRM Methodology Evaluation

In order to setup and evaluate the SILAC-PRM methodology for glycopeptides quantification, heavy-labelled IgG glycopeptides were mixed with light-labelled ones at the ratios of 5:1, 4:2, 2:4 and 1:5 before MS analysis. Data were first analyzed with XCalibur 3.0 (Thermo Fischer) software manually. For quantification, one or three fragment (transition) ions of each precursor were used for manual extraction and inspection based on the abundance, interference-free signal and representative potential to each structure.

10 ppm of mass tolerance was used for peak extraction in each PRM spectrum. For some structures, only two transitions were used for quantification. Both peak area and height of each transition were evaluated as quantification method.

D.1.7 Semi-Automated Glycopeptide Analysis Using Skyline

MS2-level quantification was performed with the software Skyline [353], similarly to Pan and colleagues [354], by inserting manually the unique glyco-transitions into the software (Figure D.2 B). All fragment ions were defined based on their chemical formula and added into Skyline manually. In addition, the presence of glycan oxonium ions was also used to confirm all types of glycopeptides with the same principle as described for XCaliburTM analysis. The peak height of each transition was used for quantification.

D.1.8 Fractional labeling quantification and analysis

For control experiments and Swainsonine-treated cells, the fractional labeling for a given glycopeptide at each time point was defined as the ratio between the measured intensity of the heavy-labeled species H and the sum of the heavy- and light-labeled species (H+L). We noticed that this type of normalization produced biased values for the heavy to light ratio in Kifunensine-treated cells, since a large intracellular pool of Man_{8-5} glycans was still present 6h after addition of the ER Man I inhibitor. This resulted in a significant underestimation of the fraction labeling for most of the high mannose species, which was not due to reduced enzyme kinetics (for example, Golgi mannosidase I is not affected by Kifunensine), but due to the residual amount of light species in the system. To account for this, the values of heavy- and light-labeled species at intermediate time points were normalized with respect to the steady-state value of heavy- and light-labeled fractions.

D.2 Model

D.2.1 Justification for the Use of First-Order Rate Equations

For an enzyme-catalyzed reaction following the Michaelis-Menten kinetics, the reaction rate r for the conversion of a generic substrate S can be written as (Eq. D.1):

$$r = \frac{V_{max}\,[S]}{K_M + [S]} \tag{D.1}$$

During pulse-chase experiments, the reaction rate for the consumption of an H-labeled substrate assumes the form in Eq. D.2:

$$r = \frac{V_{max}\,[S]^H}{K_M + [S]^L + [S]^H} \tag{D.2}$$

The model assumes intracellular steady state with respect to enzyme and substrate concentration as well as enzyme activity. Under these assumptions, the amount of substrate S is constant and can be written as (Eq. D.3):

$$S = S^L + S^H = const. \tag{D.3}$$

Since the enzyme activity is also assumed constant and the K_M value is constant by definition, the equation for the rate equation can be simplified as shown in Eq. D.4:

$$r = k\,[S]^H \tag{D.4}$$

Where the constant k accounts for the enzymatic activity and the competitive inhibition present in the system investigated. This simplification is also valid for more complex kinetic mechanisms, since the cell machinery is supposed to operate at a constant enzyme, total H+L substrate and inhibitor concentration.

D.2.2 Kinetic Theories for *in vivo* $Man_4GlcNAc_2$ Generation

Considering the L to H-labeled turnover rates for the various ER species, $Man_4GlcNAc_2$ is slightly slower than $Man_9GlcNAc_2$, but significantly faster than all other high mannose species. If all the non-folded glycoproteins in the ER could aggregate with the

same kinetic constant (Figure D.8 A), the model would predict a slower turnover rate of $Man_4GlcNAc_2$ compared to the one experimentally detected, since the total pool of $Man_9GlcNAc_2$ is lower in size than the sum of all other (slower) high mannose species. Another possibility is that aggregation occurs at the $Glc_1Man_9GlcNAc_2$ level. This species is known to interact with Calnexin and Calreticulin, chaperons responsible for disulfide bond formation. Errors in this process might lead to the formation of very unstable intermediates that could possibly be extremely prone to aggregate (Figure D.8 B). The model confirms that this is a possible behavior since it can fit the $Man_4GlcNAc_2$ data correctly for control, swainsonine- and kifunensine-treated experiments. Alternatively, it is still possible to consider every unfolded glycoprotein in the ER to be eligible for aggregation, but the propensity for this to occur decreases the more units of mannose are trimmed, due to the repeated interactions with chaperons that can stabilize the structure of the proteins (Figure D.8 C). To test this hypothesis, we assumed the aggregation rate k_{agg} to scale for high mannose species using the following relation (Eq. D.5):

$$k_{agg} = \frac{k_{agg,Man_9Glc_1}}{x^{n \cdot i}} \tag{D.5}$$

Where $kagg, Man_9Glc_1$ is the aggregation constant for the monoglucosilated glycoproteins, x and n are scaling factors and i is the number of mannose units trimmed. For the model to correctly predict the $Man_4GlcNAc_2$ kinetics, it was found that the value of x has to be lower than 10^{-4}, indicating that aggregation is prevalently happening at the $Glc_1Man_9GlcNAc_2$ level even If this mechanism is assumed.

Table D.1: ER-related parameters. Non-identifiable parameters are indicated with the notation n.i.

Kinetic Constant	Variable	Value (ctr)	Value (SWA)	Value (KIF)
Folding	$k_{folding}$	5.44E-03±1.39E-04	5.89E-03±6.29E-06	7.80E-03±1.36E-04
Cytosolic transport (ERAD)	k_T^{cyt}	1.36E-02±5.51E-03	4.33E-03±2.03E-03	n.i.
ERAD degradation	k_{deg}^{Cyt}	6.68E-03±8.37E-04	6.18E-03±2.20E-03	n.i.
Aggregation	k_{agg}	9.63E-01±9.2E-01	2.18E+00±1.24E-01	2.54E+00±1.89E+00
Lysosomal degradation	k_{deg}^{Lys}	1.12E-02±4.77E-03	1.14E-02±1.91E-03	1.33E-02±1.24E-02
Man_9 to Man_8 trimming	$k_{9\to8}$	1.17E-02±2.53E-04	9.04E-03±6.49E-04	0
Man_8 to Man_7 trimming	$k_{8\to7}$	3.52E-03±3.38E-04	3.00E-03±1.46E-04	n.i.
Man_7 to Man_6 trimming	$k_{7\to6}$	3.76E-02±1.40E-02	1.90E-02±9.71E-03	n.i.
Man_6 to Man_5 trimming	$k_{6\to5}$	1.07E-03±1.13E-04	1.22E-03±8.50E-04	n.i.

Table D.2: Golgi-related parameters. Non-identifiable parameters are indicated with the notation n.i.

Enzyme	Variable	Value (ctr)	Value (SWA)	Value (KIF)
Golgi α-mannosidase I	E_{max}	4.88E+00±1.30E-01	2.80E+00±1.80E+00	1.18E-01±6.38E-03
	z_{max}	1.50E-01±6.52E-15	1.99E-01±1.46E-02	-1.50E-02±1.08E-03
N-Acetylglucosaminyltransferase	E_{max}	2.42E+00±6.61E-01	1.22E+00±7.46E-01	n.i
	z_{max}	2.55E-01±6.65E-02	3.24E-01±3.15E-01	n.i
Golgi α-mannosidase II	E_{max}	5.28E+00±3.50E-13	0	n.i
	z_{max}	3.53E-01±2.17E-14	n.i	n.i
α-(1,6)-fucosyltransferase	E_{max}	1.55E+00±1.63E-01	2.60E+00±1.74E+00	n.i
	z_{max}	3.87E-01±3.35E-15	3.24E-01±1.37E-14	n.i
N-Acetylglucosaminyltransferase II	E_{max}	1.60E+00±1.79E-01	n.i	n.i
	z_{max}	4.78E-01±4.01E-16	n.i	n.i
Galactosyltransferase	E_{max}	1.75E-01±1.30E-14	5.02E-01±2.51E-01	n.i
	z_{max}	7.77E-01±1.29E-01	7.51E-01±1.28E-01	n.i
Sialyltransferase	E_{max}	5.61E-02±3.88E-02	2.76E-01±2.15E-01	n.i
	z_{max}	8.07E-01±5.60E-01	8.24E-01±1.00E-01	n.i
All	ω	8.16E-02±2.68E-03	8.16E-02±2.68E-03	8.16E-02±2.68E-03

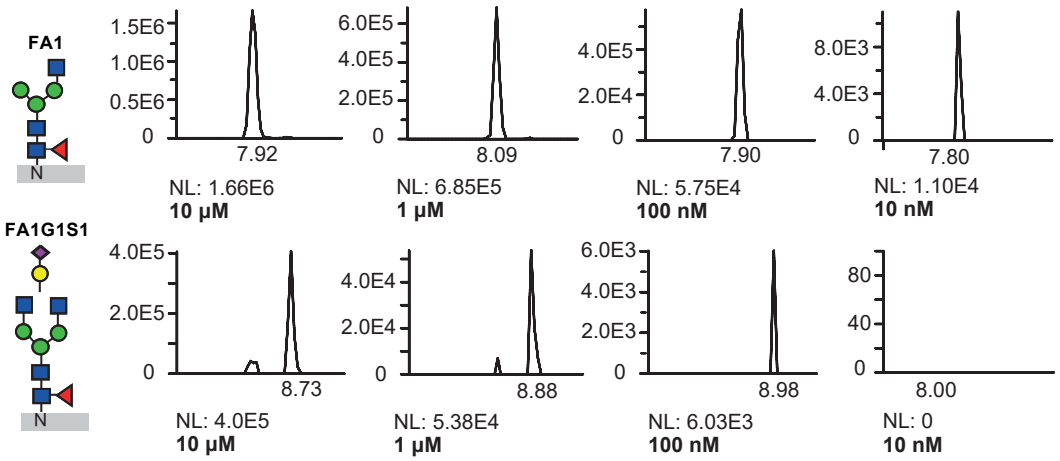

Figure D.1: Y1 ion [peptide + HexNAc] XIC of PRM scan for two IgG glycoform (FA_1 top, $FA_1G_1S_1$ bottom) from different dilutions (10 μM to 10nM). The value of the peak intensity is reported under each graph.

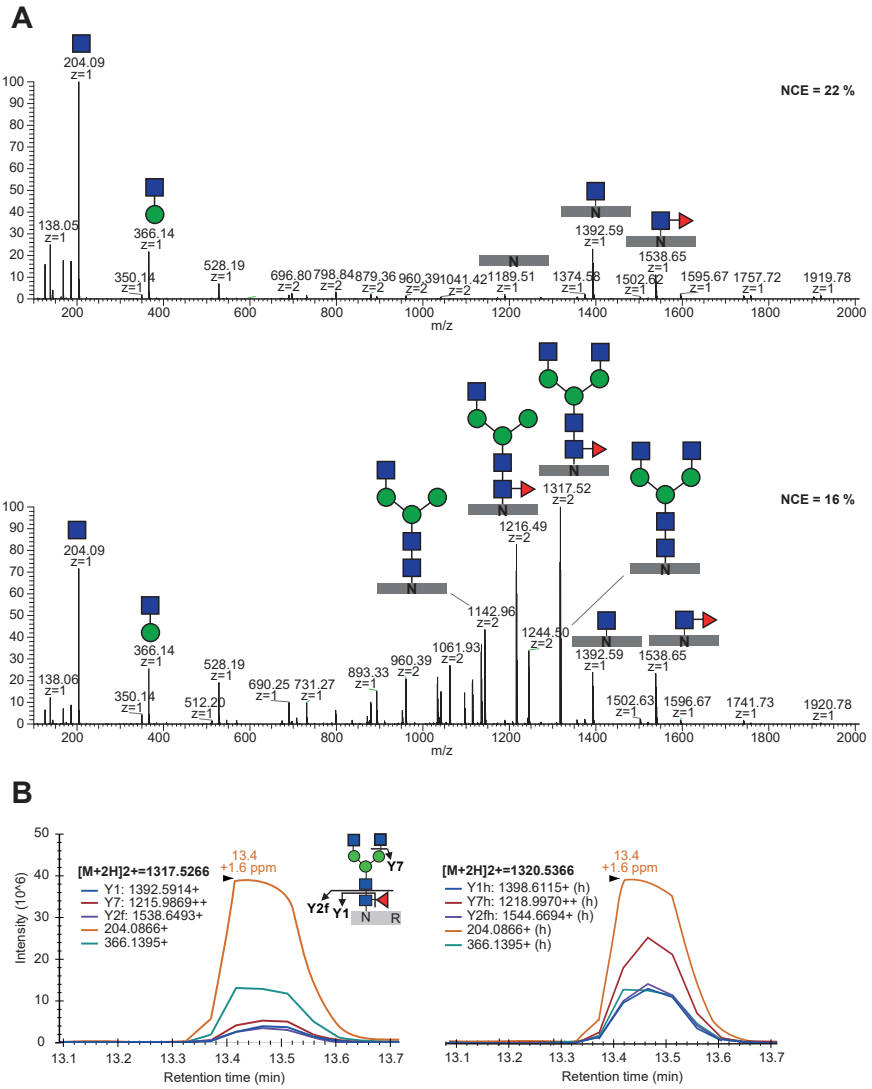

Figure D.2: (A) Representative MS2 spectrum of IgG glycopeptide bearing $FA_2GlcNAc_2$ glycan structure obtained using normalized collision energy (NCE) of 22% (top spectrum) or 16% (bottom spectrum). Mass and charge state of fragment ions are indicated above the peaks. Fragments cartoons are present above the major fragment ion used for quantification. (B) Skyline XIC of oxonium and glyco-transitions (fragment ions) from the PRM spectra of IgG FA_2 glycoform, for both the light (left) and heavy (right) glycopeptide. The precursor ion as well as the fragment ions mass and charge state are indicated for both heavy and light counterpart.

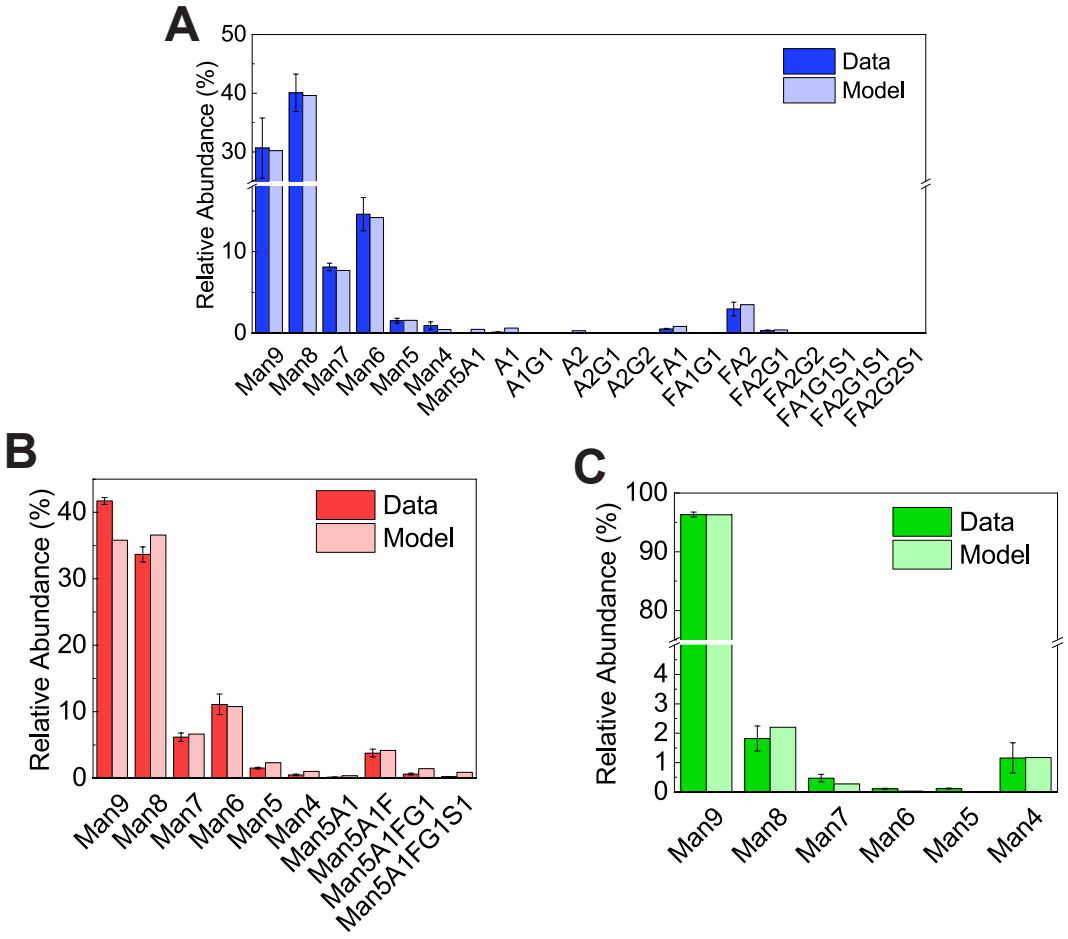

Figure D.3: Comparison between experimental data and model fitting for the intracellular glycan fractions for control (A), Swainsonine- (B) and Kifunensine- (C) treated cells (n=3).

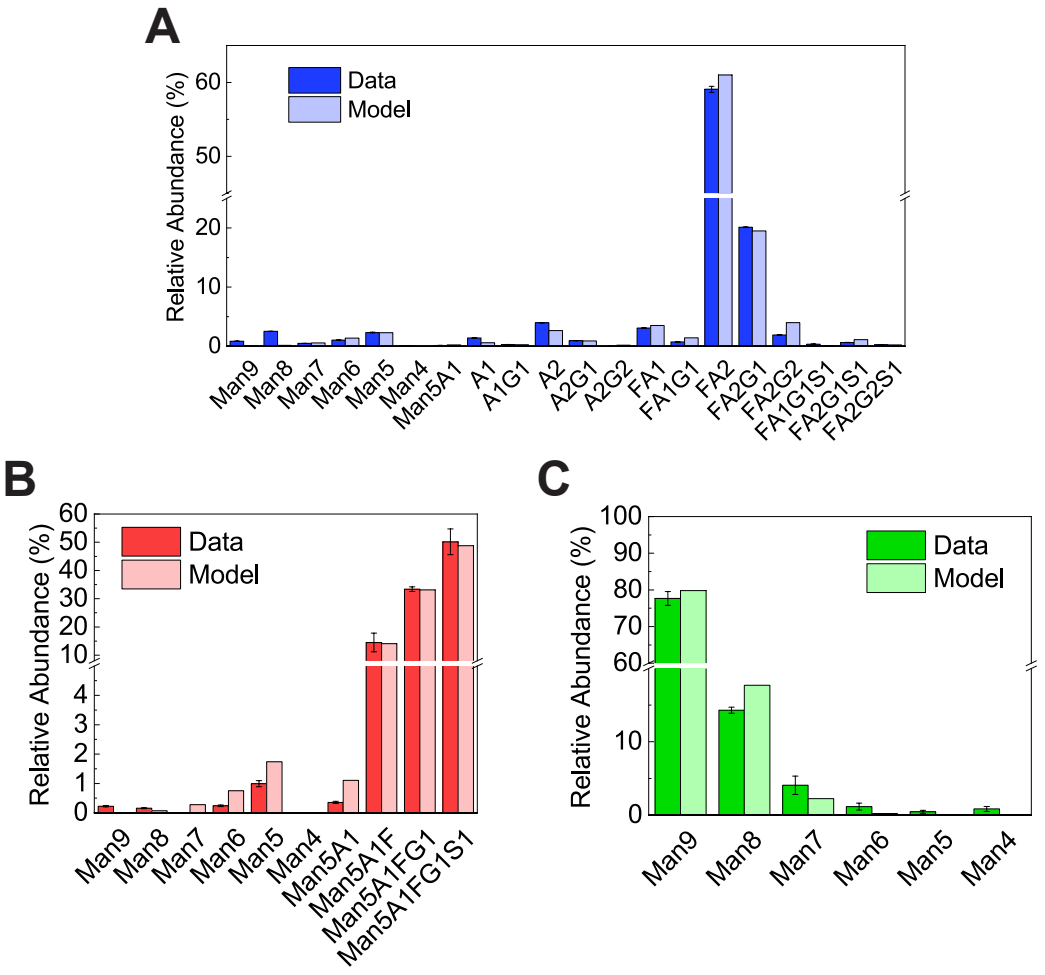

Figure D.4: Comparison between experimental data and model fitting for the secreted glycan fractions for control (A), Swainsonine- (B) and Kifunensine- (C) treated cells (n=3)

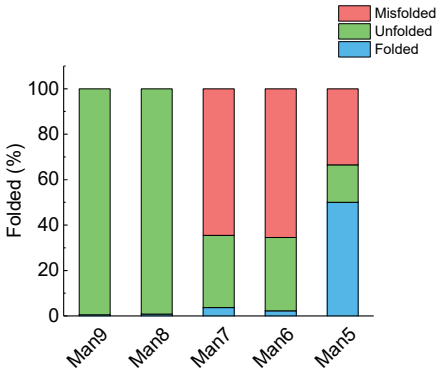

Figure D.5: Model-based estimation of the fraction of folding intermediates, misfolded and folded oligommanose structures in ER and Golgi

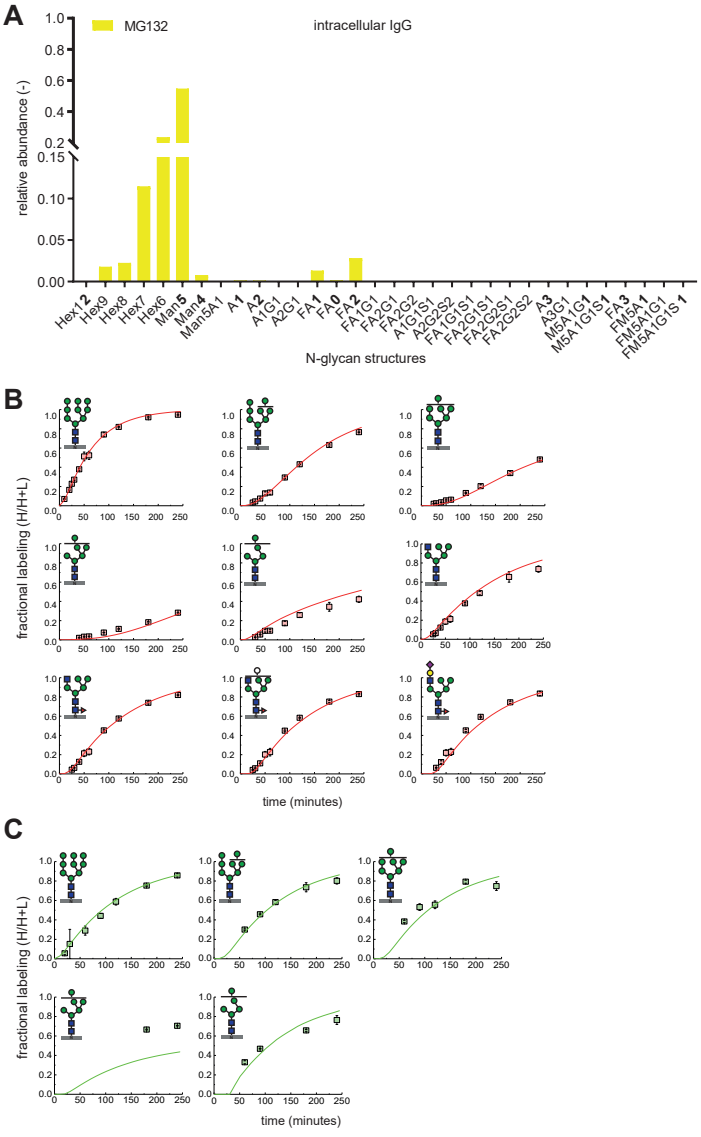

Figure D.6: (A) Steady-state intracellular N-glycan profiling of IgG purified form cells treated with MG132 (80 /*mu*M). Cells were switched to heavy SILAC medium containing MG132 and after 4 hours $5/cdot10^6$ cells were harvested and IgG purified via protein-A capture and subjected to SILAC-PRM measurements. The relative abundance of each N-glycoform (B). Fractional labeling of IgG glycopeptides bearing N-glycan intermediates under SWA treatment. Error bars show the standard deviation of three independent experiments (C) Fractional labeling of IgG glycopeptides bearing N-glycan intermediates under KIF treatment.

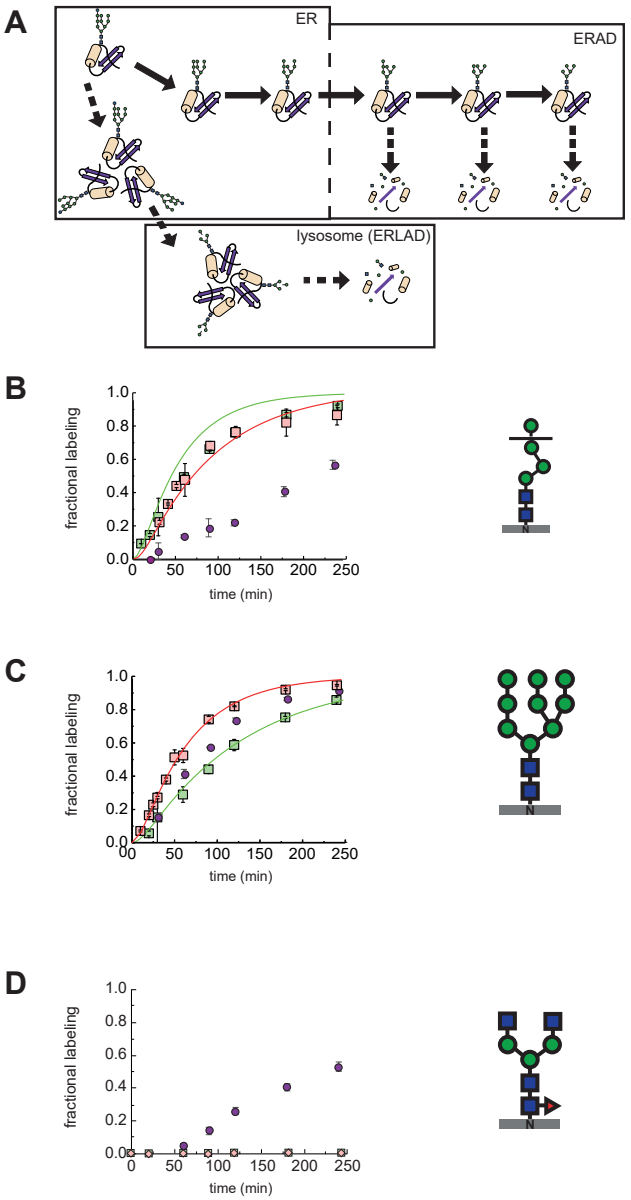

Figure D.7: (A) Schematic representation of the hypothesized mechanism for $Man_4GlcNAc_2$ generation. (B) Fractional labeling of the IgG glycopeptide bearing the $Man_4GlcNAc_2$ structure under control, SWA, KIF and BAF treatment. Fractional labeling of the IgG glycopeptide bearing the $Man_9GlcNAc_2$ (C) and $FA_2GlcNAc_2$ (D) structures under the same conditions.

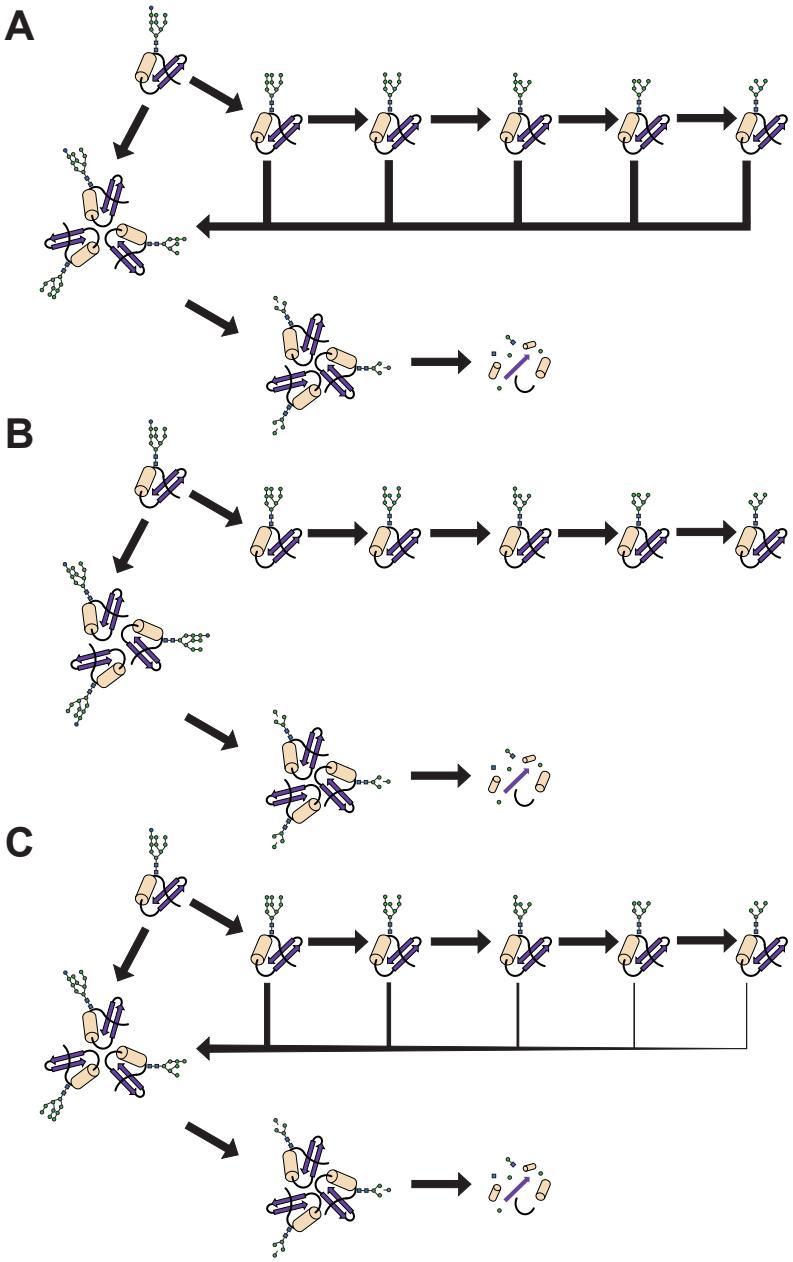

Figure D.8: (A) Every unfolded protein in the ER can aggregate, with no difference in the kinetic constant of the process. (B) Aggregation occurs mainly foe $Glc_1Man_9GlcNAc_2$-bearing structures. (C) Every unfolded protein in the ER can aggregate, but the corresponding kinetic constant decreases with the time the protein spent in the ER, represented by the trimming of mannose residues.

Bibliography

[1] G. Walsh, Biopharmaceuticals and biotechnology medicines: An issue of nomenclature. *European Journal of Pharmaceutical Sciences* 2002, 15 (2), 135–138.

[2] G. Jagschies, *Chapter 1 – Disease and Healthcare Priorities*. Elsevier Ltd., 2018.

[3] B. Montgomery, *Chapter 54 - Basics of Financial Management*. 8, Elsevier Ltd., 2017.

[4] M. A. Fischbach, J. A. Bluestone, W. A. Lim, Cell-based therapeutics: The next pillar of medicine. 2013.

[5] J. M. Reichert, Trends in US approvals: new biopharmaceuticals and vaccines. *Trends in biotechnology* 2006, 24 (7), 293–8.

[6] R. P. Evens, Pharma Success in Product Development—Does Biotechnology Change the Paradigm in Product Development and Attrition. *The AAPS journal* 2016, 18 (1), 281–5.

[7] F. Li, N. Vijayasankaran, A. Y. Shen, R. Kiss, A. Amanullah, Cell culture processes for monoclonal antibody production. *mAbs* 2010, 2 (5), 466–79.

[8] H. Liu, G. Gaza-Bulseco, D. Faldu, C. Chumsae, J. Sun, Heterogeneity of Monoclonal Antibodies. *Journal of Pharmaceutical Sciences* 2008, 97 (7), 2426–2447.

[9] A. Eon-Duval, H. Broly, R. Gleixner, Quality attributes of recombinant therapeutic proteins: an assessment of impact on safety and efficacy as part of a quality by design development approach. *Biotechnology Progress* 2012, 28 (3), 608–622.

[10] Y. Y. Lipsitz, N. E. Timmins, P. W. Zandstra, Quality cell therapy manufacturing by design. *Nat Biotechnol* 2016, 34 (4), 393–400.

[11] T. K. Villiger, E. Scibona, M. Stettler, H. Broly, M. Morbidelli, M. Soos, Controlling the time evolution of mAb N-linked glycosylation - Part II: Model-based predictions. *Biotechnology Progress* 2016, 32 (5), 1135–1148.

[12] E. Buzhor, L. Leshansky, J. Blumenthal, H. Barash, D. Warshawsky, Y. Mazor, R. Shtrichman, Cell-based therapy approaches: The hope for incurable diseases. 2014.

[13] Y. Levinson, R. G. Beri, K. Holderness, I. F. Ben-Nun, Y. Shi, E. Abraham, Bespoke cell therapy manufacturing platforms. *Biochemical Engineering Journal* 2018, 132, 262–269.

[14] I. Weissman, Stem cell therapies could change medicine... If they get the chance. *Cell Stem Cell* 2012, 10 (6), 663–665.

[15] Y. Y. Lipsitz, P. Bedford, A. H. Davies, N. E. Timmins, P. W. Zandstra, Achieving Efficient Manufacturing and Quality Assurance through Synthetic Cell Therapy Design. *Cell Stem Cell* 2017, 20 (1), 13–17.

[16] A. R. Perry, D. C. Linch, The history of bone-marrow transplantation. in *Blood Reviews*, volume 10, Pearson Professional Ltd, 215–219.

[17] G. Cossu, M. Birchall, T. Brown, P. De Coppi, E. Culme-Seymour, S. Gibbon, J. Hitchcock, C. Mason, J. Montgomery, S. Morris, F. Muntoni, D. Napier, N. Owji, A. Prasad, J. Round, P. Saprai, J. Stilgoe, A. Thrasher, J. Wilson, Lancet Commission: Stem cells and regenerative medicine. 2018.

[18] E. J. Culme-Seymour, N. L. Davie, D. A. Brindley, S. Edwards-Parton, C. Mason, A decade of cell therapy clinical trials (2000-2010). 2012.

[19] Pharmaceuticals Research & Manufacturers of America (PhRMA), Medicines in Development for Biologics 2013 Report. 2013, PhRMA: Washington DC, USA. Technical report, 2013.

[20] Center for Biologics Evaluation and Research, Regulatory Considerations for Human Cells, Tissues, and Cellular and Tissue- Based Products: Minimal Manipulation and Homologous Use. *Food and Drug Administration* 2017.

[21] M. Geukes Foppen, M. Donia, I. Svane, J. Haanen, Tumor-infiltrating lymphocytes for the treatment of metastatic cancer. *Molecular Oncology* 2015, 9 (10), 1918–1935.

[22] V. Florea, A. C. Rieger, D. L. DiFede, J. El-Khorazaty, M. Natsumeda, M. N. Banerjee, B. A. Tompkins, A. Khan, I. H. Schulman, A. M. Landin, M. Mushtaq, S. Golpanian, M. H. Lowery, J. J. Byrnes, R. C. Hendel, M. G. Cohen, K. Valasaki, M. V. Pujol, E. Ghersin, R. Miki, C. Delgado, F. Abuzeid, M. Vidro-Casiano, R. G. Saltzman, D. DaFonseca, L. V. Caceres, K. N. Ramdas, A. Mendizabal, A. W. Heldman, R. D. Mitrani, J. M. Hare, Dose comparison study of allogeneic mesenchymal stem cells in patients with ischemic cardiomyopathy (The TRIDENT study). *Circulation Research* 2017, 121 (11), 1279–1290.

[23] E. Csaszar, D. C. Kirouac, M. Yu, W. Wang, W. Qiao, M. P. Cooke, A. E. Boitano, C. Ito, P. W. Zandstra, Rapid expansion of human hematopoietic stem cells by automated control of inhibitory feedback signaling. *Cell Stem Cell* 2012, 10 (2), 218–229.

[24] Y. Lei, D. V. Schaffer, A fully defined and scalable 3D culture system for human pluripotent stem cell expansion and differentiation. *Proceedings of the National Academy of Sciences* 2013, 110 (52), E5039–E5048.

[25] M. C. Milone, B. L. Levine, Powered and controlled T-cell production. *Nature Biomedical Engineering* 2018, 2 (3), 148–150.

[26] A. Aijaz, M. Li, D. Smith, D. Khong, C. LeBlon, O. S. Fenton, R. M. Olabisi, S. Libutti, J. Tischfield, M. V. Maus, R. Deans, R. N. Barcia, D. G. Anderson, J. Ritz, R. Preti, B. Parekkadan, Biomanufacturing for clinically advanced cell therapies. *Nature Biomedical Engineering* 2018, 2 (6), 362–376.

[27] F. M. Wurm, Production of recombinant protein therapeutics in cultivated mammalian cells. *Nature biotechnology* 2004, 22 (11), 1393–8.

[28] K. Itakura, T. Hirose, R. Crea, A. D. Riggs, H. L. Heyneker, F. Bolivar, H. W. Boyer, Expression in Escherichia coli of a chemically synthesized gene for the hormone somatostatin. *Science (New York, N.Y.)* 1977, 198 (4321), 1056–63.

[29] E. Waltz, It's official: biologics are pharma's darlings. *Nature Biotechnology* 2014, 32 (2), 117–117.

[30] B. Kelley, Industrialization of mAb production technology: the bioprocessing industry at a crossroads. *mAbs* 2009, 1 (5), 443–52.

[31] F. M. Wurm, M. de Jesus, Manufacture of Recombinant Therapeutic Proteins Using Chinese Hamster Ovary Cells in Large-Scale Bioreactors. in *Biosimilars of Monoclonal Antibodies*, John Wiley & Sons, Inc., Hoboken, NJ, USA, 2016, 327–353.

[32] F. H. Gage, Cell therapy. *Nature* 1998, 392 (6679 Suppl), 18–24.

[33] V. Prasad, Immunotherapy: Tisagenlecleucel — the first approved CAR-T-cell therapy: implications for payers and policy makers. *Nature Reviews Clinical Oncology* 2017, 15 (1), 11–12.

[34] R. P. Harrison, S. Ruck, N. Medcalf, Q. A. Rafiq, Decentralized manufacturing of cell and gene therapies: Overcoming challenges and identifying opportunities. *Cytotherapy* 2017, 19 (10), 1140–1151.

[35] N. Trainor, A. Pietak, T. Smith, Rethinking clinical delivery of adult stem cell therapies. *Nature Biotechnology* 2014, 32 (8), 729–735.

[36] S. S. Farid, M. J. Jenkins, Chapter 44 - Bioprocesses for Cell Therapies 2018.

[37] M. Al-rubeai, *Animal Cell Culture*, volume 9 of *Cell Engineering*. Springer International Publishing, Cham, 2015.

[38] D. C. Kirouac, P. W. Zandstra, The Systematic Production of Cells for Cell Therapies. *Cell Stem Cell* 2008, 3, 369–381.

[39] D. Eibl, R. Eibl, Bioreactors for Mammalian Cells: General Overview. Springer, Berlin, Heidelberg, 2009, 55–82.

[40] Q. a. Rafiq, K. Coopman, C. J. Hewitt, Scale-up of human mesenchymal stem cell culture: Current technologies and future challenges. *Current Opinion in Chemical Engineering* 2013, 2 (1), 8–16.

[41] J. F. Vera, L. J. Brenner, U. Gerdemann, M. C. Ngo, U. Sili, H. Liu, J. Wilson, G. Dotti, H. E. Heslop, A. M. Leen, C. M. Rooney, Accelerated Production of Antigen-specific T Cells for Preclinical and Clinical Applications Using Gas-permeable Rapid Expansion Cultureware (G-Rex). *Journal of Immunotherapy* 2010, 33 (3), 305–315.

[42] M.-A. Forget, R. J. Tavera, C. Haymaker, R. Ramachandran, S. Malu, M. Zhang, S. Wardell, O. J. Fulbright, C. L. Toth, A. M. Gonzalez, S. T. Thorsen, E. Flores, A. Wahl, W. Peng, R. N. Amaria, P. Hwu, C. Bernatchez, A Novel Method to Generate and Expand Clinical-Grade, Genetically Modified, Tumor-Infiltrating Lymphocytes. *Frontiers in Immunology* 2017, 8 (AUG), 1–8.

[43] J. Jin, M. Sabatino, R. Somerville, J. R. Wilson, M. E. Dudley, D. F. Stroncek, S. A. Rosenberg, Simplified Method of the Growth of Human Tumor Infiltrating Lymphocytes in Gas-permeable Flasks to Numbers Needed for Patient Treatment. *Journal of Immunotherapy* 2012, 35 (3), 283–292.

[44] J. M. Bielser, M. Wolf, J. Souquet, H. Broly, M. Morbidelli, Perfusion mammalian cell culture for recombinant protein manufacturing – A critical review. *Biotechnology Advances* 2018, 36 (4), 1328–1340.

[45] M. K. Wolf, V. Lorenz, D. J. Karst, J. Souquet, H. Broly, M. Morbidelli, Development of a shake tube-based scale-down model for perfusion cultures. *Biotechnology and Bioengineering* 2018, 115 (11), 2703–2713.

[46] M. S. Croughan, J.-F. Hamel, D. I. C. Wang, Hydrodynamic effects on animal cells grown in microcarrier cultures. *Biotechnology and Bioengineering* 2000, 67 (6), 841–852.

[47] O.-w. Merten, Advances in cell culture: anchorage dependence. *Philosophical transactions of the Royal Society of London. Series B, Biological sciences* 2015, 370 (1661), 20140040.

[48] D. C. Lane, J. W. Forrester, Invited Review and Reappraisal Industrial Dynamics. *The Journal of the Operational Research Society* 2006, 48 (10), 1037.

[49] P. G. Layer, A. Robitzki, A. Rothermel, E. Willbold, H. Wilson, A. Gierer, et Al., A. Moscona, V. Shacoori, et Al., W. Müller-Klieser, P. Layer, et Al., B. Gähwiler, S. Potter, J. Morris, A. Wobus, et Al., M. Götz, et Al., U. Technau, et Al., R. Bjerkvig, et Al., G. Daston, et Al., P. Layer, et Al., A. Robitzki, et Al., B. Pardo, P. Honegger, T. Takezawa, et Al., E. Tziampazis, A. Sambanis, L. Shea, et Al., G. Steinhoff, et Al., R. Akins, et Al., M. Liu, et Al., O. Brüstle, R. McKay, S. Lee, et Al., A. Alvarez-Buylla, N. Theise, et Al., C. Orlic, et Al., E. Willbold, P. Layer, M. Perron, W. Harris, I. Ahmad, et Al., A. Fischer, T. Reh, V. Tropepe, et Al., N. Lumelsky, et Al., M. Bauer, et Al., A. Rothermel, P. Layer, P. Layer, et Al., E. Willbold, et Al., E. Willbold, et Al., A. Rothermel, et Al., Of layers and spheres: the reaggregate approach in tissue engineering. *Trends in neurosciences* 2002, 25 (3), 131–4.

[50] T.-M. Achilli, J. Meyer, J. R. Morgan, Advances in the formation, use and understanding of multi-cellular spheroids. 2012.

[51] H. Page, P. Flood, E. G. Reynaud, Three-dimensional tissue cultures: current trends and beyond. *Cell and tissue research* 2013, 352 (1), 123–31.

[52] E. Y. Lee, Y. Xia, W. S. Kim, M. H. Kim, T. H. Kim, K. J. Kim, B. S. Park, J. H. Sung, Hypoxia-enhanced wound-healing function of adipose-derived stem cells: Increase in stem cell proliferation and up-regulation of VEGF and bFGF. *Wound Repair and Regeneration* 2009, 17, 540–547.

[53] T. J. Bartosh, J. H. Ylöstalo, A. Mohammadipoor, N. Bazhanov, K. Coble, K. Claypool, R. H. Lee, H. Choi, D. J. Prockop, Aggregation of human mesenchymal stromal cells (MSCs) into 3D spheroids enhances their antiinflammatory properties. *Proceedings of the National Academy of Sciences of the United States of America* 2010, 107 (31), 13724–9.

[54] J. Wu, M. R. Rostami, D. P. Cadavid Olaya, E. S. Tzanakakis, Oxygen Transport and Stem Cell Aggregation in Stirred-Suspension Bioreactor Cultures. *PLoS ONE* 2014, 9 (7), e102486.

[55] K. G. Chen, B. S. Mallon, R. D. McKay, P. G. Robey, Human Pluripotent Stem Cell Culture: Considerations for Maintenance, Expansion, and Therapeutics. *Cell Stem Cell* 2014, 14 (1), 13–26.

[56] M. Donia, S. M. Larsen, Ö. Met, I. M. Svane, Simplified protocol for clinical-grade tumor-infiltrating lymphocyte manufacturing with use of the Wave bioreactor. *Cytotherapy* 2014, 16 (8), 1117–1120.

[57] S. Eaker, E. Abraham, J. Allickson, T. A. Brieva, D. Baksh, T. R. Heathman, B. Mistry, N. Zhang, Bioreactors for cell therapies: Current status and future advances. *Cytotherapy* 2017, 19 (1), 9–18.

[58] A. W. Nienow, On impeller circulation and mixing effectiveness in the turbulent flow regime. *Chemical Engineering Science* 1997, 52 (15), 2557–2565.

[59] V. Jossen, C. van den Bos, R. Eibl, D. Eibl, Manufacturing human mesenchymal stem cells at clinical scale: process and regulatory challenges. 2018.

[60] T. K. Villiger, B. Neunstoecklin, D. J. Karst, E. Lucas, M. Stettler, H. Broly, M. Morbidelli, M. Soos, Experimental and CFD physical characterization of animal cell bioreactors: From micro- to production scale. *Biochemical Engineering Journal* 2018, 131, 84–94.

[61] C. Kropp, H. Kempf, C. Halloin, D. Robles-Diaz, A. Franke, T. Scheper, K. Kinast, T. Knorpp, T. O. Joos, A. Haverich, U. Martin, R. Zweigerdt, R. Olmer, Impact of Feeding Strategies on the Scalable Expansion of Human Pluripotent Stem Cells in Single-Use Stirred Tank Bioreactors. *STEM CELLS Translational Medicine* 2016, 5 (10), 1289–1301.

[62] D. Voisard, F. Meuwly, P. A. Ruffieux, G. Baer, A. Kadouri, Potential of cell retention techniques for large-scale high-density perfusion culture of suspended mammalian cells. *Biotechnology and Bioengineering* 2003, 82 (7), 751–765.

[63] F. Dos Santos, A. Campbell, A. Fernandes-Platzgummer, P. Z. Andrade, J. M. Gimble, Y. Wen, S. Boucher, M. C. Vemuri, C. L. Da Silva, J. M. S. Cabral, A xenogeneic-free bioreactor system for the clinical-scale expansion of human mesenchymal stem/stromal cells. *Biotechnology and Bioengineering* 2014, 111 (6), 1116–1127.

[64] H. Kempf, B. Andree, R. Zweigerdt, Large-scale production of human pluripotent stem cell derived cardiomyocytes. *Advanced Drug Delivery Reviews* 2016, 96, 18–30.

[65] P. C. Collins, W. M. Miller, E. T. Papoutsakis, Stirred culture of peripheral and cord blood hematopoietic cells offers advantages over traditional static systems for clinically relevant applications. *Biotechnology and Bioengineering* 1998, 59 (5), 534–543.

[66] A. E. Foster, K. Forrester, D. J. Gottlieb, G. W. Barton, J. A. Romagnoli, K. F. Bradstock, Large-scale expansion of cytomegalovirus-specific cytotoxic T cells in suspension culture. *Biotechnology and Bioengineering* 2004, 85 (2), 138–146.

[67] X. Wang, I. Rivière, Clinical manufacturing of CAR T cells: foundation of a promising therapy. *Molecular Therapy—Oncolytics* 2016, (February), 1–7.

[68] M.-F. Clincke, C. Mölleryd, Y. Zhang, E. Lindskog, K. Walsh, V. Chotteau, Very high density of CHO cells in perfusion by ATF or TFF in WAVE bioreactor™. Part I. Effect of the cell density on the process. *Biotechnology Progress* 2013, 29 (3), 754–767.

[69] T. Kaartinen, A. Luostarinen, P. Maliniemi, J. Keto, M. Arvas, H. Belt, J. Koponen, A. Loskog, S. Mustjoki, K. Porkka, S. Ylä-Herttuala, M. Korhonen, Low interleukin-2 concentration favors generation of early memory T cells over effector phenotypes during chimeric antigen receptor T-cell expansion 2017.

[70] L. Gattinoni, D. E. Speiser, M. Lichterfeld, C. Bonini, T memory stem cells in health and disease. *Nat Med* 2017, 23 (1), 18–27.

[71] J. Petricciani, T. Hayakawa, G. Stacey, J. H. Trouvin, I. Knezevic, Scientific considerations for the regulatory evaluation of cell therapy products. *Biologicals* 2017, 50, 20–26.

[72] T. R. Heathman, A. W. Nienow, M. J. McCall, K. Coopman, B. Kara, C. J. Hewitt, The translation of cell-based therapies: clinical landscape and manufacturing challenges. *Regenerative Medicine* 2015.

[73] K. Maeda, Kazuhisa, New Method of Measurement of Epidermal Turnover in Humans. *Cosmetics* 2017, 4 (4), 47.

[74] Y. Barrandon, H. Green, Three clonal types of keratinocyte with different capacities for multiplication. *Proceedings of the National Academy of Sciences of the United States of America* 1987, 84 (8), 2302–6.

[75] C. Blanpain, E. Fuchs, Epidermal stem cells of the skin. *Annual review of cell and developmental biology* 2006, 22, 339–73.

[76] S. Kumar, B. B. Mahajan, S. Kaur, A. Singh, Grafting of burns with cultured epithelium prepared from autologous epidermal cells. *Lancet (London, England)* 1981, 1 (8211), 75–8.

[77] Z. Li, P. Maitz, Cell therapy for severe burn wound healing. *Burns & Trauma* 2018, 6 (1), 13.

[78] T. Hirsch, T. Rothoeft, N. Teig, J. W. Bauer, G. Pellegrini, L. De Rosa, D. Scaglione, J. Reichelt, A. Klausegger, D. Kneisz, O. Romano, A. S. Seconetti, R. Contin, E. Enzo, I. Jurman, S. Carulli, F. Jacobsen, T. Luecke, M. Lehnhardt, M. Fischer, M. Kueckelhaus, D. Quaglino, M. Morgante, S. Bicciato, S. Bondanza, M. De Luca, Regeneration of the entire human epidermis using transgenic stem cells. *Nature Publishing Group* 2017, 551, 3–2.

[79] G. Cotsarelis, S.-Z. Cheng, G. Dong, T.-T. Sun, R. M. Lavker, Existence of slow-cycling limbal epithelial basal cells that can be preferentially stimulated to proliferate: Implications on epithelial stem cells. *Cell* 1989, 57 (2), 201–209.

[80] G. Pellegrini, D. Ardigò, G. Milazzo, G. Iotti, P. Guatelli, D. Pelosi, M. De Luca, Navigating Market Authorization: The Path Holoclar Took to Become the First Stem Cell Product Approved in the European Union. *Stem Cells Translational Medicine* 2018, 7 (1), 146–154.

[81] G. Pellegrini, C. E. Traverso, A. T. Franzi, M. Zingirian, R. Cancedda, M. De Luca, Long-term restoration of damaged corneal surfaces with autologous cultivated corneal epithelium. *Lancet* 1997, 349 (9057), 990–993.

[82] O. Baylis, F. Figueiredo, C. Henein, M. Lako, S. Ahmad, 13 Years of cultured limbal epithelial cell therapy: A review of the outcomes. *Journal of Cellular Biochemistry* 2011, 112 (4), 993–1002.

[83] I. Henig, T. Zuckerman, Hematopoietic stem cell transplantation-50 years of evolution and future perspectives. *Rambam Maimonides medical journal* 2014, 5 (4), e0028.

[84] L. Gragert, M. Eapen, E. Williams, J. Freeman, S. Spellman, R. Baitty, R. Hartzman, J. D. Rizzo, M. Horowitz, D. Confer, M. Maiers, HLA Match Likelihoods for Hematopoietic Stem-Cell Grafts in the U.S. Registry. *New England Journal of Medicine* 2014, 371 (4), 339–348.

[85] C. G. Brunstein, J. A. Gutman, D. J. Weisdorf, A. E. Woolfrey, T. E. DeFor, T. A. Gooley, M. R. Verneris, F. R. Appelbaum, J. E. Wagner, C. Delaney, Allogeneic hematopoietic cell transplantation for hematologic malignancy: relative risks and benefits of double umbilical cord blood. *Blood* 2010, 116 (22), 4693–4699.

[86] K. K. Ballen, E. Gluckman, H. E. Broxmeyer, Umbilical cord blood transplantation: the first 25 years and beyond. 2013.

[87] J. Kiernan, P. Damien, M. Monaghan, R. Shorr, L. Mcintyre, D. Fergusson, A. Tinmouth, D. Allan, Clinical Studies of Ex Vivo Expansion to Accelerate Engraftment After Umbilical Cord Blood Transplantation: A Systematic Review. *Transfusion Medicine Reviews* 2017, 31, 173–182.

[88] M. de Lima, I. McNiece, S. N. Robinson, M. Munsell, M. Eapen, M. Horowitz, A. Alousi, R. Saliba, J. D. McMannis, I. Kaur, P. Kebriaei, S. Parmar, U. Popat, C. Hosing, R. Champlin, C. Bollard, J. J. Molldrem, R. B. Jones, Y. Nieto, B. S. Andersson, N. Shah, B. Oran, L. J. Cooper, L. Worth, M. H. Qazilbash, M. Korbling, G. Rondon, S. Ciurea, D. Bosque, I. Maewal, P. J. Simmons, E. J. Shpall, Cord-Blood Engraftment with Ex Vivo Mesenchymal-Cell Coculture. *New England Journal of Medicine* 2012, 367 (24), 2305–2315.

[89] M. De Lima, J. Mcmannis, A. Gee, K. Komanduri, D. Couriel, B. S. Andersson, C. Hosing, I. Khouri, R. Jones, R. Champlin, S. Karandish, T. Sadeghi, T. Peled, F. Grynspan, Y. Daniely, A. Nagler, E. J. Shpall, Transplantation of ex vivo expanded cord blood cells using the copper chelator tetraethylenepentamine: a phase I/II clinical trial. *Bone Marrow Transplantation* 2008, 41, 771–778.

[90] M. E. Horwitz, N. J. Chao, D. A. Rizzieri, G. D. Long, K. M. Sullivan, C. Gasparetto, J. P. Chute, A. Morris, C. McDonald, B. Waters-Pick, P. Stiff, S. Wease, A. Peled, D. Snyder, E. G. Cohen, H. Shoham, E. Landau, E. Friend, I. Peleg, D. Aschengrau, D. Yackoubov, J. Kurtzberg, T. Peled, Umbilical cord blood expansion with nicotinamide provides long-term multilineage engraftment. *Journal of Clinical Investigation* 2014, 124 (7), 3121–3128.

[91] J. E. Wagner, C. G. Brunstein, A. E. Boitano, J. Jones, M. P. Cooke, C. C. B. Correspondence, T. E. Defor, D. Mckenna, D. Sumstad, B. R. Blazar, J. Tolar, C. Le, C. C. Bleul, Phase I/II Trial of StemRegenin-1 Expanded Umbilical Cord Blood Hematopoietic Stem Cells Supports Testing as a Stand-Alone Graft Cell Stem Cell Phase I/II Trial of StemRegenin-1 Expanded Umbilical Cord Blood Hematopoietic Stem Cells Supports Testing as a . *Cell Stem Cell* 2016, 18, 144–155.

[92] S. Kumar, H. Geiger, HSC Niche Biology and HSC Expansion Ex Vivo. 2017.

[93] C. Delaney, S. Heimfeld, C. Brashem-Stein, H. Voorhies, R. L. Manger, I. D. Bernstein, Notch-mediated expansion of human cord blood progenitor cells capable of rapid myeloid reconstitution. *Nature Medicine* 2010, 16 (2), 232–236.

[94] C. H. June, S. R. Riddell, T. N. Schumacher, Adoptive cellular therapy : A race to the finish line. *Science Translational Medicine* 2015, 7 (280), 1–8.

[95] L. M. Muul, P. J. Spiess, E. P. Director, S. A. Rosenberg, Identification of specific cytolytic immune responses against autologous tumor in humans bearing malignant melanoma. *Journal of immunology (Baltimore, Md. : 1950)* 1987, 138 (3), 989–95.

[96] N. J. Dwarshuis, K. Parratt, A. Santiago-Miranda, K. Roy, Cells as advanced therapeutics: State-of-the-art, challenges, and opportunities in large scale biomanufacturing of high-quality cells for adoptive immunotherapies. *Advanced Drug Delivery Reviews* 2017, 114, 222–239.

[97] M. E. Dudley, J. C. Yang, R. Sherry, M. S. Hughes, R. Royal, U. Kammula, P. F. Robbins, J. Huang, D. E. Citrin, S. F. Leitman, J. Wunderlich, N. P. Restifo, A. Thomasian, S. G. Downey, F. O. Smith, J. Klapper, K. Morton, C. Laurencot, D. E. White, S. A. Rosenberg, Adoptive cell therapy for patients with metastatic melanoma: Evaluation of intensive myeloablative chemoradiation preparative regimens. *Journal of Clinical Oncology* 2008, 26 (32), 5233–5239.

[98] M. C. Pandolfino, N. Labarrière, M. H. Tessier, A. Cassidanius, S. Bercegeay, P. Lemarre, F. Dehaut, B. Dréno, F. Jotereau, High-scale expansion of melanoma-reactive TIL by a polyclonal stimulus: predictability and relation with disease advancement. *Cancer immunology, immunotherapy : CII* 2001, 50 (3), 134–140.

[99] T. Zuliani, J. David, S. Bercegeay, M. C. Pandolfino, I. Rodde-Astier, A. Khammari, C. Coissac, B. Delorme, S. Saïagh, B. Dréno, Value of large scale expansion of tumor infiltrating lymphocytes in a compartmentalised gas-permeable bag: Interests for adoptive immunotherapy. *Journal of Translational Medicine* 2011, 9.

[100] C. C. Malone, P. M. Schiltz, A. D. MacKintosh, L. D. Beutel, F. S. Heinemann, R. O. Dillman, Characterization of Human Tumor-Infiltrating Lymphocytes Expanded in Hollow-Fiber Bioreactors for Immunotherapy of Cancer. *Cancer Biotherapy and Radiopharmaceuticals* 2001, 16 (5), 381–390.

[101] R. A. Knazek, Y.-W. Wu, P. M. Aebersold, S. A. Rosenberg, Culture of human tumor infiltrating lymphocytes in hollow fiber bioreactors. *Journal of Immunological Methods* 1990, 127 (1), 29–37.

[102] M. E. Dudley, C. A. Gross, R. P. T. Somerville, Y. Hong, N. P. Schaub, S. F. Rosati, D. E. White, D. Nathan, N. P. Restifo, S. M. Steinberg, J. R. Wunderlich, U. S. Kammula, R. M. Sherry, J. C. Yang, G. Q. Phan, M. S. Hughes, C. M. Laurencot, S. A. Rosenberg, Randomized selection design trial evaluating CD8+-enriched versus unselected tumor-infiltrating lymphocytes for adoptive cell therapy for patients with melanoma. *Journal of clinical oncology : official journal of the American Society of Clinical Oncology* 2013, 31 (17), 2152–9.

[103] S. L. Goff, M. E. Dudley, D. E. Citrin, R. P. Somerville, J. R. Wunderlich, D. N. Danforth, D. A. Zlott, J. C. Yang, R. M. Sherry, U. S. Kammula, C. A. Klebanoff, M. S. Hughes, N. P. Restifo, M. M. Langhan, T. E. Shelton, L. Lu, M. L. M. Kwong, S. Ilyas, N. D. Klemen, E. C. Payabyab, K. E. Morton, M. A. Toomey, S. M. Steinberg, D. E. White, S. A. Rosenberg, Randomized, prospective evaluation comparing intensity of lymphodepletion before adoptive transfer of tumor-infiltrating lymphocytes for patients with metastatic melanoma. *Journal of Clinical Oncology* 2016, 34 (20), 2389–2397.

[104] A. Sadeghi, L. Pauler, C. Annerén, A. Friberg, D. Brandhorst, O. Korsgren, T. H. Tötterman, Large-scale bioreactor expansion of tumor-infiltrating lymphocytes. *Journal of Immunological Methods* 2011, 364, 94–100.

[105] M. Hall, H. Liu, M. Malafa, B. Centeno, P. J. Hodul, J. Pimiento, S. Pilon-Thomas, A. A. Sarnaik, Expansion of tumor-infiltrating lymphocytes (TIL) from human pancreatic tumors. *Journal for ImmunoTherapy of Cancer* 2016, 4 (1), 61.

[106] W. A. Lim, C. H. June, The Principles of Engineering Immune Cells to Treat Cancer. *Cell* 2017, 168 (4), 724–740.

[107] C. H. June, R. S. O'Connor, O. U. Kawalekar, S. Ghassemi, M. C. Milone, CAR T cell immunotherapy for human cancer. 2018.

[108] J. Hartmann, M. Schüßler-Lenz, A. Bondanza, C. J. Buchholz, Clinical development of CAR T cells—challenges and opportunities in translating innovative treatment concepts. *EMBO Molecular Medicine* 2017, 9 (9), 1183–1197.

[109] S. A. Rosenberg, N. P. Restifo, Adoptive cell transfer as personalized immunotherapy for human cancer. *Science* 2015, 348 (6230), 62–68.

[110] P. Vormittag, R. Gunn, S. Ghorashian, F. S. Veraitch, A guide to manufacturing CAR T cell therapies. *Current Opinion in Biotechnology* 2018, 53, 164–181.

[111] L. R. Neal, S. R. Bailey, M. M. Wyatt, J. S. Bowers, K. Majchrzak, M. H. Nelson, C. Haupt, C. M. Paulos, J. C. Varela, The Basics of Artificial Antigen Presenting Cells in T Cell-Based Cancer Immunotherapies. *Journal of immunology research and therapy* 2017, 2 (1), 68–79.

[112] D. L. Porter, B. L. Levine, N. Bunin, E. A. Stadtmauer, S. M. Luger, S. Goldstein, A. Loren, J. Phillips, S. Nasta, A. Perl, S. Schuster, D. Tsai, A. Sohal, E. Veloso, S. Emerson, C. H. June, A phase 1 trial of donor lymphocyte infusions expanded and activated ex vivo via CD3/CD28 costimulation. *Blood* 2006, 107 (4), 1325–31.

[113] L. Xiao, C. Chen, Z. Li, S. Zhu, J. C. Tay, X. Zhang, S. Zha, J. Zeng, W. K. Tan, X. Liu, W. J. Chng, S. Wang, Large-scale expansion of Vγ9Vδ2 T cells with engineered K562 feeder cells in G-Rex vessels and their use as chimeric antigen receptor–modified effector cells. *Cytotherapy* 2018, 20 (3), 420–435.

[114] R. J. Brentjens, M. L. Davila, I. Riviere, J. Park, X. Wang, L. G. Cowell, S. Bartido, J. Stefanski, C. Taylor, M. Olszewska, O. Borquez-Ojeda, J. Qu, T. Wasielewska, Q. He, Y. Bernal, I. V. Rijo, C. Hedvat, R. Kobos, K. Curran, P. Steinherz, J. Jurcic, T. Rosenblat, P. Maslak, M. Frattini, M. Sadelain, CD19-Targeted T Cells Rapidly Induce Molecular Remissions in Adults with Chemotherapy-Refractory Acute Lymphoblastic Leukemia. *Science Translational Medicine* 2013, 5 (177), 177ra38–177ra38.

[115] D. Hollyman, J. Stefanski, M. Przybylowski, S. Bartido, O. Borquez-Ojeda, C. Taylor, R. Yeh, V. Capacio, M. Olszewska, J. Hosey, M. Sadelain, R. J. Brentjens, I. Rivière, Manufacturing validation of biologically functional T cells targeted to CD19 antigen for autologous adoptive cell therapy. *Journal of immunotherapy (Hagerstown, Md. : 1997)* 2009, 32 (2), 169–80.

[116] U. Mock, L. Nickolay, B. Philip, G. W.-K. Cheung, H. Zhan, I. C. D. Johnston, A. D. Kaiser, K. Peggs, M. Pule, A. J. Thrasher, W. Qasim, Automated manufacturing of chimeric antigen receptor T cells for adoptive immunotherapy using CliniMACS Prodigy. *Cytotherapy* 2016, 18 (8), 1002–1011.

[117] J. A. Bluestone, J. H. Buckner, M. Fitch, S. E. Gitelman, S. Gupta, M. K. Hellerstein, K. C. Herold, A. Lares, M. R. Lee, K. Li, W. Liu, S. A. Long, L. M. Masiello, V. Nguyen, A. L. Putnam, M. Rieck, P. H. Sayre, Q. Tang, Type 1 diabetes immunotherapy using polyclonal regulatory T cells. *Science Translational Medicine* 2015, 7 (315).

[118] P. Trzonkowski, R. Bacchetta, M. Battaglia, D. Berglund, H. R. Bohnenkamp, A. ten Brinke, A. Bushell, N. Cools, E. K. Geissler, S. Gregori, S. Marieke van Ham, C. Hilkens, J. A. Hutchinson, G. Lombardi, J. A. Madrigal, N. Marek-Trzonkowska, E. M. Martinez-Caceres, M. G. Roncarolo, S. Sanchez-Ramon, A. Saudemont, B. Sawitzki, Hurdles in therapy with regulatory T cells. *Science translational medicine* 2015, 7 (304), 304ps18.

[119] J. L. Riley, C. H. June, B. R. Blazar, Human T Regulatory Cell Therapy: Take a Billion or So and Call Me in the Morning. *Immunity* 2009, 30 (5), 656–665.

[120] Q. Tang, J. A. Bluestone, Regulatory T-cell therapy in transplantation: moving to the clinic. *Cold Spring Harbor perspectives in medicine* 2013, 3 (11).

[121] M. Romano, S. L. Tung, L. A. Smyth, G. Lombardi, Treg therapy in transplantation: a general overview. *Transplant International* 2017, 30 (8), 745–753.

[122] N. Safinia, N. Grageda, C. Scottà, S. Thirkell, L. J. Fry, T. Vaikunthanathan, R. I. Lechler, G. Lombardi, Cell Therapy in Organ Transplantation: Our Experience on the Clinical Translation of Regulatory T Cells. *Frontiers in Immunology* 2018, 9 (3), 1003.

[123] J. M. Mathew, J. H-Voss, A. LeFever, I. Konieczna, C. Stratton, J. He, X. Huang, L. Gallon, A. Skaro, M. J. Ansari, J. R. Leventhal, A Phase I Clinical Trial with Ex Vivo Expanded Recipient Regulatory T cells in Living Donor Kidney Transplants. *Scientific reports* 2018, 8 (1), 7428.

[124] M. Miyara, D. Chader, A. Burlion, J. Goldstein, D. Sterlin, F. Norol, H. Trebeden-Nègre, L. Claër, S. Sakaguchi, G. Marodon, Z. Amoura, G. Gorochov, Combination of IL-2, rapamycin, DNA methyltransferase and histone deacetylase inhibitors for the expansion of human regulatory T cells. *Oncotarget* 2016, 1–12.

[125] K. L. Hippen, S. C. Merkel, D. K. Schirm, C. M. Sieben, D. Sumstad, D. M. Kadidlo, D. H. McKenna, J. S. Bromberg, B. L. Levine, J. L. Riley, C. H. June, P. Scheinberg, D. C. Douek, J. S. Miller, J. E. Wagner, B. R. Blazar, Massive ex vivo expansion of human natural regulatory T cells (T(regs)) with minimal loss of in vivo functional activity. *Sci Transl Med* 2011, 3 (83), 83ra41.

[126] M. G. Morvan, L. L. Lanier, NK cells and cancer: you can teach innate cells new tricks. *Nature reviews. Cancer* 2016, 16 (1), 7–19.

[127] K. Rezvani, R. Rouce, E. Liu, E. Shpall, Engineering Natural Killer Cells for Cancer Immunotherapy. 2017.

[128] M. Granzin, S. Soltenborn, S. Müller, J. Kollet, M. Berg, A. Cerwenka, R. W. Childs, V. Huppert, Fully automated expansion and activation of clinical-grade natural killer cells for adoptive immunotherapy. *Cytotherapy* 2015.

[129] R. W. Childs, M. Carlsten, Therapeutic approaches to enhance natural killer cell cytotoxicity against cancer: the force awakens. *Nature Reviews Drug Discovery* 2015, 14 (7), 487–498.

[130] J. Spanholtz, F. Preijers, M. Tordoir, C. Trilsbeek, J. Paardekooper, T. de Witte, N. Schaap, H. Dolstra, Clinical-Grade Generation of Active NK Cells from Cord Blood Hematopoietic Progenitor Cells for Immunotherapy Using a Closed-System Culture Process. *PLoS ONE* 2011, 6 (6), e20740.

[131] T. Sutlu, B. Stellan, M. Gilljam, H. C. Quezada, H. Nahi, G. Gahrton, E. Alici, Clinical-grade, large-scale, feeder-free expansion of highly active human natural killer cells for adoptive immunotherapy using an automated bioreactor. *Cytotherapy* 2010, 12 (8), 1044–1055.

[132] M. Boyiadzis, M. Agha, R. L. Redner, A. Sehgal, A. Im, J. Z. Hou, R. Farah, K. A. Dorritie, A. Raptis, S. H. Lim, H. Wang, N. Lapteva, Z. Mei, L. H. Butterfield, C. M. Rooney, T. L. Whiteside, Phase 1 clinical trial of adoptive immunotherapy using "off-the-shelf" activated natural killer cells in patients with refractory and relapsed acute myeloid leukemia. *Cytotherapy* 2017, 19 (10), 1225–1232.

[133] S. Anguille, E. L. Smits, E. Lion, V. F. Van Tendeloo, Z. N. Berneman, Clinical use of dendritic cells for cancer therapy 2014.

[134] K. Palucka, J. Banchereau, Cancer immunotherapy via dendritic cells. *Nature reviews. Cancer* 2012, 12 (4), 265–77.

[135] R. L. Sabado, S. Balan, N. Bhardwaj, Dendritic cell-based immunotherapy. *Cell Research* 2017, 27157, 74–95.

[136] M. Saxena, S. Balan, V. Roudko, N. Bhardwaj, Towards superior dendritic-cell vaccines for cancer therapy. *Nature Biomedical Engineering* 2018, 2 (6), 341–346.

[137] P. W. Kantoff, C. S. Higano, N. D. Shore, E. R. Berger, E. J. Small, D. F. Penson, C. H. Redfern, A. C. Ferrari, R. Dreicer, R. B. Sims, Y. Xu, M. W. Frohlich, P. F. Schellhammer, Sipuleucel-T Immunotherapy for Castration-Resistant Prostate Cancer. *New England Journal of Medicine* 2010, 363 (5), 411–422.

[138] C. van den Bos, R. Keefe, C. Schirmaier, M. McCaman, Therapeutic Human Cells: Manufacture for Cell Therapy/Regenerative Medicine. in *Cardiovascular Ultrasound*, volume 4, Springer, Berlin, Heidelberg, 2013, 61–97.

[139] P. Menasché, V. Vanneaux, A. Hagège, A. Bel, B. Cholley, A. Parouchev, I. Cacciapuoti, R. Al-Daccak, N. Benhamouda, H. Blons, O. Agbulut, L. Tosca, J.-H. Trouvin, J.-R. Fabreguettes, V. Bellamy, D. Charron, E. Tartour, G. Tachdjian, M. Desnos, J. Larghero, Transplantation of Human Embryonic Stem Cell–Derived Cardiovascular Progenitors for Severe Ischemic Left Ventricular Dysfunction. *Journal of the American College of Cardiology* 2018, 71 (4), 429–438.

[140] Y.-W. Liu, B. Chen, X. Yang, J. A. Fugate, F. A. Kalucki, A. Futakuchi-Tsuchida, L. Couture, K. W. Vogel, C. A. Astley, A. Baldessari, J. Ogle, C. W. Don, Z. L. Steinberg, S. P. Seslar, S. A. Tuck, H. Tsuchida, A. V. Naumova, S. K. Dupras, M. S. Lyu, J. Lee, D. W. Hailey, H. Reinecke, L. Pabon, B. H. Fryer, W. R. MacLellan, R. S. Thies, C. E. Murry, Human embryonic stem cell–derived cardiomyocytes restore function in infarcted hearts of non-human primates. *Nature Biotechnology* 2018, 36 (7), 597–605.

[141] P. Hematti, Mesenchymal stromal cells and fibroblasts: a case of mistaken identity? *Cytotherapy* 2012, 14 (5), 516–21.

[142] M. Dominici, K. Le Blanc, I. Mueller, I. Slaper-Cortenbach, F. Marini, D. Krause, R. Deans, a. Keating, D. Prockop, E. Horwitz, Minimal criteria for defining multipotent mesenchymal stromal cells. The International Society for Cellular Therapy position statement. *Cytotherapy* 2006, 8 (4), 315–317.

[143] R. A. Denu, S. Nemcek, D. D. Bloom, A. D. Goodrich, J. Kim, D. F. Mosher, P. Hematti, Fibroblasts and Mesenchymal Stromal/Stem Cells Are Phenotypically Indistinguishable. *Acta Haematologica* 2016, 85–97.

[144] P. Bianco, X. Cao, P. S. Frenette, J. J. Mao, P. G. Robey, P. J. Simmons, C.-Y. Wang, The meaning, the sense and the significance: translating the science of mesenchymal stem cells into medicine. *Nature medicine* 2013, 19 (1), 35–42.

[145] B. Sacchetti, A. Funari, C. Remoli, G. Giannicola, G. Kogler, S. Liedtke, G. Cossu, M. Serafini, M. Sampaolesi, E. Tagliafico, E. Tenedini, I. Saggio, P. Robey, M. Riminucci, P. Bianco, No Identical "Mesenchymal Stem Cells" at Different Times and Sites: Human Committed Progenitors of Distinct Origin and Differentiation Potential Are Incorporated as Adventitial Cells in Microvessels. *Stem Cell Reports* 2016, 6 (6), 897–913.

[146] U. Galderisi, T. Squillaro, G. Peluso, Clinical Trials With Mesenchymal Stem Cells: An Update. *Cell Transplantation* 2016, 25, 829–848.

[147] A. Trounson, C. McDonald, Stem Cell Therapies in Clinical Trials: Progress and Challenges. 2015.

[148] R. R. Sharma, K. Pollock, A. Hubel, D. McKenna, Mesenchymal stem or stromal cells: A review of clinical applications and manufacturing practices. *Transfusion* 2014, 54 (5), 1418–1437.

[149] J. Rowley, E. Abraham, A. Campbell, H. Brandwein, S. Oh, Meeting lot-size challenges of manufacturing adherent cells for therapy. 2012.

[150] F. de la Portilla, F. Alba, D. García-Olmo, J. M. Herrerías, F. X. González, A. Galindo, Expanded allogeneic adipose-derived stem cells (eASCs) for the treatment of complex perianal fistula in Crohn's disease: results from a multicenter phase I/IIa clinical trial. *International Journal of Colorectal Disease* 2013, 28 (3), 313–323.

[151] P. Nold, C. Brendel, A. Neubauer, G. Bein, H. Hackstein, Good manufacturing practice-compliant animal-free expansion of human bone marrow derived mesenchymal stroma cells in a closed hollow-fiber-based bioreactor. *Biochemical and Biophysical Research Communications* 2013, 430 (1), 325–330.

[152] C. Weber, D. Freimark, R. Pörtner, P. Pino-Grace, S. Pohl, C. Wallrapp, P. Geigle, P. Czermak, Expansion of Human Mesenchymal Stem Cells in a Fixed-Bed Bioreactor System Based on Non-Porous Glass Carrier – Part B: Modeling and Scale-up of the System. *The International Journal of Artificial Organs* 2010, 33 (11), 782–795.

[153] A. W. Nienow, C. J. Hewitt, T. R. Heathman, V. A. Glyn, G. N. Fonte, M. P. Hanga, K. Coopman, Q. A. Rafiq, Agitation conditions for the culture and detachment of hMSCs from microcarriers in multiple bioreactor platforms. *Biochemical Engineering Journal* 2016, 108, 24–29.

[154] T. Lawson, D. E. Kehoe, A. C. Schnitzler, P. J. Rapiejko, K. A. Der, K. Philbrick, S. Punreddy, S. Rigby, R. Smith, Q. Feng, J. R. Murrell, M. S. Rook, Process development for expansion of human mesenchymal stromal cells in a 50 L single-use stirred tank bioreactor. *Biochemical Engineering Journal* 2017, 120, 49–62.

[155] N. Timmins, M. Kiel, M. Günther, C. Heazlewood, M. Doran, G. Brooke, K. Atkinson, Closed system isolation and scalable expansion of human placental mesenchymal stem cells. *Biotechnology and Bioengineering* 2012, 109 (7), 1817–1826.

[156] A. K.-L. Chen, Y. K. Chew, H. Y. Tan, S. Reuveny, S. K. Weng Oh, Increasing efficiency of human mesenchymal stromal cell culture by optimization of microcarrier concentration and design of medium feed. *Cytotherapy* 2015, 17 (2), 163–173.

[157] J. Wu, T. Yamauchi, J. C. Izpisua Belmonte, An overview of mammalian pluripotency. *Development* 2016, 143 (10), 1644–1648.

[158] A. De Los Angeles, F. Ferrari, R. Xi, Y. Fujiwara, N. Benvenisty, H. Deng, K. Hochedlinger, R. Jaenisch, S. Lee, H. G. Leitch, M. W. Lensch, E. Lujan, D. Pei, J. Rossant, M. Wernig, P. J. Park, G. Q. Daley, Hallmarks of pluripotency. *Nature* 2015, 525 (7570), 469–78.

[159] A. D. Celiz, J. G. W. Smith, R. Langer, D. G. Anderson, D. A. Winkler, D. A. Barrett, M. C. Davies, L. E. Young, C. Denning, M. R. Alexander, Materials for stem cell factories of the future. *Nature Materials* 2014, 13 (6), 570–579.

[160] M. Mandai, A. Watanabe, Y. Kurimoto, Y. Hirami, C. Morinaga, T. Daimon, M. Fujihara, H. Akimaru, N. Sakai, Y. Shibata, M. Terada, Y. Nomiya, S. Tanishima, M. Nakamura, H. Kamao, S. Sugita, A. Onishi, T. Ito, K. Fujita, S. Kawamata, M. J. Go, C. Shinohara, K.-i. Hata, M. Sawada, M. Yamamoto, S. Ohta, Y. Ohara, K. Yoshida, J. Kuwahara, Y. Kitano, N. Amano, M. Umekage, F. Kitaoka, A. Tanaka, C. Okada, N. Takasu, S. Ogawa, S. Yamanaka, M. Takahashi, Autologous Induced Stem-Cell–Derived Retinal Cells for Macular Degeneration. *New England Journal of Medicine* 2017, 376 (11), 1038–1046.

[161] Y. Y. Lipsitz, C. Woodford, T. Yin, J. H. Hanna, P. W. Zandstra, Modulating cell state to enhance suspension expansion of human pluripotent stem cells. *Proceedings of the National Academy of Sciences of the United States of America* 2018, 115 (25), 6369–6374.

[162] M. M. Adil, D. V. Schaffer, Expansion of human pluripotent stem cells. *Current Opinion in Chemical Engineering* 2017, 15 (Cm), 24–35.

[163] K. Watanabe, M. Ueno, D. Kamiya, A. Nishiyama, M. Matsumura, T. Wataya, J. B. Takahashi, S. Nishikawa, S.-i. Nishikawa, K. Muguruma, Y. Sasai, A ROCK inhibitor permits survival of dissociated human embryonic stem cells. *Nature biotechnology* 2007, 25 (6), 681–686.

[164] M. Amit, J. Chebath, V. Margulets, I. Laevsky, Y. Miropolsky, K. Shariki, M. Peri, I. Blais, G. Slutsky, M. Revel, J. Itskovitz-Eldor, Suspension Culture of Undifferentiated Human Embryonic and Induced Pluripotent Stem Cells. *Stem Cell Reviews and Reports* 2010, 6 (2), 248–259.

[165] Y. Y. Lipsitz, P. D. Tonge, P. W. Zandstra, Chemically controlled aggregation of pluripotent stem cells. *Biotechnology and Bioengineering* 2018, 115 (8), 2061–2066.

[166] L. da Cruz, K. Fynes, O. Georgiadis, J. Kerby, Y. H. Luo, A. Ahmado, A. Vernon, J. T. Daniels, B. Nommiste, S. M. Hasan, S. B. Gooljar, A.-J. F. Carr, A. Vugler, C. M. Ramsden, M. Bictash, M. Fenster, J. Steer, T. Harbinson, A. Wilbrey, A. Tufail, G. Feng, M. Whitlock, A. G. Robson, G. E. Holder, M. S. Sagoo, P. T. Loudon, P. Whiting, P. J. Coffey, Phase 1 clinical study of an embryonic stem cell–derived retinal pigment epithelium patch in age-related macular degeneration. *Nature Publishing Group* 2018.

[167] T. C. Schulz, Concise Review: Manufacturing of Pancreatic Endoderm Cells for Clinical Trials in Type 1 Diabetes. *STEM CELLS Translational Medicine* 2015, 4 (8), 927–931.

[168] P. Salmikangas, N. Kinsella, P. Chamberlain, Chimeric Antigen Receptor T-Cells (CAR T-Cells) for Cancer Immunotherapy - Moving Target for Industry? *Pharmaceutical research* 2018, 35 (8), 152.

[169] M. J. Farrell, M. B. Fisher, A. H. Huang, J. I. Shin, K. M. Farrell, R. L. Mauck, Functional properties of bone marrow-derived MSC-based engineered cartilage are unstable with very long-term in vitro culture. *Journal of Biomechanics* 2014, 47 (9), 2173–2182.

[170] D. J. Prockop, M. Brenner, W. E. Fibbe, E. Horwitz, K. Le Blanc, D. G. Phinney, P. J. Simmons, L. Sensebe, A. Keating, Defining the risks of mesenchymal stromal cell therapy. *Cytotherapy* 2010, 12 (5), 576–578.

[171] M. Ruella, J. Xu, D. M. Barrett, J. A. Fraietta, T. J. Reich, D. E. Ambrose, M. Klichinsky, O. Shestova, P. R. Patel, I. Kulikovskaya, F. Nazimuddin, V. G. Bhoj, E. J. Orlando, T. J. Fry, H. Bitter, S. L. Maude, B. L. Levine, C. L. Nobles, F. D. Bushman, R. M. Young, J. Scholler, S. I. Gill, C. H. June, S. A. Grupp, S. F. Lacey, J. J. Melenhorst, Induction of resistance to chimeric antigen receptor T cell therapy by transduction of a single leukemic B cell. *Nature Medicine* 2018, 24 (10), 1499–1503.

[172] Y. Y. Lipsitz, W. D. Milligan, I. Fitzpatrick, E. Stalmeijer, S. S. Farid, K. Y. Tan, D. Smith, R. Perry, J. Carmen, A. Chen, C. Mooney, J. Fink, A roadmap for cost-of-goods planning to guide economic production of cell therapy products. *Cytotherapy* 2017, 19 (12), 1383–1391.

[173] J. Beers, D. R. Gulbranson, N. George, L. I. Siniscalchi, J. Jones, J. A. Thomson, G. Chen, Passaging and colony expansion of human pluripotent stem cells by enzyme-free dissociation in chemically defined culture conditions. *Nature Protocols* 2012, 7 (11), 2029–2040.

[174] J. Bardy, A. K. Chen, Y. M. Lim, S. Wu, S. Wei, H. Weiping, K. Chan, S. Reuveny, S. K. Oh, Microcarrier Suspension Cultures for High-Density Expansion and Differentiation of Human Pluripotent Stem Cells to Neural Progenitor Cells. *Tissue Engineering Part C: Methods* 2013, 19 (2), 166–180.

[175] D. E. Kehoe, D. Jing, L. T. Lock, E. S. Tzanakakis, Scalable Stirred-Suspension Bioreactor Culture of Human Pluripotent Stem Cells 2010, 16 (2), 405–421.

[176] L. T. Lock, E. S. Tzanakakis, Expansion and differentiation of human embryonic stem cells to endoderm progeny in a microcarrier stirred-suspension culture. *Tissue engineering. Part A* 2009, 15 (8), 2051–2063.

[177] Y. Nie, V. Bergendahl, D. J. Hei, J. M. Jones, S. P. Palecek, Scalable culture and cryopreservation of human embryonic stem cells on microcarriers. *Biotechnology Progress* 2009, 25 (1), 20–31.

[178] S. K. Oh, A. K. Chen, Y. Mok, X. Chen, U.-M. Lim, A. Chin, A. B. Choo, S. Reuveny, Long-term microcarrier suspension cultures of human embryonic stem cells. *Stem Cell Research* 2009, 2 (3), 219–230.

[179] D. a. Fluri, P. D. Tonge, H. Song, R. P. Baptista, N. Shakiba, S. Shukla, G. Clarke, A. Nagy, P. W. Zandstra, Derivation, expansion and differentiation of induced pluripotent stem cells in continuous suspension cultures. *Nature Methods* 2012, 9 (5), 509–516.

[180] D. Steiner, H. Khaner, M. Cohen, S. Even-Ram, Y. Gil, P. Itsykson, T. Turetsky, M. Idelson, E. Aizenman, R. Ram, Y. Berman-Zaken, B. Reubinoff, Derivation, propagation and controlled differentiation of human embryonic stem cells in suspension. *Nature biotechnology* 2010, 28 (4), 361–364.

[181] C. Kropp, D. Massai, R. Zweigerdt, Progress and challenges in large-scale expansion of human pluripotent stem cells. *Process Biochemistry* 2017, 59, 244–254.

[182] S. Abbasalizadeh, M. R. Larijani, A. Samadian, H. Baharvand, Bioprocess Development for Mass Production of Size-Controlled Human Pluripotent Stem Cell Aggregates in Stirred Suspension Bioreactor. *Tissue Engineering Part C: Methods* 2012, 18 (11), 831–851.

[183] Y. Wang, B. K. Chou, S. Dowey, C. He, S. Gerecht, L. Cheng, Scalable expansion of human induced pluripotent stem cells in the defined xeno-free E8 medium under adherent and suspension culture conditions. *Stem Cell Research* 2013, 11 (3), 1103–1116.

[184] B. Abecasis, T. Aguiar, É. Arnault, R. Costa, P. Gomes-Alves, A. Aspegren, M. Serra, P. M. Alves, Expansion of 3D human induced pluripotent stem cell aggregates in bioreactors: Bioprocess intensification and scaling-up approaches. *Journal of Biotechnology* 2017, 246, 81–93.

[185] M. M. Hunt, G. Meng, D. E. Rancourt, I. D. Gates, M. S. Kallos, Factorial Experimental Design for the Culture of Human Embryonic Stem Cells as Aggregates in Stirred Suspension Bioreactors Reveals the Potential for Interaction Effects Between Bioprocess Parameters. *Tissue Engineering Part C: Methods* 2014, 20 (1), 76–89.

[186] H. Kempf, R. Olmer, C. Kropp, M. Rückert, M. Jara-Avaca, D. Robles-Diaz, A. Franke, D. A. Elliott, D. Wojciechowski, M. Fischer, A. Roa Lara, G. Kensah, I. Gruh, A. Haverich, U. Martin, R. Zweigerdt, Controlling Expansion and

Cardiomyogenic Differentiation of Human Pluripotent Stem Cells in Scalable Suspension Culture. *Stem Cell Reports* 2014, 3 (6), 1132–1146.

[187] C. K. Kwok, Y. Ueda, A. Kadari, K. Günther, S. Ergün, A. Heron, A. C. Schnitzler, M. Rook, F. Edenhofer, Scalable stirred suspension culture for the generation of billions of human induced pluripotent stem cells using single-use bioreactors. *Journal of Tissue Engineering and Regenerative Medicine* 2018, 12 (2), e1076–e1087.

[188] D. Nampe, R. Joshi, K. Keller, N. I. zur Nieden, H. Tsutsui, Impact of fluidic agitation on human pluripotent stem cells in stirred suspension culture. *Biotechnology and Bioengineering* 2017, 114 (9), 2109–2120.

[189] C. . Eline, L. Bauwens, R. Peerani, S. Niebruegge, K. A. Woodhouse, E. Kumacheva, M. Husain, P. W. Zandstra, Control of Human Embryonic Stem Cell Colony and Aggregate Size Heterogeneity Influences Differentiation Trajectories. *STEM CELLS* 2008, 26, 2300–2310.

[190] R. Krawetz, J. T. Taiani, S. Liu, G. Meng, X. Li, M. S. Kallos, D. E. Rancourt, Large-scale expansion of pluripotent human embryonic stem cells in stirred-suspension bioreactors. *Tissue engineering. Part C, Methods* 2010, 16 (4), 573–582.

[191] M. R. Larijani, A. Seifinejad, B. Pournasr, V. Hajihoseini, S.-N. Hassani, M. Totonchi, M. Yousefi, F. Shamsi, G. H. Salekdeh, H. Baharvand, Long-Term Maintenance of Undifferentiated Human Embryonic and Induced Pluripotent Stem Cells in Suspension. *Stem Cells and Development* 2011, 20 (11), 1911–1923.

[192] R. Olmer, A. Haase, S. Merkert, W. Cui, J. Paleček, C. Ran, A. Kirschning, T. Scheper, S. Glage, K. Miller, E. C. Curnow, E. S. Hayes, U. Martin, Long term expansion of undifferentiated human iPS and ES cells in suspension culture using a defined medium. *Stem Cell Research* 2010, 5, 51–64.

[193] H. Singh, P. Mok, T. Balakrishnan, S. N. B. Rahmat, R. Zweigerdt, Up-scaling single cell-inoculated suspension culture of human embryonic stem cells. *Stem Cell Research* 2010, 4 (3), 165–179.

[194] R. Zweigerdt, R. Olmer, H. Singh, A. Haverich, U. Martin, Scalable expansion of human pluripotent stem cells in suspension culture. *Nature protocols* 2011, 6 (5), 689–700.

[195] T. G. Otsuji, J. Bin, A. Yoshimura, M. Tomura, D. Tateyama, I. Minami, Y. Yoshikawa, K. Aiba, J. E. Heuser, T. Nishino, K. Hasegawa, N. Nakatsuji, A 3D sphere culture system containing functional polymers for large-scale human pluripotent stem cell production. *Stem Cell Reports* 2014, 2 (5), 734–745.

[196] L. Wallman, E. Åkesson, D. Ceric, P. H. Andersson, K. Day, O. Hovatta, S. Falci, T. Laurell, E. Sundström, Biogrid—a microfluidic device for large-scale enzyme-free dissociation of stem cell aggregates. *Lab on a Chip* 2011, 11 (19), 3241.

[197] S. Niebruegge, C. L. Bauwens, R. Peerani, N. Thavandiran, S. Masse, E. Sevaptisidis, K. Nanthakumar, K. Woodhouse, M. Husain, E. Kumacheva, P. W. Zandstra, Generation of human embryonic stem cell-derived mesoderm and cardiac cells using size-specified aggregates in an oxygen-controlled bioreactor. *Biotechnology and Bioengineering* 2009, 102 (2), 493–507.

[198] F. Huchet, A. Liné, J. Morchain, Evaluation of local kinetic energy dissipation rate in the impeller stream of a Rushton turbine by time-resolved PIV. *Chemical Engineering Research and Design* 2009, 87 (4), 369–376.

[199] W. Bujalski, A. Nienow, S. Chatwin, M. Cooke, The dependency on scale of power numbers of Rushton disc turbines. *Chemical Engineering Science* 1987, 42 (2), 317–326.

[200] D. J. Karst, E. Serra, T. K. Villiger, M. Soos, M. Massimo, Characterization and comparison of ATF and TFF in stirred bioreactors for the continuous production of therapeutic proteins. *Biochemical Engineering Journal* 2015, (submitted).

[201] M. Soos, L. Ehrl, M. U. Baebler, M. Morbidelli, Aggregate Breakup in a Contracting Nozzle. *Langmuir* 2010, 26 (1), 10–18.

[202] S. Sart, J. Bejoy, Y. Li, Characterization of 3D pluripotent stem cell aggregates and the impact of their properties on bioprocessing. *Process Biochemistry* 2017, 59, 276–288.

[203] B. P. Weegman, P. Nash, A. L. Carlson, K. J. Voltzke, Z. Geng, M. Jahani, B. B. Becker, K. K. Papas, M. T. Firpo, Nutrient Regulation by Continuous Feeding Removes Limitations on Cell Yield in the Large-Scale Expansion of Mammalian Cell Spheroids. *PLoS ONE* 2013, 8 (10), e76611.

[204] T. K. Villiger, M. Morbidelli, M. Soos, Experimental determination of maximum effective hydrodynamic stress in multiphase flow using shear sensitive aggregates. *AIChE Journal* 2015, 61 (5), 1735–1744.

[205] M. S. Croughan, E. S. Sayre, D. I. C. Wang, Viscous reduction of turbulent damage in animal cell culture. *Biotechnology and Bioengineering* 1989, 33 (7), 862–872.

[206] E. Y. L. Fok, P. W. Zandstra, Shear-controlled single-step mouse embryonic stem cell expansion and embryoid body-based differentiation. *Stem cells* 2005, 23, 1333–1342.

[207] A. Sen, M. S. Kallos, L. a. Behie, Effects of Hydrodynamics on Cultures of Mammalian Neural Stem Cell Aggregates in Suspension Bioreactors. *Industrial & Engineering Chemistry Research* 2001, 40, 5350–5357.

[208] N. Ma, K. W. Koelling, J. J. Chalmers, Fabrication and use of a transient contractional flow device to quantify the sensitivity of mammalian and insect cells to hydrodynamic forces. *Biotechnology and Bioengineering* 2002, 80 (4), 428–437.

[209] B. Neunstoecklin, M. Stettler, T. Solacroup, H. Broly, M. Morbidelli, M. Soos, Determination of the maximum operating range of hydrodynamic stress in mammalian cell culture. *Journal of Biotechnology* 2015, 194, 100–109.

[210] Y. Lei, D. Jeong, J. Xiao, D. V. Schaffer, Developing defined and scalable 3D culture systems for culturing human pluripotent stem cells at high densities. *Cellular and Molecular Bioengineering* 2014, 7 (2), 172–183.

[211] J. J. Chalmers, Mixing, aeration and cell damage, 30+ years later: What we learned, how it affected the cell culture industry and what we would like to know more about. 2015.

[212] J. Wu, J. C. Izpisua Belmonte, Dynamic Pluripotent Stem Cell States and Their Applications. 2015.

[213] L. A. Johnson, R. A. Morgan, M. E. Dudley, L. Cassard, J. C. Yang, M. S. Hughes, U. S. Kammula, R. E. Royal, R. M. Sherry, J. R. Wunderlich, C.-C. R. Lee, N. P. Restifo, S. L. Schwarz, A. P. Cogdill, R. J. Bishop, H. Kim, C. C. Brewer, S. F. Rudy, C. VanWaes, J. L. Davis, A. Mathur, R. T. Ripley, D. A. Nathan, C. M. Laurencot, S. A. Rosenberg, Gene therapy with human and mouse T-cell receptors mediates cancer regression and targets normal tissues expressing cognate antigen. *Blood* 2009, 114 (3), 535–546.

[214] D. E. White, S. L. Topalian, J. C. Yang, U. Kammula, D. M. Berman, J. Gea-Banacloche, R. E. Royal, L. J. Rogers, M. M. Pelletier, S. A. Jones, A. C. Filie, D. P. Mangiameli, S. A. Mavroukakis, S. A. Rosenberg, M. R. Robinson, R. M. Sherry, M. E. Dudley, N. P. Restifo, A. Abati, J. R. Wunderlich, G. J. Gracia, Adoptive Cell Transfer Therapy Following Non-Myeloablative but Lymphodepleting Chemotherapy for the Treatment of Patients With Refractory Metastatic Melanoma. *Journal of Clinical Oncology* 2005, 23 (10), 2346–2357.

[215] C. Yee, Adoptive T cell therapy: points to consider. *Current Opinion in Immunology* 2018, 51, 197–203.

[216] X. Dai, Y. Mei, D. Cai, W. Han, Standardizing CAR-T therapy: Getting it scaled up. *Biotechnology Advances* 2018, 37 (December 2018), 239–245.

[217] E. Lugli, M. H. Dominguez, L. Gattinoni, P. K. Chattopadhyay, D. L. Bolton, K. Song, N. R. Klatt, J. M. Brenchley, M. Vaccari, E. Gostick, D. A. Price, T. A. Waldmann, N. P. Restifo, G. Franchini, M. Roederer, Superior T memory stem cell persistence supports long-lived T cell memory. *Journal of Clinical Investigation* 2013, 123 (2), 594–599.

[218] L. Gattinoni, C. A. Klebanoff, N. P. Restifo, Paths to stemness: building the ultimate antitumour T cell. *Nature reviews. Cancer* 2012, 12 (10), 671–84.

[219] M. Sukumar, J. Liu, Y. Ji, M. Subramanian, J. G. Crompton, Z. Yu, R. Roychoudhuri, D. C. Palmer, P. Muranski, E. D. Karoly, R. P. Mohney, C. A. Klebanoff, A. Lal, T. Finkel, N. P. Restifo, L. Gattinoni, Inhibiting glycolytic metabolism enhances CD8+T cell memory and antitumor function. *Journal of Clinical Investigation* 2013, 123 (10), 4479–4488.

[220] R. J. Kishton, M. Sukumar, N. P. Restifo, Metabolic Regulation of T Cell Longevity and Function in Tumor Immunotherapy. 2017.

[221] N. Cieri, B. Camisa, F. Cocchiarella, M. Forcato, G. Oliveira, E. Provasi, A. Bondanza, C. Bordignon, J. Peccatori, F. Ciceri, M. T. Lupo-Stanghellini, F. Mavilio, A. Mondino, S. Bicciato, A. Recchia, C. Bonini, IL-7 and IL-15 instruct the generation of human memory stem T cells from naive precursors. *Blood* 2013, 121 (4), 573–84.

[222] Y. Xu, M. Zhang, C. A. Ramos, A. Durett, E. Liu, O. Dakhova, H. Liu, C. J. Creighton, A. P. Gee, H. E. Heslop, C. M. Rooney, B. Savoldo, G. Dotti, Closely related T-memory stem cells correlate with in vivo expansion of CAR.CD19-T cells and are preserved by IL-7 and IL-15. *Blood* 2014, 123 (24), 3750–3759.

[223] L. Gattinoni, X. S. Zhong, D. C. Palmer, Y. Ji, C. S. Hinrichs, Z. Yu, C. Wrzesinski, A. Boni, L. Cassard, L. M. Garvin, C. M. Paulos, P. Muranski, N. P. Restifo, Wnt signaling arrests effector T cell differentiation and generates CD8+ memory stem cells. *Nat Med* 2009, 15 (7), 808–813.

[224] Y. Kagoya, M. Nakatsugawa, Y. Yamashita, T. Ochi, T. Guo, M. Anczurowski, K. Saso, M. O. Butler, C. H. Arrowsmith, N. Hirano, BET bromodomain inhibition enhances T cell persistence and function in adoptive immunotherapy models. *Journal of Clinical Investigation* 2016, 126 (9), 3479–3494.

[225] E. L. Pearce, M. C. Walsh, P. J. Cejas, G. M. Harms, H. Shen, L. S. Wang, R. G. Jones, Y. Choi, Enhancing CD8 T-cell memory by modulating fatty acid metabolism. *Nature* 2009, 460 (7251), 103–107.

[226] R. Urak, M. Walter, L. Lim, C. W. Wong, L. E. Budde, S. Thomas, S. J. Forman, X. Wang, Ex vivo Akt inhibition promotes the generation of potent CD19CAR T cells for adoptive immunotherapy. *Journal for ImmunoTherapy of Cancer* 2017, 5.

[227] M. D. D. Buck, D. O'Sullivan, R. I. I. Klein Geltink, J. D. D. Curtis, C. H. Chang, D. E. E. Sanin, J. Qiu, O. Kretz, D. Braas, G. J. J. van der Windt, Q. Chen, S. C. C. Huang, C. M. M. O'Neill, B. T. T. Edelson, E. J. J. Pearce, H. Sesaki, T. B. B. Huber, A. S. S. Rambold, E. L. L. Pearce, Mitochondrial Dynamics Controls T Cell Fate through Metabolic Programming. *Cell* 2016, 166 (1), 63–76.

[228] R. P. Somerville, M. E. Dudley, Bioreactors get personal. 2012.

[229] J. A. Sánchez Pérez, E. M. Rodríguez Porcel, J. L. Casas López, J. M. Fernández Sevilla, Y. Chisti, Shear rate in stirred tank and bubble column bioreactors. *Chemical Engineering Journal* 2006, 124, 1–5.

[230] C. P. Peter, Y. Suzuki, J. Büchs, Hydromechanical stress in shake flasks: correlation for the maximum local energy dissipation rate. *Biotechnology and Bioengineering* 2006, 93 (6), 1164–1176.

[231] O. Karnieli, O. M. Friedner, J. G. Allickson, N. Zhang, S. Jung, D. Fiorentini, E. Abraham, S. S. Eaker, T. K. Yong, A. Chan, S. Griffiths, A. K. Wehn, S. Oh, A consensus introduction to serum replacements and serum-free media for cellular therapies. *Cytotherapy* 2017, 19, 155–169.

[232] C. Mason, N. L. Davie, J. A. Rowley, D. W. Smith, E. J. Culme-Seymour, D. A. Brindley, Peak serum: implications of serum supply for cell therapy manufacturing. *Regenerative Medicine* 2011, 7 (1), 7–13.

[233] Y.-L. Kim, Y.-J. Im, Y.-K. Lee, N.-C. Ha, Y.-S. Bae, S.-M. Lim, F. Okajima, D.-S. Im, Albumin functions as an inhibitor of T cell adhesion in vitro. *Biochemical and Biophysical Research Communications* 2006, 351 (4), 953–957.

[234] S. Golding, S. P. Young, Iron Requirements of Human Lymphocytes: Relative Contributions of Intra- and Extra-Cellular Iron. *Scandinavian Journal of Immunology* 1995, 41 (3), 229–236.

[235] K. Nagira, T. Hara, M. Hayashida, K. Osada, M. Shiga, K. Sasamoto, K. Kina, H. Murakami, Development of a protein-free medium with iron salts replacing transferrin for a human-human hybridoma. 1995.

[236] M. Lochner, L. Berod, T. Sparwasser, Fatty acid metabolism in the regulation of T cell function. 2015.

[237] J. G. Crompton, M. Sukumar, R. Roychoudhuri, D. Clever, A. Gros, R. L. Eil, E. Tran, K.-i. Hanada, Z. Yu, D. C. Palmer, S. P. Kerkar, R. D. Michalek, T. Upham, A. Leonardi, N. Acquavella, E. Wang, F. M. Marincola, L. Gattinoni, P. Muranski, M. S. Sundrud, C. A. Klebanoff, S. A. Rosenberg, D. T. Fearon, N. P. Restifo, Akt Inhibition Enhances Expansion of Potent Tumor-Specific Lymphocytes with Memory Cell Characteristics. *Cancer Research* 2015, 75 (2), 296–305.

[238] K. O. Cameron, D. W. Kung, A. S. Kalgutkar, R. G. Kurumbail, R. Miller, C. T. Salatto, J. Ward, J. M. Withka, S. K. Bhattacharya, M. Boehm, K. A. Borzilleri, J. A. Brown, M. Calabrese, N. L. Caspers, E. Cokorinos, E. L. Conn, M. S. Dowling, D. J. Edmonds, H. Eng, D. P. Fernando, R. Frisbie, D. Hepworth, J. Landro, Y. Mao, F. Rajamohan, A. R. Reyes, C. R. Rose, T. Ryder, A. Shavnya, A. C. Smith, M. Tu, A. C. Wolford, J. Xiao, Discovery and Preclinical Characterization of 6-Chloro-5-[4-(1-hydroxycyclobutyl)phenyl]-1 H -indole-3-carboxylic Acid (PF-06409577), a Direct Activator of Adenosine Monophosphate-activated Protein Kinase (AMPK), for the Potential Treatment of Diabetic Nephropathy. *Journal of Medicinal Chemistry* 2016, 59 (17), 8068–8081.

[239] C. A. Klebanoff, J. G. Crompton, A. J. Leonardi, T. N. Yamamoto, S. S. Chandran, R. L. Eil, M. Sukumar, S. K. Vodnala, J. Hu, Y. Ji, D. Clever, M. A. Black, D. Gurusamy, M. J. Kruhlak, P. Jin, D. F. Stroncek, L. Gattinoni, S. A. Feldman, N. P. Restifo, Inhibition of AKT signaling uncouples T cell differentiation from expansion for receptor-engineered adoptive immunotherapy. *JCI Insight* 2017, 2 (23).

[240] E. E. Vincent, P. P. Coelho, J. Blagih, T. Griss, B. Viollet, R. G. Jones, Differential effects of AMPK agonists on cell growth and metabolism. *Oncogene* 2015, 34 (28), 3627–3639.

[241] H. Bohnenkamp, U. Hilbert, T. Noll, Bioprocess development for the cultivation of human T-lymphocytes in a clinical scale. *Cytotechnology* 2002, 38 (1-3), 135–145.

[242] R. J. Purrott, N. Vulpis, D. C. Lloyd, The influence of incubation temperature on the rate of human lymphocyte proliferation in vitro. *Experientia* 1981, 37 (4), 407–408.

[243] K. Sunley, M. Butler, Strategies for the enhancement of recombinant protein production from mammalian cells by growth arrest. *Biotechnology Advances* 2010, 28 (3), 385–394.

[244] K. S. Carswell, E. T. Papoutsakis, Culture of human T cells in stirred bioreactors for cellular immunotherapy applications: Shear, proliferation, and the IL-2 receptor. *Biotechnology and Bioengineering* 2000, 68 (3), 328–338.

[245] Y. Nakagawa, Y. Negishi, M. Shimizu, M. Takahashi, M. Ichikawa, H. Takahashi, Effects of extracellular pH and hypoxia on the function and development of antigen-specific cytotoxic T lymphocytes. *Immunology Letters* 2015, 167 (2), 72–86.

[246] J. B. Sieck, T. Cordes, W. E. Budach, M. H. Rhiel, Z. Suemeghy, C. Leist, T. K. Villiger, M. Morbidelli, M. Soos, Development of a Scale-Down Model of hydrodynamic stress to study the performance of an industrial CHO cell line under simulated production scale bioreactor conditions. *Journal of Biotechnology* 2013, 164 (1), 41–49.

[247] A. Carreau, B. E. Hafny-Rahbi, A. Matejuk, C. Grillon, C. Kieda, Why is the partial oxygen pressure of human tissues a crucial parameter? Small molecules and hypoxia. *Journal of Cellular and Molecular Medicine* 2011, 15 (6), 1239–1253.

[248] J. Jin, N. Gkitsas, V. S. Fellowes, J. Ren, S. A. Feldman, C. S. Hinrichs, D. F. Stroncek, S. L. Highfill, Enhanced clinical-scale manufacturing of TCR transduced T-cells using closed culture system modules. *Journal of Translational Medicine* 2018, 16 (13).

[249] C. L. Mackall, R. G. Majzner, C. M. Yuan, L. Zhang, J. F. Shern, M. Sabatino, T. J. Fountaine, D. S. Dimitrov, N. N. Shah, D. F. Stroncek, H. Qin, S. Nguyen, Y. Feng, S. Martin, D. W. Lee, H. Shalabi, T. J. Fry, P. Wolters, M. Stetler-Stevenson, C. Delbrook, B. Dropulic, R. J. Orentas, S. Ramakrishna, B. Yates, CD22-targeted CAR T cells induce remission in B-ALL that is naive or resistant to CD19-targeted CAR immunotherapy. *Nature Medicine* 2017.

[250] S. Maude, M. Pulsipher, M. Boyer, S. Grupp, S. Davies, Efficacy and Safety of CTL019 in the First US Phase II Multicenter Trial in Pediatric Relapsed/Refractory Acute Lymphoblastic Leukemia: Results of an Interim Analysis. *Blood* 2016, 126 (23), 681.

[251] P. F. Robbins, S. H. Kassim, T. L. N. Tran, J. S. Crystal, R. A. Morgan, S. A. Feldman, J. C. Yang, M. E. Dudley, J. R. Wunderlich, R. M. Sherry, U. S. Kammula, M. S. Hughes, N. P. Restifo, M. Raffeld, C.-C. R. Lee, Y. F. Li, M. El-Gamil, S. A. Rosenberg, Cancer Therapy: Clinical A Pilot Trial Using Lymphocytes Genetically Engineered with an NY-ESO-1-Reactive T-cell Receptor: Long-term Follow-up and Correlates with Response. *Clin Cancer Res* 2015, 21 (5).

[252] S. He, Y. Liu, L. Meng, H. Sun, Y. Wang, Y. Ji, J. Purushe, P. Chen, C. Li, J. Madzo, J. P. Issa, J. Soboloff, R. Reshef, B. Moore, L. Gattinoni, Y. Zhang, Ezh2 phosphorylation state determines its capacity to maintain CD8+T memory precursors for antitumor immunity. *Nature Communications* 2017, 8 (1).

[253] E. H. Ma, M. C. Poffenberger, A. H-T Wong, R. G. Jones, C. Author, The role of AMPK in T cell metabolism and function. *Current Opinion in Immunology* 2017, 46, 45–52.

[254] D. Finlay, D. A. Cantrell, Metabolism, migration and memory in cytotoxic T cells. 2011.

[255] X. Liu, R. R. Chhipa, S. Pooya, M. Wortman, S. Yachyshin, L. M. L. Chow, A. Kumar, X. Zhou, Y. Sun, B. Quinn, C. McPherson, R. E. Warnick, A. Kendler, S. Giri, J. Poels, K. Norga, B. Viollet, G. A. Grabowski, B. Dasgupta, Discrete mechanisms of mTOR and cell cycle regulation by AMPK agonists independent of AMPK. *Proceedings of the National Academy of Sciences* 2014, 111 (4), E435–E444.

[256] L. S. Hami, C. Green, N. Leshinsky, E. Markham, K. Miller, S. Craig, GMP production and testing of Xcellerated T Cells for the treatment of patients with CLL. *Cytotherapy* 2004, 6 (6), 554–562.

[257] B. L. Levine, J. Miskin, K. Wonnacott, C. Keir, Global Manufacturing of CAR T-Cell Therapy. *Molecular Therapy - Methods & Clinical Development* 2016, 4 (March), 92–101.

[258] R. P. Somerville, L. Devillier, M. R. Parkhurst, S. A. Rosenberg, M. E. Dudley, Clinical scale rapid expansion of lymphocytes for adoptive cell transfer therapy in the WAVE ® bioreactor. *Journal of Translational Medicine* 2012, 10 (1).

[259] R. K. Iyer, P. A. Bowles, H. Kim, A. Dulgar-Tulloch, Industrializing Autologous Adoptive Immunotherapies: Manufacturing Advances and Challenges. *Frontiers in Medicine* 2018, 5, 150.

[260] P. Kaiser, M. Werner, V. Jérôme, R. Freitag, Scale-up of the ex vivo expansion of encapsulated primary human T lymphocytes. *Biotechnology and Bioengineering* 2018, (February), 2632–2642.

[261] S. F. Lacey, E. J. Orlando, Determinants of response and resistance to CD19 chimeric antigen receptor (CAR) T cell therapy of chronic lymphocytic leukemia. *Nature Medicine* 2018.

[262] M. Aebi, R. Bernasconi, S. Clerc, M. Molinari, N-glycan structures: recognition and processing in the ER. *Trends in Biochemical Sciences* 2010, 35 (2), 74–82.

[263] Y. van Kooyk, G. A. Rabinovich, Protein-glycan interactions in the control of innate and adaptive immune responses. 2008.

[264] R. D. Wright, D. Cooper, Glycobiology of leukocyte trafficking in inflammation. *Glycobiology* 2014, 24 (12), 1242–1251.

[265] T. S. Raju, S. E. Lang, Diversity in structure and functions of antibody sialylation in the Fc. *Current Opinion in Biotechnology* 2014, 30, 147–152.

[266] K. W. Moremen, M. Tiemeyer, A. V. Nairn, Vertebrate protein glycosylation: diversity, synthesis and function. *Nature Reviews Molecular Cell Biology* 2012, 13 (7), 448–462.

[267] J. Breitling, M. Aebi, N-linked protein glycosylation in the endoplasmic reticulum. *Cold Spring Harbor Perspectives in Biology* 2013, 5 (8), a013359–a013359.

[268] N. Cherepanova, S. Shrimal, R. Gilmore, N-linked glycosylation and homeostasis of the endoplasmic reticulum. *Current Opinion in Cell Biology* 2016, 41, 57–65.

[269] D. F. Zielinska, F. Gnad, K. Schropp, J. R. Wiśniewski, M. Mann, Mapping N-Glycosylation Sites across Seven Evolutionarily Distant Species Reveals a Divergent Substrate Proteome Despite a Common Core Machinery. *Molecular Cell* 2012, 46 (4), 542–548.

[270] S. W. Mast, K. W. Moremen, Family 47 α-Mannosidases in N-Glycan Processing. in *Methods in Enzymology*, volume 415, 2006, 31–46.

[271] P. Stanley, Golgi glycosylation. *Cold Spring Harbor Perspectives in Biology* 2011, 3 (4), 1–13.

[272] H. Schachter, Biosynthetic controls that determine the branching and microheterogeneity of protein-bound oligosaccharides. *Biochemistry and cell biology = Biochimie et biologie cellulaire* 1986, 64 (3), 163–81.

[273] H. Schachter, The 'yellow brick road' to branched complex N -glycans. *Glycobiology* 1991, 1 (5), 453–461.

[274] A. Dell, A. Galadari, F. Sastre, P. Hitchen, Similarities and differences in the glycosylation mechanisms in prokaryotes and eukaryotes. 2010.

[275] I. J. del Val, K. M. Polizzi, C. Kontoravdi, A theoretical estimate for nucleotide sugar demand towards Chinese Hamster Ovary cellular glycosylation. *Scientific Reports* 2016, 6 (1), 28547.

[276] A. Varki, Factors controlling the glycosylation potential of the Golgi apparatus. *Trends in Cell Biology* 1998, 8 (1), 34–40.

[277] I. Hang, C. W. Lin, O. C. Grant, S. Fleurkens, T. K. Villiger, M. Soos, M. Morbidelli, R. J. Woods, R. Gauss, M. Aebi, Analysis of site-specific N-glycan remodeling in the endoplasmic reticulum and the Golgi. *Glycobiology* 2015, 25 (12), 1335–1349.

[278] K. Khatri, J. A. Klein, M. R. White, O. C. Grant, N. Leymarie, R. J. Woods, K. L. Hartshorn, J. Zaia, Integrated Omics and Computational Glycobiology Reveal Structural Basis for Influenza A Virus Glycan Microheterogeneity and Host Interactions. *Molecular & Cellular Proteomics* 2016, 15 (6), 1895–1912.

[279] B. J. Scallon, S. H. Tam, S. G. McCarthy, A. N. Cai, T. S. Raju, Higher levels of sialylated Fc glycans in immunoglobulin G molecules can adversely impact functionality. *Molecular Immunology* 2007, 44 (7), 1524–1534.

[280] K. J. Doores, L. Kong, S. A. Krumm, K. M. Le, D. Sok, U. Laserson, F. Garces, P. Poignard, I. A. Wilson, D. R. Burton, Two Classes of Broadly Neutralizing Antibodies within a Single Lineage Directed to the High-Mannose Patch of HIV Envelope. *Journal of Virology* 2015, 89 (2), 1105–1118.

[281] M. Butler, M. Spearman, The choice of mammalian cell host and possibilities for glycosylation engineering. *Current Opinion in Biotechnology* 2014, 30, 107–112.

[282] P. Hossler, S. F. Khattak, Z. J. Li, Optimal and consistent protein glycosylation in mammalian cell culture. *Glycobiology* 2009, 19 (9), 936–949.

[283] L.-X. Wang, J. V. Lomino, Emerging Technologies for Making Glycan-Defined Glycoproteins. *ACS Chemical Biology* 2012, 7 (1), 110–122.

[284] Y. Durocher, M. Butler, Expression systems for therapeutic glycoprotein production. *Current Opinion in Biotechnology* 2009, 20 (6), 700–707.

[285] E. Grabenhorst, P. Schlenke, S. Pohl, M. Nimtz, H. S. Conradt, Genetic engineering of recombinant glycoproteins and the glycosylation pathway in mammalian host cells. 1999.

[286] S. J. North, H.-H. Huang, S. Sundaram, J. Jang-Lee, A. T. Etienne, A. Trollope, S. Chalabi, A. Dell, P. Stanley, S. M. Haslam, Glycomics Profiling of Chinese Hamster Ovary Cell Glycosylation Mutants Reveals N -Glycans of a Novel Size and Complexity. *Journal of Biological Chemistry* 2010, 285 (8), 5759–5775.

[287] S. K. Patnaik, P. Stanley, Lectin-Resistant CHO Glycosylation Mutants. in *Methods in Enzymology*, 2006, 159–182.

[288] P. A. Gleeson, J. Feeney, R. C. Hughes, Structures of N-glycans of a ricin-resistant mutant of baby hamster kidney cells. Synthesis of high-mannose and hybrid N-glycans. *Biochemistry* 1985, 24 (2), 493–503.

[289] Q. Wang, M. Stuczynski, Y. Gao, M. J. Betenbaugh, Strategies for Engineering Protein N-Glycosylation Pathways in Mammalian Cells. in *Glyco-Engineering: Methods and Protocols*, 2015, 287–305.

[290] Q. Zhou, S. Shankara, A. Roy, H. Qiu, S. Estes, A. McVie-Wylie, K. Culm-Merdek, A. Park, C. Pan, T. Edmunds, Development of a simple and rapid method for producing non-fucosylated oligomannose containing antibodies with increased effector function. *Biotechnology and Bioengineering* 2008, 99 (3), 652–665.

[291] P. Zhang, K. F. Chan, R. Haryadi, M. Bardor, Z. Song, CHO Glycosylation Mutants as Potential Host Cells to Produce Therapeutic Proteins with Enhanced Efficacy. in *Advances in Biochemical Engineering/Biotechnology*, volume 131, 2012, 63–87.

[292] N. Lin, J. Mascarenhas, N. R. Sealover, H. J. George, J. Brooks, K. J. Kayser, B. Gau, I. Yasa, P. Azadi, S. Archer-Hartmann, Chinese hamster ovary (CHO) host cell engineering to increase sialylation of recombinant therapeutic proteins by modulating sialyltransferase expression. *Biotechnology Progress* 2015, 31 (2), 334–346.

[293] M. C. Ryczko, J. Pawling, R. Chen, A. M. Abdel Rahman, K. Yau, J. K. Copeland, C. Zhang, A. Surendra, D. S. Guttman, D. Figeys, J. W. Dennis, Metabolic Reprogramming by Hexosamine Biosynthetic and Golgi N-Glycan Branching Pathways. *Scientific Reports* 2016, 6 (1), 23043.

[294] V. Faid, G. Evjen, O. K. Tollersrud, J. C. Michalski, W. Morelle, Site-specific glycosylation analysis of the bovine lysosomal α-mannosidase. *Glycobiology* 2006, 16 (5), 440–461.

[295] S. Hua, C. C. Nwosu, J. S. Strum, R. R. Seipert, H. J. An, A. M. Zivkovic, J. B. German, C. B. Lebrilla, Site-specific protein glycosylation analysis with glycan isomer differentiation. *Analytical and Bioanalytical Chemistry* 2012, 403 (5), 1291–1302.

[296] L. F. Zacchi, B. L. Schulz, N-glycoprotein macroheterogeneity: biological implications and proteomic characterization. *Glycoconjugate Journal* 2016, 33 (3), 359–376.

[297] X. Yu, K. Baruah, D. J. Harvey, S. Vasiljevic, D. S. Alonzi, B. D. Song, M. K. Higgins, T. A. Bowden, C. N. Scanlan, M. Crispin, Engineering hydrophobic protein-carbohydrate interactions to fine-tune monoclonal antibodies. *Journal of the American Chemical Society* 2013, 135 (26), 9723–9732.

[298] W. Chen, L. Kong, S. Connelly, J. M. Dendle, Y. Liu, I. A. Wilson, E. T. Powers, J. W. Kelly, Stabilizing the CH2 Domain of an Antibody by Engineering in an Enhanced Aromatic Sequon. *ACS Chemical Biology* 2016, 11 (7), 1852–1861.

[299] I. Jimenez del Val, J. M. Nagy, C. Kontoravdi, A dynamic mathematical model for monoclonal antibody N-linked glycosylation and nucleotide sugar donor transport within a maturing Golgi apparatus. *Biotechnology Progress* 2011, 27 (6), 1730–1743.

[300] N. Shah, D. A. Kuntz, D. R. Rose, Golgi -mannosidase II cleaves two sugars sequentially in the same catalytic site. *Proceedings of the National Academy of Sciences* 2008, 105 (28), 9570–9575.

[301] G. Tian, S. Xiang, R. Noiva, W. J. Lennarz, H. Schindelin, The crystal structure of yeast protein disulfide isomerase suggests cooperativity between its active sites. *Cell* 2006, 124 (1), 61–73.

[302] S. C. Hubbard, Regulation of glycosylation. The influence of protein structure on N-linked oligosaccharide processing. *Journal of Biological Chemistry* 1988, 263 (36), 19303–19317.

[303] R. B. Trimble, F. Maley, F. K. Chu, Glycoprotein biosynthesis in yeast. Protein conformation affects processing of high mannose oligosaccharides on carboxypeptidase Y and invertase. *Journal of Biological Chemistry* 1983, 258 (4), 2562–2567.

[304] C. H. Hsu, S. Park, D. E. Mortenson, B. L. Foley, X. Wang, R. J. Woods, D. A. Case, E. T. Powers, C. H. Wong, H. J. Dyson, J. W. Kelly, The Dependence of Carbohydrate-Aromatic Interaction Strengths on the Structure of the Carbohydrate. *Journal of the American Chemical Society* 2016, 138 (24), 7636–7648.

[305] A. N. Murray, W. Chen, A. Antonopoulos, S. R. Hanson, R. L. Wiseman, A. Dell, S. M. Haslam, D. L. Powers, E. T. Powers, J. W. Kelly, Enhanced Aromatic Sequons Increase Oligosaccharyltransferase Glycosylation Efficiency and Glycan Homogeneity. *Chemistry and Biology* 2015, 22 (8), 1052–1062.

[306] J. L. Price, D. L. Powers, E. T. Powers, J. W. Kelly, Glycosylation of the enhanced aromatic sequon is similarly stabilizing in three distinct reverse turn contexts. *Proceedings of the National Academy of Sciences* 2011, 108 (34), 14127–14132.

[307] J. L. Price, E. K. Culyba, W. Chen, A. N. Murray, S. R. Hanson, C. H. Wong, E. T. Powers, J. W. Kelly, N-glycosylation of enhanced aromatic sequons to increase glycoprotein stability. *Biopolymers* 2012, 98 (3), 195–211.

[308] P. Hsieh, M. R. Rosner, P. W. Robbins, Host-dependent variation of asparagine-linked oligosaccharides at individual glycosylation sites of sindbis virus glycoproteins. *Journal of Biological Chemistry* 1983, 258 (4), 2548–2554.

[309] J. Gu, Y. Sato, Y. Kariya, T. Isaji, N. Taniguchi, T. Fukuda, A mutual regulation between cell-cell adhesion and N-glycosylation: Implication of the bisecting GlcNAc for biological functions. 2009.

[310] R. Niwa, E. Shoji-Hosaka, M. Sakurada, T. Shinkawa, K. Uehida, K. Nakamura, K. Matsushima, R. Ueda, N. Hanai, K. Shitara, Defucosylated Chimeric Anti-CC Chemokine Receptor 4 IgG1 with Enhanced Antibody-Dependent Cellular Cytotoxicity Shows Potent Therapeutic Activity to T-Cell Leukemia and Lymphoma. *Cancer Research* 2004, 64 (6), 2127–2133.

[311] R. G. Werner, K. Kopp, M. Schlueter, Glycosylation of therapeutic proteins in different production systems. in *Acta Paediatrica, International Journal of Paediatrics*, volume 96, 17–22.

[312] B. Yin, Y. Gao, C. yu Chung, S. Yang, E. Blake, M. C. Stuczynski, J. Tang, H. F. Kildegaard, M. R. Andersen, H. Zhang, M. J. Betenbaugh, Glycoengineering of Chinese hamster ovary cells for enhanced erythropoietin N-glycan branching and sialylation. *Biotechnology and Bioengineering* 2015, 112 (11), 2343–2351.

[313] N. Yamane-Ohnuki, S. Kinoshita, M. Inoue-Urakubo, M. Kusunoki, S. Iida, R. Nakano, M. Wakitani, R. Niwa, M. Sakurada, K. Uchida, K. Shitara, M. Satoh, Establishment of FUT8 knockout Chinese hamster ovary cells: An ideal host cell line for producing completely defucosylated antibodies with enhanced antibody-dependent cellular cytotoxicity. *Biotechnology and Bioengineering* 2004, 87 (5), 614–622.

[314] F. Schwarz, M. Aebi, Mechanisms and principles of N-linked protein glycosylation. 2011.

[315] A. Varki, R. D. Cummings, J. D. Esko, P. Stanley, G. W. Hart, M. Aebi, A. G. Darvill, T. Kinoshita, N. H. Packer, J. H. Prestegard, R. L. Schnaar, P. H. Seeberger, *Essentials of glycobiology, third edition*. 2017.

[316] S. Shrimal, R. Gilmore, Oligosaccharyltransferase structures provide novel insight into the mechanism of asparagine-linked glycosylation in prokaryotic and eukaryotic cells. *Glycobiology* 2018.

[317] C. Hammond, I. Braakman, A. Helenius, Role of N-linked oligosaccharide recognition, glucose trimming, and calnexin in glycoprotein folding and quality control. *Proceedings of the National Academy of Sciences* 2006, 91 (3), 913–917.

[318] C. Appenzeller-Herzog, The ER-Golgi intermediate compartment (ERGIC): in search of its identity and function. *Journal of Cell Science* 2006, 119 (11), 2173–2183.

[319] P. Zhang, S. Woen, T. Wang, B. Liau, S. Zhao, C. Chen, Y. Yang, Z. Song, M. R. Wormald, C. Yu, P. M. Rudd, Challenges of glycosylation analysis and control: An integrated approach to producing optimal and consistent therapeutic drugs. 2016.

[320] J. I. Aikawa, I. Matsuo, Y. Ito, In vitro mannose trimming property of human ER α-1,2 mannosidase i. *Glycoconjugate Journal* 2012, 29 (1), 35–45.

[321] K. Fujiyama, Y. Ido, R. Misaki, D. G. Moran, I. Yanagihara, T. Honda, S. I. Nishimura, T. Yoshida, T. Seki, Human N-Acetylglucosaminyltransferase I. Expression in Escherichia coli as a soluble enzyme, and application as an immobilized enzyme for the chemoenzymatic synthesis of N-linked oligosaccharides. *Journal of Bioscience and Bioengineering* 2001, 92 (6), 569–574.

[322] J. REN, F. J. CASTELLINO, R. K. BRETTHAUER, Purification and properties of α -mannosidase II from Golgi-like membranes of baculovirus-infected Spodoptera frugiperda (IPLB-SF-21AE) cells. *Biochemical Journal* 2015, 324 (3), 951–956.

[323] D. R. P. Tulsiani, O. Touster, The purification and characterization of mannosidase IA from rat liver Golgi membranes. *Journal of Biological Chemistry* 1988, 263 (11), 5408–5417.

[324] Q. Yang, L. X. Wang, Mammalian α-1,6-fucosyltransferase (FUT8) is the sole enzyme responsible for the N-acetylglucosaminyltransferase I-independent core fucosylation of high-mannose N-glycans. *Journal of Biological Chemistry* 2016, 291 (21), 11064–11071.

[325] W. G. Dunphy, R. Brands, J. E. Rothman, Attachment of terminal N-acetylglucosamine to asparagine-linked oligosaccharides occurs in central cisternae of the golgi stack. *Cell* 1985, 40 (2), 463–472.

[326] A. Velasco, L. Hendricks, K. W. Moremen, D. R. Tulsiani, O. Touster, M. G. Farquhar, Cell type-dependent variations in the subcellular distribution of α-mannosidase I and II. *Journal of Cell Biology* 1993, 122 (1), 39–51.

[327] C. Rabouille, N. Hui, F. Hunte, R. Kieckbusch, E. G. Berger, G. Warren, T. Nilsson, Mapping the distribution of Golgi enzymes involved in the construction of complex oligosaccharides. *Journal of cell science* 1995, 108 (Pt 4, 1617–27.

[328] A. Hassinen, A. Rivinoja, A. Kauppila, S. Kellokumpu, Golgi N-glycosyltransferases form both homo- and heterodimeric enzyme complexes in live cells. *Journal of Biological Chemistry* 2010, 285 (23), 17771–17777.

[329] T. Nilsson, J. Lucocq, D. Mackay, G. Warren, The membrane spanning domain of beta-1,4-galactosyltransferase specifies trans Golgi localization. *The EMBO Journal* 2018, 10 (12), 3567–3575.

[330] S. Sha, C. Agarabi, K. Brorson, D. Y. Lee, S. Yoon, N-Glycosylation Design and Control of Therapeutic Monoclonal Antibodies. 2016.

[331] P. Hossler, L. T. Goh, M. M. Lee, W. S. Hu, GlycoVis: Visualizing glycan distribution in the protein N-glycosylation pathway in mammalian cells. *Biotechnology and Bioengineering* 2006, 95 (5), 946–960.

[332] F. J. Krambeck, S. V. Bennun, M. R. Andersen, M. J. Betenbaugh, Model-based analysis of N-glycosylation in Chinese hamster ovary cells. *PLoS ONE* 2017, 12 (5).

[333] R. Amanchy, D. E. Kalume, A. Pandey, Stable Isotope Labeling with Amino Acids in Cell Culture (SILAC) for Studying Dynamics of Protein Abundance and Posttranslational Modifications. *Science Signaling* 2005, 2005 (267), pl2–pl2.

[334] T. M. Duarte, N. Carinhas, L. C. Barreiro, M. J. Carrondo, P. M. Alves, A. P. Teixeira, Metabolic responses of CHO cells to limitation of key amino acids. *Biotechnology and Bioengineering* 2014, 111 (10), 2095–2106.

[335] J. Deisenhofer, Crystallographic Refinement and Atomic Models of a Human Fc Fragment and Its Complex with Fragment B of Protein A from Staphylococcus aureus at 2.9- and 2.8-Å Resolution. *Biochemistry* 1981, 20 (9), 2361–2370.

[336] L. Nicoud, J. Jagielski, D. Pfister, S. Lazzari, J. Massant, M. Lattuada, M. Morbidelli, Kinetics of Monoclonal Antibody Aggregation from Dilute toward Concentrated Conditions. *Journal of Physical Chemistry B* 2016, 120 (13), 3267–3280.

[337] R. Bernasconi, M. Molinari, ERAD and ERAD tuning: Disposal of cargo and of ERAD regulators from the mammalian ER. 2011.

[338] A. A. Heemskerk, M. Wuhrer, J. M. Busnel, C. A. Koeleman, M. H. Selman, G. Vidarsson, R. Kapur, B. Schoenmaker, R. J. Derks, A. M. Deelder, O. A. Mayboroda, Coupling porous sheathless interface MS with transient-ITP in neutral capillaries for improved sensitivity in glycopeptide analysis. *Electrophoresis* 2013, 34 (3), 383–387.

[339] M. Sanda, L. Zhang, N. J. Edwards, R. Goldman, Site-specific analysis of changes in the glycosylation of proteins in liver cirrhosis using data-independent workflow with soft fragmentation. *Analytical and Bioanalytical Chemistry* 2017, 409 (2), 619–627.

[340] M. K. Doherty, D. E. Hammond, M. J. Clague, S. J. Gaskell, R. J. Beynon, Turnover of the human proteome: Determination of protein intracellular stability by dynamic SILAC. *Journal of Proteome Research* 2009, 8 (1), 104–112.

[341] K. T. Pan, C. C. Chen, H. Urlaub, K. H. Khoo, Adapting Data-Independent Acquisition for Mass Spectrometry-Based Protein Site-Specific N-Glycosylation Analysis. *Analytical Chemistry* 2017, 89 (8), 4532–4539.

[342] Y. Xiang, K. Karaveg, K. W. Moremen, Substrate recognition and catalysis by GH47 α-mannosidases involved in Asn-linked glycan maturation in the mammalian secretory pathway. *Proceedings of the National Academy of Sciences* 2016, 113 (49), E7890–E7899.

[343] M. Oh-eda, H. Nakagawa, T. O. Akama, K. Lowitz, M. Misago, K. W. Moremen, M. N. Fukuda, Overexpression of the Golgi-localized enzyme α-mannosidase IIx in Chinese hamster ovary cells results in the conversion of hexamannosyl-N-acetylchitobiose to tetramannosyl-N-acetylchitobiose in the N-glycan-processing pathway. *European Journal of Biochemistry* 2001, 268 (5), 1280–1288.

[344] D. Chui, M. Oh-Eda, Y. F. Liao, K. Panneerselvam, A. Lal, K. W. Marek, H. H. Freeze, K. W. Moremen, M. N. Fukuda, J. D. Marth, Alpha-mannosidase-II deficiency results in dyserythropoiesis and unveils an alternate pathway in oligosaccharide biosynthesis. *Cell* 1997, 90 (1), 157–167.

[345] T. Noda, M. G. Farquhar, A non-autophagic pathway for diversion of ER secretory proteins to lysosomes. *Journal of Cell Biology* 1992, 119 (1), 85–97.

[346] I. Fregno, E. Fasana, T. J. Bergmann, A. Raimondi, M. Loi, T. Soldà, C. Galli, R. D'Antuono, D. Morone, A. Danieli, P. Paganetti, E. van Anken, M. Molinari, ER-to-lysosome-associated degradation of proteasome-resistant ATZ polymers occurs via receptor-mediated vesicular transport. *The EMBO Journal* 2018, 37 (17), e99259.

[347] I. Fregno, M. Molinari, Endoplasmic reticulum turnover: ER-phagy and other flavors in selective and non-selective ER clearance. *F1000Research* 2018, 7, 454.

[348] R. Gauss, K. Kanehara, P. Carvalho, D. T. W. Ng, M. Aebi, A Complex of Pdi1p and the Mannosidase Htm1p Initiates Clearance of Unfolded Glycoproteins from the Endoplasmic Reticulum. *Molecular Cell* 2011, 42 (6), 782–793.

[349] M. Crispin, D. J. Harvey, V. T. Chang, C. Yu, A. R. Aricescu, E. Y. Jones, S. J. Davis, R. A. Dwek, P. M. Rudd, Inhibition of hybrid- and complex-type glycosylation reveals the presence of the GlcNAc transferase I-independent fucosylation pathway. *Glycobiology* 2006, 16 (8), 748–756.

[350] H. Torikai, A. Reik, F. Soldner, E. H. Warren, C. Yuen, Y. Zhou, D. L. Crossland, H. Huls, N. Littman, Z. Zhang, S. S. Tykodi, P. Kebriaei, D. A. Lee, J. C. Miller, E. J. Rebar, M. C. Holmes, R. Jaenisch, R. E. Champlin, P. D. Gregory, L. J. N. Cooper, Toward eliminating HLA class I expression to generate universal cells from allogeneic donors. *Blood* 2013, 122 (8), 1341–9.

[351] C. Guyot, S. Lerouge, Can we achieve the perfect injectable scaffold for cell therapy? *Future science OA* 2018, 4 (4), FSO284.

[352] J. R. Wiśniewski, A. Zougman, N. Nagaraj, M. Mann, Universal sample preparation method for proteome analysis. *Nature methods* 2009, 6 (5), 359–62.

[353] B. MacLean, D. M. Tomazela, N. Shulman, M. Chambers, G. L. Finney, B. Frewen, R. Kern, D. L. Tabb, D. C. Liebler, M. J. MacCoss, Skyline: An open source document editor for creating and analyzing targeted proteomics experiments. *Bioinformatics* 2010, 26 (7), 966–968.

[354] N. Hosokawa, L. O. Tremblay, B. Sleno, Y. Kamiya, I. Wada, K. Nagata, K. Kato, A. Herscovics, EDEM1 accelerates the trimming of α1,2-linked mannose on the C branch of N-glycans. *Glycobiology* 2010, 20 (5), 567–575.

Höhenring 7
8052 Zurich, Switzerland
+41 764 406 875
ernesto.scibona@gmail.com
Italian, born 14/09/1990
Unmarried
European Driving License B

Ernesto Scibona

Curriculum Vitæ

Research & Work Experience

March 2015 - Present — **Ph.D Candidate**, *ETH Zurich, Institute for Chemical- and Bioengineering, Group Morbidelli*, Switzerland, dissertation title: Experimental and modeling framework for the production for cell and protein-based biopharmaceutical products. Supervisor: Prof. Massimo Morbidelli.

- Led the development of a processes for the production of human stem and T cell-based therapies.
- Developed a mathematical description of protein synthesis.
- Provided data analysis support for industrial partners.
- Presented the research work at major international conferences (over 250 attendees).

March 2012 - June 2012 — **Lab assistant**, *Universitá di Bologna, Department of Civil, Chemical, Environmental, and Materials Engineering, Prof. Nadia Lotti's Laboratory*, Italy.

- Responsible for the characterization of biodegradable polymers.

Education

Sept. 2012 - Dec. 2014 — **Master Degree in Biongineering**, *Politecnico di Milano*, Italy.
Track: Cells, Tissues and Biotechnology.
Final Grade: 110/110 cum Laude. Average Grade: 29.0/30.

March 2014 - Dec. 2014 — **Invited Visiting Student**, *ETH Zurich*, Switzerland.
Master thesis in the Institute of Chemical and Bioengineering, Morbidelli Group.

Sept. 2009 - July. 2012 — **First Level Degree in Bioengineering**, *Universitá di Bologna*, Italy.
Final Grade: 110/110 cum Laude. Average Grade: 28.2/30

Awards

2010 — Premio di studio a favore di studenti meritevoli iscritti a Corsi di studio dell'Università di Bologna (Merit Scolarship, Top 0.5% student).

Skills

Languages	Italian (mother tongue), English (full professional proficiency), German (intermediate).
Expertise	Biomanufacturing processes, cell-based therapies, mathematical models.
Programming	MatLab, Fortran, C (basics), Java (basics).
IT Skills	Adobe Illustrator, Adobe CQ5, MS Office.

Personal Interests

Sports	Soccer (team captain for university tournament), gym, hiking.
Hobbies	Cooking, reading (non-fiction, philosophy), chess.

List of Publications

Losfeld, M. E., Scibona, E., Lin, C. W., Villiger, T. K., Gauss, R., Morbidelli, M., & Aebi, M. (2017). Influence of protein/glycan interaction on site-specific glycan heterogeneity. The FASEB Journal, 31(10), 4623-4635.

Karst, D. J., Scibona, E., Serra, E., Bielser, J. M., Souquet, J., Stettler, M., ... & Villiger, T. K. (2017). Modulation and modeling of monoclonal antibody N-linked glycosylation in mammalian cell perfusion reactors. Biotechnology and bioengineering, 114(9), 1978-1990.

Villiger, T. K., Scibona, E., Stettler, M., Broly, H., Morbidelli, M., & Soos, M. (2016). Controlling the time evolution of mAb N-linked glycosylation-Part II: Model-based predictions. Biotechnology progress, 32(5), 1135-1148.

Conference Proceedings

E. Scibona, M. Perra, L. Ayala-Solares, M. Morbidelli, Bioprocess optimization for the expansion of early memory T cells in serum-free conditions, World Advanced Therapies & Regenerative Medicine Congress (2018), London, UK (poster)

E. Scibona, M. Perra, L. Ayala-Solares, M. Morbidelli, Bioprocess optimization for the expansion of early memory T cells in serum-free conditions, Cell Culture Engineering XVI (2018), Tampa, FL, USA (poster)

E. Scibona, F. Iocchi, M. Morbidelli, High density ex vivo expansion of stem cell aggregates in stirred perfusion bioreactors, Scale-up and Manufacturing of Cell-based Therapies V (2017), San Diego, CA, USA (oral talk)

T. K. Villiger, E. Scibona, M. Morbidelli, M. Soos, Modeling and Modulating N-Linked Glycosylation – Differences and Similarities in Fed-Batch and Continuous Cultures, AIChE Annual Meeting (2014), Atlanta, GA, USA (oral talk)